Structural changes in single chromatin fibers induced by tension and torsion
Meng, H.

Cover Page

Universiteit Leiden

Structural Changes in Single Chromatin Fibers Induced by Tension and Torsion

He Meng

Structural Changes in Single Chromatin Fibers Induced by Tension and Torsion

Proefschrift

ter verkrijging van

de graad van Doctor aan de Universiteit Leiden,

op gezag van Rector Magnificus prof. mr. C. J. J. M. Stolker,

volgens besluit van het College voor Promoties

te verdedigen op donderdag 9 oktober 2014

klokke 11:15 uur

door

He Meng

geboren te Jilin, China

in 1985

Promotiecommissie

Promotor:	Prof. dr. T. Schmidt	(Universiteit Leiden)
Co-promotor:	Dr. ir. S. J. T. van Noort	(Universiteit Leiden)
Overige leden:	Dr. R. T. Dame	(Universiteit Leiden)
	Prof. dr. N. H. Dekker	(Technische Universiteit Delft)
	Prof. dr. E. R. Eliel	(Universiteit Leiden)
	Prof. dr. N. Gilbert	(The University of Edinburgh, UK)
	Prof. dr. M. van Hecke	(Universiteit Leiden)
	Prof. dr. H. Schiessel	(Universiteit Leiden)

"If I have seen further, it is by standing on the shoulders of Giants."

— Isaac Newton, *a letter to Robert Hooke in 1676*

vi

Contents

x

Chapter 1

Introduction

In this thesis, we describe the mechanical properties of chromatin, the ubiquitous DNA protein complex that organizes our genome, at the single-molecule level. This chapter briefly introduces the structural properties of DNA, nucleosomes and chromatin. We introduce the theory to describe the elastic and topological characteristics of DNA and discuss the single molecule technique, magnetic tweezers, which is used in this thesis to study the structural changes of DNA and chromatin under tension and torsion. Finally, we provide a brief overview of the contents of this thesis.

Almost 60 years have passed since the discovery of the right-handed helical structure of DNA [1]. The unique structure of DNA enables genetic and epi-genetic information to be stored and regulated in prokaryotes and eukaryotes. Prokaryotes are single-celled organism that lack a cell nucleus, and their DNA, though compacted by supercoiling and a host of DNA organizing proteins, floats freely in the cytoplasm. Eukaryotic cells, in contrast, have intracellular organelles that organize the cellular contents into compartments. In human cells, for instance, our genes consist of 3 billion base pairs (bp) of DNA that are packed in the nucleus. DNA is under constant mechanical stress and exists in various structures. This organization of DNA is highly dynamic with various enzymes stretching and twisting the helix. This dynamical structure plays a role in regulating transcription, replication and mitosis. Understanding the role of DNA compaction in gene regulation represents one of the most challenging questions in current life sciences. To address this question, we need better physical descriptions of DNA and its higher order organization, chromatin.

1.1 DNA, nucleosomes and chromatin

DNA in cells typically consists of two complementary polynucleotide chains that are interwound, forming a doublestranded helix, though other shapes, such as G-quadruplexes and Holliday junctions may also occur. Among several known conformations, B-DNA prevails under physiological conditions (Fig. 1.1A). B-DNA is a right handed helix with a pitch of 10.5 bp per helical turn (3.4 nm) and a diameter of 2.0 nm. The human genome DNA consisting of 3 billion bp is therefore about 1 meter long when stretched out. Without physical constraints, it may fold into a swollen coil occupying volume of 10^7 μm^3 [2]. In the nucleus of a typical human cell however, it is condensed into a volume of about 500 μm^3. This formidable magnitude of condensation into the nucleus is achieved by several steps of compaction involving a choice of structural proteins. The complex of DNA and those structural proteins is known as chromatin.

The basic repeating unit of chromatin is the nucleosome, consisting of 147 bp of DNA wrapped 1.7 times around a wedge-shaped histone octamer. The octamer is composed of a (H3-H4)$_2$ tetramer and two H2A-H2B dimers (Fig. 1.1B) [6]. In vitro studies revealed that the nucleosome is highly dynamic and undergoes spontaneous, re-

A

2 nm

10 bp = 3.4 nm

B

12 nm

147 bp = 6 nm

C

~30 nm

~5000 bp ≈ 50 nm
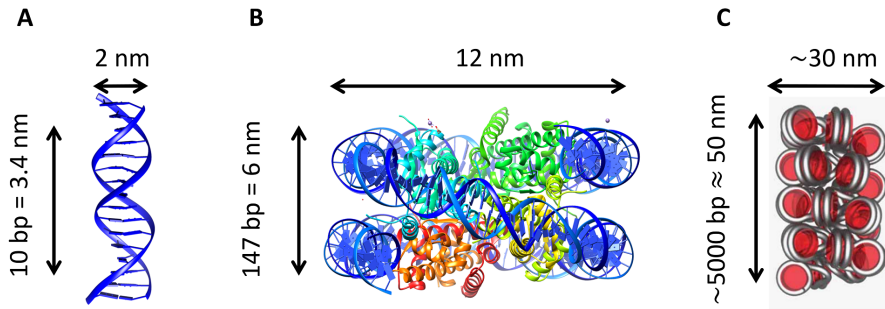
Figure 1.1: Overview of several levels of DNA organization with typical dimensions. (A) The crystal structure of B-DNA (3BSE) [3] shows a right-handed chirality with about 10 bp per helical turn. (B) The nucleosome crystal structure (1KX4) [4] shows 147 bp of DNA wrapped around a histone octamer with a left-handed chirality. (C) Schematic drawing of a folded chromatin fiber with one-start solenoid model proposed in [5]. The nucleosome arrays are connected by 30-60 bp of linker DNA.

versible unwrapping of part of the DNA from the histone core [7]. Although there are no sequence-specific interactions between histones and DNA bases, certain DNA sequences have a strong preference to form a nucleosome. The chromatin fibers studied in this thesis are reconstituted with tandem arrays of the Widom 601 sequence [8, 9]. This DNA sequence was selected from a random DNA pool to bind with high affinity to the histone octamer. Even though 601 sequence is widely used in vitro research, only recently was the mechanism of its strong affinity explained by a statistical mechanics model [10].

Nucleosomes are connected by short DNA segments (linker DNA) into nucleosome arrays, which fold into chromatin fibers by interactions with neighboring nucleosomes. Although the structure of chromatin fibers has been heavily debated for 30 years, in vitro it is commonly found that these fibers form condensed 30 nm fibers under physiological conditions (Fig. 1.1C). Several parameters determine the conformation and the degree of compaction of the 30 nm fiber, such as the linker DNA length, salt concentration and histone post transcriptional modifications. The linker DNA varies in nature between 10 and 90 bp [11]. Two groups of competing models, the "one start" solenoid model and the "two start" zigzag model have been proposed to explain the chromatin structure [12]. In the solenoid model, consecutive nucleosomes interact with each other

and follow a helical trajectory. This model is supported by the Electron Microscopy experiments on reconstituted chromatin fibers with 30-60 bp of linker DNA [13]. In the zigzag model, two rows of nucleosomes twist into a double helix, so that alternate nucleosomes become interacting partners. This model is supported by the crystal structure of a tetranucleosome array with 20 bp of linker DNA [14].

1.2   DNA supercoiling

Overwinding (positive) or underwinding (negative) the DNA double helix results in DNA supercoiling, which is an expression of the torsional strain on the helix. DNA supercoiling plays an important role in DNA compaction such as the formation of nucleosomes and the higher order chromatin structures. The DNA wraps around the histone core in a left-handed helix, therefore it is negatively supercoiled. Additionally, DNA supercoiling acts as an important feature during replication and transcription. During transcription, the double helix is underwound, gets melted and forms a transcription bubble [15]. DNA is also thought to experience the torsional stress created by RNA polymerase II [16], when RNA polymerase II is bound to the nuclear matrix and processes through a torsionally constrained DNA domain. However, how chromatin fibers respond to the torsional stress is not well understood. To further answer this question, we need physical and mathematical descriptions of DNA supercoiling.

The term topology is used in mathematical studies of shapes, to quantify the structural properties that are conserved under continuous deformations, including stretching and bending. It is commonly used to describe the conformation change of supercoiled DNA. A torsionally constrained DNA segment with no free rotation of its ends, is called a topological domain. An example of a topological domain is circular DNA.

In our studies, we create a topological domain from a linear DNA fragment, using multiple anchor points to stick the DNA to a glass slide and a bead. A topological domain is characterized by its linking number (Lk). The linking number is defined as the number of times that the two DNA strands are interwound, independent of the exact conformation. The linking number of a relaxed B-DNA molecule with N bp is

$$Lk_0 = N/10.5 \, . \tag{1.1}$$

A

B
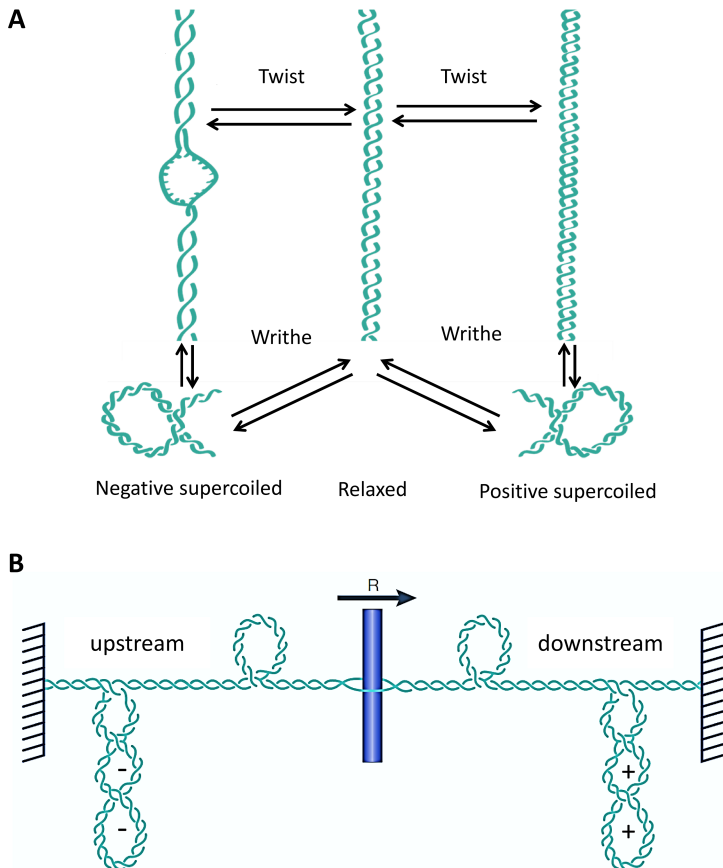
Figure 1.2: The topological properties of DNA. (A) DNA can exist as a relaxed molecule (center) having a right-handed chirality without any supercoiling as schematically depicted in the center. Overwinding (right) DNA can over-twist the DNA or form a plectonemic structure. Underwinding DNA may undertwist DNA, induce DNA denaturation to form DNA melting bubble or form a plectonemic structure. (B) A graphical illustration of the "twin supercoil domain" based on [17]. R is RNA polymerase II. If R is moving from left to right, the DNA in font of the polymerase (downstream) becomes overwound, or positively supercoiled; the DNA behind the polymerase (upstream) becomes underwound, or negatively supercoiled.

Two parameters that describe changes in DNA conformation are twist (Tw) and writhe (Wr). Twist refers to the helical winding of the DNA strands around each other in a helical conformation, whereas writhe is a measure of the looping of the double helix, quantified by the number of times it crosses itself. Without supercoiling, Lk_o equals Tw_o. Over or under-winding the DNA molecule will change Lk. This change in the linking number can be distributed into the two ways (shown in Fig. 1.2A),

$$\Delta Lk = Lk - Lk_o = Tw - Tw_o + Wr = \Delta Tw + Wr \qquad (1.2)$$

The response to positive and negative supercoiling is not symmetric. Because of the chirality of DNA, it may be denatured by negative supercoiling to form a melted bubble, which has no intrinsic twist.

In eukaryotic cells, many activities that require DNA to be unwound (and rewound) involve the process of supercoiling. During transcription, for example, a RNA polymerase II can generate about seven DNA supercoils per second in a topological domain [18]. A popular model to describe the mechanism of RNA polymerase II is the "twin supercoiled domain" model [19, 20] (Fig. 1.2B). In this model, the RNA polymerase II moves along the DNA helix, and generates positive supercoiling ahead and negative supercoiling behind. However, the natural substrate for RNA polymerase II is a chromatin fiber consisting of several tens of nucleosomes (a typical length of a gene) rather than naked DNA. The effects of supercoiling therefore need to be considered in the context of chromatin, but unfortunately, we know very little about its mechanical properties. The idea that the supercoiling may be transmitted along chromatin was raised twenty-five years ago but how the chromatin fiber responds to supercoiling has nonetheless remained unclear [21, 22]. One hypothesis based on the "twin supercoiled domain" model is that positive supercoiling ahead of the RNA polymerase II will destabilize nucleosomes and negative supercoiling behind will promote reassembly of nucleosomes [23, 24]. Manipulating chromatin by single-molecule techniques can provide insight into this fundamental question.

1.3 Magnetic tweezers

In this thesis, we used magnetic tweezers as a tool to manipulate single DNA molecules or chromatin fibers and study their response to torsional stress. Magnetic and optical

tweezers have been developed in the past twenty years. Force spectroscopy studies on DNA or DNA-protein complexes have given lots of structural insights on the single molecule level. In 1996, Strick et al. measured the response of a single supercoiled DNA to a stretching force [25]. A single DNA molecule was anchored on a glass cover slip, and at the other end to a superparamagnetic bead (Fig. 1.3A). A magnet, placed above the flow cell, exerted a force on the bead and hence on the DNA molecule. The magnetic force exerted on the bead depends on the gradient of the magnetic field [26, 27]:

$$F = \frac{1}{2}\nabla(\overrightarrow{m(B)} \cdot \overrightarrow{B})$$ (1.3)
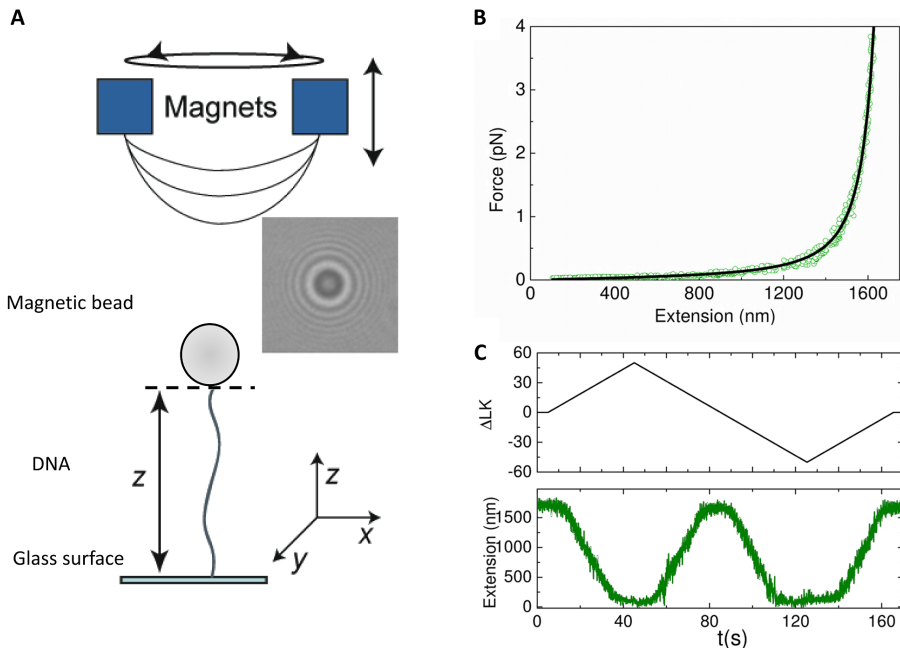
Figure 1.3: Magnetic tweezers set up and the mechanical properties of DNA. (A) A schematic drawing of the setup with an image of the bead. (B) A force-extension curve of a bare DNA molecule with 5.2 kbp. A fit by worm like chain model gives the contour length of 1750 nm, persistence length of 50 nm. (C) The real time measurements of DNA extension versus excess linking number.

where $\overrightarrow{B}$ is the external magnetic field and $\overrightarrow{m(B)}$ is the magnetic moment induced in the paramagnetic bead. The micrometer-sized bead can be tracked by ordinary light

microscopy. The position of the bead in three dimensions is determined by image analysis: the position in the x and y directions is obtained from the center of the diffraction rings with nanometer precision. The position in the z direction can also be extracted from the diffraction pattern by comparison with reference images, which measured the diffraction pattern of the bead at known distances from the focal plane.

The force can be calculated from the amplitude of the Brownian fluctuations. The Brownian motion of the bead is restricted by the DNA tether and varies with the applied force. The force follows from equipartition theorem [25]:

$$F = \frac{k_B T}{< \triangle x^2 >} < z > .$$
(1.4)

$k_B T$ is the product of the Boltzmann constant, k_B, and the temperature, T. At room temperature, $k_B T = 4.1$ pN nm. $< \triangle x^2 >$ is the variance of the bead excursions in the x-direction and $< z >$ is the extension of the DNA tether. The forces range from sub-piconewton to tens of piconewtons. The spatial resolution is several nanometers and temporal resolution is in the order of tens of milliseconds [28].

One should notice that due to the limited frame rate of the camera, $< \triangle x^2 >$ can be underestimated at large forces or with short tethers. Therefore, rather than using Equation 1.4 directly, the fluctuations in position are transferred into the frequency domain, and the power spectrum of the motion is further analyzed. More details about force calibration can be found in [29, 30]. Here we calibrated the force as a function of the magnet position, and use this relation to calculate the force during an experiment [31]. A major advantage of this method is that one does not need long (> minutes) calibration times, and long exposures to large forces, which is detrimental to our chromatin fibers.

During a magnetic tweezers experiment, the height of the bead that we measured is relative to the focal plane of the microscope. We subtract the relative position of the bead at a certain force with the position of the bead at the lowest force (< 0.03 pN) to obtain the extension of the tether. However, this extension is sometimes shorter than what we expected, because the tether may not always be attached to the bottom of the bead. When it is attached at the side of the bead, this leads an apparent extension shorter than the exact value [32, 33]. We correct this by adding an offset correction according to the expected contour length of the tether, using the well-documented worm-like chain properties of DNA (Fig. 1.3B, and described in the next section).

An advantage of the magnetic tweezers with respect to (traditional) optical tweezers is its ability to control the excess linking number of a single tether. Rotating the pair of magnets rotates the bead, and induces either over or under-winding of the DNA. The extension of the tether response to supercoiling can be detected in real time (Fig. 1.3C).

1.4 Mechanical properties of DNA and nucleosomes

Knowing the elastic properties of double stranded DNA is the first step to understand the mechanical properties of a chromatin fiber. The elasticity of double stranded DNA has been investigated extensively using magnetic and optical tweezers [34, 35]. A DNA molecule in solution bends locally as a result of thermal fluctuations. Such fluctuations shorten the end-to-end distance of the molecule and is called entropic elasticity. A model named the Worm like chain (WLC) is commonly used to describe this entropic elasticity. The WLC model envisions an isotropic rod that is continuously flexible, as opposed to other polymer models, like the freely jointed chain, which has discrete rigid sections that are linked by flexible hinges. The correlation of the rod's local direction reduces with distance s along the curve following an exponential decay $e^{-|s|/A}$. The decay length, A, is called the persistence length of the rod and defines its flexibility. The persistence length of double-stranded DNA is around 50 nm under physiological conditions [26].

An analytical solution of the force-extension relation for WLC is not known, but an interpolation formula to the numerical solution, given by Marko and Siggia [36] is commonly used:

$$F = \frac{k_B T}{A} \left(\frac{1}{4(1 - \frac{z}{L_o})^2} - \frac{1}{4} + \frac{z}{L_o} \right) \tag{1.5}$$

where z is the end-to-end distance of the tether and L_o is the contour length. For B-DNA the contour length is the number of base pairs times 0.34 nm. A typical force-extension curve of DNA with 5200 bp is shown in Fig. 1.3B.

The mechanical properties of nucleosomes and chromatin have been studied for fifteen years, but there is far less consensus about their interpretation [37]. Brower-Toland et al. [38] first showed that the nucleosome unwraps in two steps. Two 25 nm

steps occur at forces around 5 pN and 15 pN. These stepsizes have been suggested to correspond to the outer turn and inner turn unwrapping of DNA. A DNA spool model proposed by Kulic and Schiessel [39] was able to explain nucleosome unwrapping under tension. Recently, a study of nucleosome unwrapping under torsion was presented [40]. Interestingly, torque has only a moderate influence on nucleosome unwrapping: positive torque slightly increases the unwrapping force for the outer turn, but decreases the unwrapping force for the inner turn. The structure and the mechanical properties of a chromatin fiber in which nucleosomes interact are still poorly understood, and this will be the main subject of this thesis.

1.5   Statistical mechanics

In this thesis we use statistical mechanics to describe the mechanical properties of DNA and chromatin. We define different states of DNA and the chromatin fiber that each have a distinct force and linking number dependent extension and free energy. Statistical mechanics is used to describe the properties of this system in thermodynamic equilibrium.

We consider a system at a constant temperature T, with a fixed number of constituent particles. Each state that the system can occupy, is defined by a specific set of conformations of the system and is marked as i, $(i = 1, 2, 3...)$ with the total energy E_i in each state. The partition function is defined as

$$Z = \sum_i exp(-\frac{E_i}{k_B T}) \tag{1.6}$$

The probability P_i that the system occupies state i is

$$P_i = \frac{1}{Z} exp(-\frac{E_i}{k_B T}) \tag{1.7}$$

In single-molecule studies, it is more convenient for us to calculate the probability P_i of the molecule occurring as a partially folded state when the temperature (T) and the force (F) are specified for a system at 1 atm [41].

$$P_i(T, F) = \frac{1}{Z} exp(-\frac{\Delta G_i(T, z_i) - F z_i}{k_B T}) \tag{1.8}$$

The $\Delta G_i(T, z_i)$ are the free energies at constant T and average extension z_i of state

i. The partition function ensures that the probabilities sum up to one, i.e. $\sum P_i = 1$. Using the partition function, we can calculate the statistical average value of any physical quantity in the system, for instance, for a quantity marked as x, the mean value of x is

$$< x > = \sum_i x_i P_i \tag{1.9}$$

1.6   Outline of this thesis

This thesis reports experimental work on the mechanical properties of the chromatin fiber under tension and torsion. It also contains the theoretical modeling to quantitatively understand the data and enables us to interpret the data in terms of the structural changes of the chromatin fiber at the single molecule level.

Chapter 2 reports the coexistence of twisted, plectonemic and melted states of DNA in a small topological domain. Magnetic tweezers measurements indicate the coexistence of these three states at sub-picoNewton force and linking number densities about −0.06. A broadening of the transitions between the three states is found when the size of a topological domain is limited to several kilobasepairs. We present a statistical mechanics model for such DNA domains by calculating the full partition function. Real-time analysis of short DNA tethers at constant force and torque shows discrete levels of extension, representing discontinuous changes in the size of the melting bubble, which should reflect the underlying DNA sequence. Our results provide a comprehensive picture of the structure of underwound DNA at low force and torque and could have important consequences for various biological processes, in particular those that depend on local DNA melting, such as the initiation of replication and transcription.

Chapter 3 describes force spectroscopy of torsionally unconstrained chromatin fibers reconstituted with 601 sequence repeats. We show that the experimental data has variations between different fibers that can be attributed to the heterogeneity in the composition of individual fibers. Comparison to force-extension curves of single nucleosome and chromatin fibers of 20 bp and 50 bp linker DNA reveals distinct physical properties of chromatin (un)folding. We propose that the unfolding of a chromatin fiber goes through four different nucleosome conformations and introduce a statistical mechanics model that quantitatively describes the extension of individual fibers in response to forces up to 30 pN. This quantitative analysis allows for a structural interpretation of all physical processes that define chromatin folding.

Chapter 4 reports the elasticity of torsionally constrained chromatin fibers. By applying tension and torsion with magnetic tweezers, we find that the fiber has a strong asymmetric response to supercoiling. Negative supercoiling stabilizes the fiber against unfolding. Positive supercoiling on the other hand can be absorbed by the fiber. When the force exceeds ~2.0 pN, the fiber unfolds and unwraps one turn of DNA. The amount of unfolding depends on the extend of supercoiling. The anisotropic response reflects the chirality of a left-handed helix. A statistical mechanics model is presented, which captures the full complexity of chromatin folding and unfolding at different degree of supercoiling. These results reveal for the first time the topology of a folded chromatin fiber and present a new description of DNA and chromatin under torsional stress.

References I

[1] Watson, J., and F. Crick. 1953. Molecular Structure of Nucleic Acids. *Nature*. 171:737–738.

[2] Schiessel, H. 2003. The physics of chromatin. *Journal of physics: condensed matter*. 15:R699–R774.

[3] Narayana, N., and M. a. Weiss. 2009. Crystallographic analysis of a sex-specific enhancer element: sequence-dependent DNA structure, hydration, and dynamics. *Journal of molecular biology*. 385:469–90.

[4] Davey, C. a., D. F. Sargent, K. Luger, A. W. Maeder, and T. J. Richmond. 2002. Solvent mediated interactions in the structure of the nucleosome core particle at 1.9 a resolution. *Journal of molecular biology*. 319:1097–113.

[5] Kruithof, M., F.-T. Chien, A. Routh, C. Logie, D. Rhodes, and J. van Noort. 2009. Single-molecule force spectroscopy reveals a highly compliant helical folding for the 30-nm chromatin fiber. *Nature structural & molecular biology*. 16:534–40.

[6] Luger, K., A. W. Ma, R. K. Richmond, D. F. Sargent, and T. J. Richmond. 1997. Crystal structure of the nucleosome core particle at 2 . 8 A resolution. *Nature*. 389:251–260.

[7] Koopmans, W. J. a., R. Buning, T. Schmidt, and J. van Noort. 2009. spFRET using alternating excitation and FCS reveals progressive DNA unwrapping in nucleosomes. *Biophysical journal*. 97:195–204.

[8] Lowary, P. T., and J. Widom. 1998. New DNA sequence rules for high affinity binding to histone octamer and sequence-directed nucleosome positioning. *Journal of molecular biology*. 276:19–42.

[9] Makde, R. D., J. R. England, H. P. Yennawar, and S. Tan. 2010. Structure of RCC1 chromatin factor bound to the nucleosome core particle. *Nature*. 467:562–6.

[10] van der Heijden, T., J. J. F. a. van Vugt, C. Logie, and J. van Noort. 2012. Sequence-based prediction of single nucleosome positioning and genome-wide nucleosome occupancy. *Proceedings of the National Academy of Sciences of the United States of America*. 109:E2514–22.

[11] Szerlong, H. J., and J. C. Hansen. 2011. Nucleosome distribution and linker DNA: connecting nuclear function to dynamic chromatin structure. *Biochemistry and cell biology = Biochimie et biologie cellulaire*. 89:24–34.

[12] Luger, K., M. L. Dechassa, and D. J. Tremethick. 2012. New insights into nucleosome and chromatin structure: an ordered state or a disordered affair? *Nature reviews. Molecular cell biology*. 13:436–47.

[13] Robinson, P. J. J., L. Fairall, V. a. T. Huynh, and D. Rhodes. 2006. EM measurements define the dimensions of the "30-nm" chromatin fiber: evidence for a compact, interdigitated structure. *Proceedings of the National Academy of Sciences of the United States of America*. 103:6506–11.

[14] Schalch, T., S. Duda, D. F. Sargent, and T. J. Richmond. 2005. X-ray structure of a tetranucleosome and its implications for the chromatin fibre. *Nature*. 436:138–41.

[15] Murakami, K. S., S. Masuda, E. A. Campbell, O. Muzzin, and S. A. Darst. 2002. Structural basis of transcription initiation: an RNA polymerase holoenzyme-DNA complex. *Science*. 296:1285–90.

[16] Ma, J., L. Bai, and M. D. Wang. 2013. Transcription under torsion. *Science*. 340:1580–3.

[17] Wang, J. C. 2002. Cellular roles of DNA topoisomerases: a molecular perspective. *Nature reviews. Molecular cell biology*. 3:430–40.

[18] Darzacq, X., Y. Shav-Tal, V. de Turris, Y. Brody, S. M. Shenoy, R. D. Phair, and R. H. Singer. 2007. In vivo dynamics of RNA polymerase II transcription. *Nature structural & molecular biology*. 14:796–806.

[19] Liu, L. F., and J. C. Wang. 1987. Supercoiling of the DNA template during transcription. *Proceedings of the National Academy of Sciences of the United States of America*. 84:7024–7027.

[20] Wang, J. C., and A. S. Lynch. 1993. Transcription and DNA supercoiling. *Current opinion in genetics & development*. 3:764–8.

[21] Patient, R. K., and J. Allan. 1989. Active chromatin. *Current opinion in cell biology*. 1:454–459.

[22] Gilbert, N., and J. Allan. 2014. Supercoiling in DNA and chromatin. *Current Opinion in Genetics & Development*. 25:15–21.

[23] Clark, D. J., and G. Felsenfeld. 1992. A nucleosome Core Is Transferred out of the Path of a Transcribing polymerase. *Cell*. 71:11–22.

[24] Li, B., M. Carey, and J. L. Workman. 2007. The role of chromatin during transcription. *Cell*. 128:707–19.

[25] Strick, T. R., J. F. Allemand, D. Bensimon, A. Bensimon, and V. Croquette. 1996. The elasticity of a single supercoiled DNA molecule. *Science*. 271:1835–7.

[26] Smith, S. B., L. Finzi, and C. Bustamante. 1992. Direct mechanical measurements of the elasticity of single DNA molecules by using magnetic beads. *Science*. 258:1122–6.

[27] Lipfert, J., X. Hao, and N. H. Dekker. 2009. Quantitative modeling and optimization of magnetic tweezers. *Biophysical journal*. 96:5040–9.

[28] De Vlaminck, I., and C. Dekker. 2012. Recent advances in magnetic tweezers. *Annual review of biophysics*. 41:453–72.

[29] Neuman, K. C., and A. Nagy. 2008. Single-molecule force spectroscopy : optical tweezers , magnetic tweezers and atomic force microscopy. *Nature methods*. 5:491–505.

[30] te Velthuis, A. J. W., J. W. J. Kerssemakers, J. Lipfert, and N. H. Dekker. 2010. Quantitative guidelines for force calibration through spectral analysis of magnetic tweezers data. *Biophysical journal*. 99:1292–302.

[31] Kruithof, M., F. Chien, M. de Jager, and J. van Noort. 2008. Subpiconewton dynamic force spectroscopy using magnetic tweezers. *Biophysical journal*. 94:2343–8.

[32] Klaue, D., and R. Seidel. 2009. Torsional Stiffness of Single Superparamagnetic Microspheres in an External Magnetic Field. *Physical Review Letters*. 102:028302.

[33] De Vlaminck, I., T. Henighan, M. T. J. van Loenhout, D. R. Burnham, and C. Dekker. 2012. Magnetic forces and DNA mechanics in multiplexed magnetic tweezers. *PloS one*. 7:e41432.

[34] Bustamante, C., S. B. Smith, J. Liphardt, and D. Smith. 2000. Single-molecule studies of DNA mechanics. *Current opinion in structural biology*. 10:279–85.

[35] Gross, P., N. Laurens, L. B. Oddershede, U. Bockelmann, E. J. G. Peterman, and G. J. L. Wuite. 2011. Quantifying how DNA stretches, melts and changes twist under tension. *Nature Physics*. 7:731–736.

[36] Marko, J. F., and E. D. Siggia. 1995. Stretching DNA. *Macromolecules*. 28:8759–8770.

[37] Chien, F.-T., and J. van Noort. 2009. 10 Years of Tension on Chromatin: Results From Single Molecule Force Spectroscopy. *Current pharmaceutical biotechnology*. 10:474–85.

[38] Brower-Toland, B. D., C. L. Smith, R. C. Yeh, J. T. Lis, C. L. Peterson, and M. D. Wang. 2002. Mechanical disruption of individual nucleosomes reveals a reversible multistage release of DNA. *Proceedings of the National Academy of Sciences of the United States of America*. 99:1960–5.

[39] Kulić, I., and H. Schiessel. 2004. DNA Spools under Tension. *Physical Review Letters*. 92:228101.

[40] Sheinin, M. Y., M. Li, M. Soltani, K. Luger, and M. D. Wang. 2013. Torque modulates nucleosome stability and facilitates H2A/H2B dimer loss. *Nature communications*. 4:2579.

[41] Tinoco, I., and C. Bustamante. 2002. The effect of force on thermodynamics and kinetics of single molecule reactions. *Biophysical chemistry*. 101-102:513–33.

Chapter 2

Coexistence of Twisted, Plectonemic, and Melted DNA in Small Topological Domains[1]

DNA responds to small changes in force and torque by over- or under-twisting, forming plectonemes, and/or melting bubbles. Though transitions between either twisted and plectonemic conformations or twisted and melted conformations have been described as first order phase transitions, we report here a broadening of these transitions when the size of a topological domain spans several kilobase pairs. Magnetic tweezers measurements indicate the coexistence of three conformations at sub-pN force and linking number densities around -0.06. We present a statistical physics model for DNA domains of several kilobase pairs by calculating the full partition function that describes this 3-state coexistence. Real-time analysis of short DNA tethers at constant force and torque shows discrete levels of extension, representing discontinuous changes in the size of the melting bubble, which should reflect the underlying DNA sequence. Our results provide a comprehensive picture of the structure of under-wound DNA at low force and torque and could have important consequences for various biological processes, in particular those that depend on local DNA melting, such as the initiation of replication and transcription.

---

[1]The contents of this chapter are based on : H. Meng, J. Bosman, T. van der Heijden and J. van Noort, "Coexistence of Twisted, Plectonemic, and Melted DNA in Small Topological Domains." *Biophysical Journal*. 106:1174-1181 (2014).

2.1 Introduction

In vivo, DNA is maintained in a negatively supercoiled state in small topological domains of several kilobase pairs (kbps) [1, 2]. This supercoiling forms the driving force for DNA compaction into chromosomes and has been implicated in regulating all processes involving DNA [3]. Access to DNA by polymerases, for example, requires melting of a small amount of DNA and may be a rate limiting step in the initiation of transcription and replication [4]. The processive motion of these polymerases in topologically fixed domains can lead to accumulation of force and torque which has been suggested to play an important role in DNA homeostasis [5–8]. It is therefore important to understand how force and torque affect the conformation of DNA.

Using force spectroscopy techniques such as magnetic and optical tweezers, it is possible to control both the force and the torque on single DNA molecules [9–11]. Seminal work by Strick and coworkers showed that under- and over-twisting of DNA leads to plectonemic structures, i.e. supercoils, at stretching forces below $0.5\,pN$ [12]. Above $1.0\,pN$ and negative torque, small dAdT rich regions of double-stranded(ds)DNA melt and form single-stranded (ss)DNA bubbles [13, 14]. At higher force ($F > 2.5\,pN$) and larger negative torque ($\Gamma < -11\,pN\,nm$), a left-handed structure L-DNA [15] forms. Large positive torque and force, on the other hand, induce a highly over-twisted state called P-DNA [16]. Thus, a rich variation of conformations accommodates physical stress and torque in DNA.

Statistical mechanics has been successfully employed to describe these remarkable features of DNA [17, 18]. In these reports, the DNA tether is assumed to be long enough to neglect thermal fluctuations between different conformations. For a DNA tether with a finite number of base pairs (i.e. several kbps) held at low forces ($F < 1.2\,pN$) and moderate linking number densities ($|\sigma| < 0.06$), representing physiologically relevant conditions [19], coexistence of three states has been suggested [20]. However, detailed analysis of the extension of short DNA molecules in this low force and torque range is lacking.

In the current article, we provide an extended experimental data set and introduce a numerical 3-state model that shows the coexistence of three states in the same topological domain. We performed magnetic tweezers experiments on DNA molecules of several kbps and measured twist-extension curves in real time. This resolved simultaneously the rather large fluctuations in extension due to the presence of different states,

and revealed a discontinuous change in the size of the melting bubbles that we attribute to differences in DNA sequence. Though we do not explicitly take the DNA sequence into account in our statistical physics model, there are indications that suggest that the phase-diagram can be affected by it. Together, these findings provide a quantitative understanding of DNA melting in small topological domains at forces and degrees of supercoiling that are representative for the conditions that occur in the living cell.

2.2 Materials and methods

2.2.1 Magnetic tweezers

The home-built magnetic tweezers has been described by Kruithof et al [21]. During an experiment, a DNA molecule was constrained between the end of a superparamagnetic bead with diameter of $1 \, \mu m$ and the surface of a microscope coverslip. Twist was induced by rotating the magnetic field at 1 turn/s. The extension of DNA was measured in real time at a frame rate of 60 Hz with a CCD camera (Pulnix TM-6710CL).

2.2.2 DNA constructs

Two DNA constructs were studied based on Plasmid pGem-3Z (3kb) and Puc18 with 25 repeats of the 601 sequence (8.5kb) (A gift from D. Rhodes, Singapore). Both plasmids were digested with BsaI and BseYI yielding linear fragments of 2410 and 6960 bp respectively with corresponding sticky ends on either side. Digoxigenin and biotin-labeled handles were produced with PCR using biotin-dUTP and digoxigen-dUTP on the pGem-3Z template using the following primers: 5' GAT AAA TCT GGA GCC GGT GA 3' and 5' CTC CAA GCT GGG CTG TGT 3'. After PCR amplification, these fragments were digested with BsaI and BseYI and ligated to the previously digested DNA backbone.

2.2.3 Sample preparation

A clean cover slip was coated with 1% polystyrene-tuolene solution. The coverslip was then mounted on a poly-di-methysiloxane (PDMS, Dow Corning) flow cell containing a $10 \times 40 \times 0.4 \, mm$ flow channel. The flow cell was incubated with 1 µg/ml anti-digoxigenin for 2 hours and 2% BSA (w/v) solution overnight. 20 ng/ml DNA in

10 $mM\, Hepes\, pH\, 7.6$, 100 $mM\, KAc$ and 10 $mM\, NaN_3$ was flushed into the flow cell and incubated for 10 minutes, followed by flushing in 1 μm diameter streptavidin-coated superparamagnetic microspheres (MyOne, Invitrogen) in the same buffer after 10 minutes.

2.3   Results

We consider a DNA molecule consisting of N base pairs. When DNA is torsionally unconstrained, the linking number Lk_o equals 1 helical turn per 10.4 bp [22]. In the case of a torsionally constrained molecule, torque builds up as one end of the molecule is twisted ΔLk turns. This change in twist can be expressed in the linking number density, $\sigma \equiv \Delta Lk/Lk_o$. Here, we will examine the situation where three states, i.e. twisted (t), plectonemic (p), and melted (m) DNA occur simultaneously in the same molecule (Fig. 2.1). In this model, the base pairs in the molecule are divided amongst these three states:

$$N = n_t + n_p + n_m,\qquad\qquad(2.1)$$

where n_i ($i = t, p, m$) is the number of base pairs in each state. The excess linking number is conserved and distributed amongst these three states:

$$\Delta Lk = \Delta Lk_t + \Delta Lk_p + \Delta Lk_m.\qquad\qquad(2.2)$$

The linking number density in the entire domain can thus be written as:

$$\sigma_{tot} = \frac{n_t}{N}\sigma_t + \frac{n_p}{N}\sigma_p + \frac{n_m}{N}\sigma_m,\qquad\qquad(2.3)$$

in which σ_i ($i = t, p, m$) is defined as the linking number density in each state ($\sigma_i = \frac{\Delta Lk_i}{n_i/10.4}$). The total free energy G equals the sum of the free energy in each state following:

$$G = n_t G_t + n_p G_p + n_m G_m,\qquad\qquad(2.4)$$

in which G_i represents the free energy per base pair in state i. In general, G_i can depend

on both the force and linking number density [15, 17]:

$$G_i(F, \sigma_i) = -g_i(F) + \frac{c_i(F)}{2}(\sigma_i - \sigma_{o,i})^2 + \varepsilon_i, \tag{2.5}$$

where $g_i(F)$ is the stretching free energy and $c_i(F)$ is the force dependent twist modulus. For the twisted and melted state, the stretching free energy is described by a wormlike chain [17], whereas stretching of plectonemic DNA is force independent because it has zero extension. $\sigma_{o,i}$ is the degree of twist in each state in absence of torque. ε_i is the melting energy for base pair separation, which is zero for twisted and plectonemic DNA. Though the melting energy is sequence dependent, we will assume an average value of $1.6\,k_B T$ [23] per base pair. All parameters in Equation 2.5 are summarized in Table S1.

Previous work by Marko [17] reported an analytical solution for the distribution of states based on equating the torque in each state. In analogy with other phase transitions, only a single point in the phase diagram was reported to represent a 3 phase coexistence. However, thermal fluctuations are not negligible in finite systems, such as a single topological domain of several kbps, allowing for a population of additional states that would remain unobserved in the thermodynamic limit. An analytical solution for such a three-state system has not been reported. Because of the finite number of states we can numerically calculate the full partition function, using Equations 2.1, 2.3 and 2.4. The probability to be in a conformation defined by n_t, n_p, σ_t and σ_p equals:

$$P(F, \sigma_{tot}) = Z^{-1} exp\left(\frac{-G(F, \sigma_{tot}, \sigma_t, \sigma_p, n_t, n_p)}{k_B T}\right), \tag{2.6}$$

with the partition function:

$$Z = \sum_{\sigma_p = -\infty}^{\infty} \sum_{\sigma_t = -\infty}^{\infty} \sum_{n_p = N - n_s}^{N} \sum_{n_s = 0}^{N} exp\left(\frac{-G(F, \sigma_{tot}, \sigma_t, \sigma_p, n_t, n_p)}{k_B T}\right). \tag{2.7}$$

Using Equation 2.4 the extension z of a DNA molecule with contour length L in a state comprising n_t stretched base pairs and n_m melted base pairs can be written as :

$$\frac{z(F, \sigma_{tot})}{L} = \frac{1}{N}\left(-\frac{\partial G}{\partial F}\right) = \frac{n_t}{N}\left(-\frac{\partial G_t}{\partial F}\right) + \frac{n_m}{N}\left(-\frac{\partial G_m}{\partial F}\right). \tag{2.8}$$

Combining Equations 2.6 and 2.8 yields for the expected extension:

$$< \frac{z(F,\sigma_{tot})}{L} > = Z^{-1} \sum_{\sigma_p=-\infty}^{\infty} \sum_{\sigma_t=-\infty}^{\infty} \sum_{n_p=N-n_s}^{N} \sum_{n_s=0}^{N} \frac{z(F,\sigma_{tot})}{L} exp\left(\frac{-G(F,\sigma_{tot},\sigma_t,\sigma_p,n_t,n_p)}{k_B T}\right). \quad (2.9)$$

The mean value and variance of all other parameters that describe the conformation of the molecule are calculated likewise.
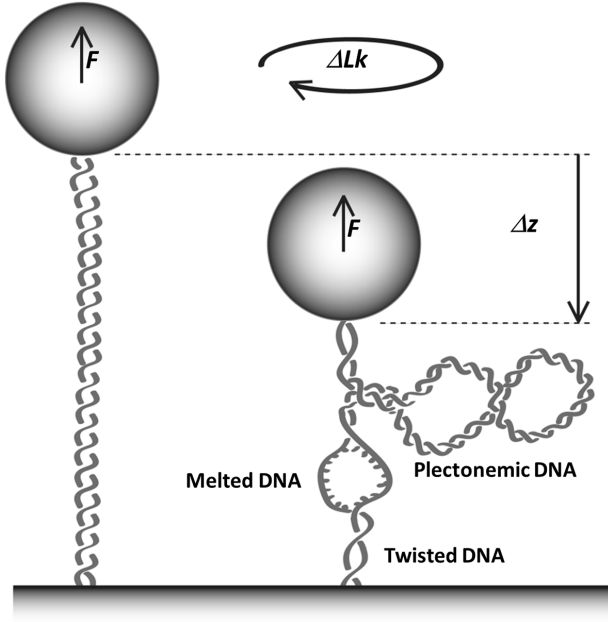
Figure 2.1: Schematic illustration of the conformational changes of a DNA molecule in a magnetic tweezers set up (not to scale). A DNA molecule is tethered between a superparamagnetic bead and a glass surface. Force and torque on the DNA molecule is applied by an external pair of magnets (not shown) to the bead. Here, we consider the coexistence of three states: twisted, plectonemic, and melted DNA.

2.3.1   3-state coexistence

We used magnetic tweezers to control the force and twist exerted on a single DNA molecule (Fig. 2.1). Briefly, the experimental setup consists of a DNA molecule that is anchored between a glass surface and a superparamagnetic bead. The position and the rotation of a pair of external magnets determines the force and twist applied to the
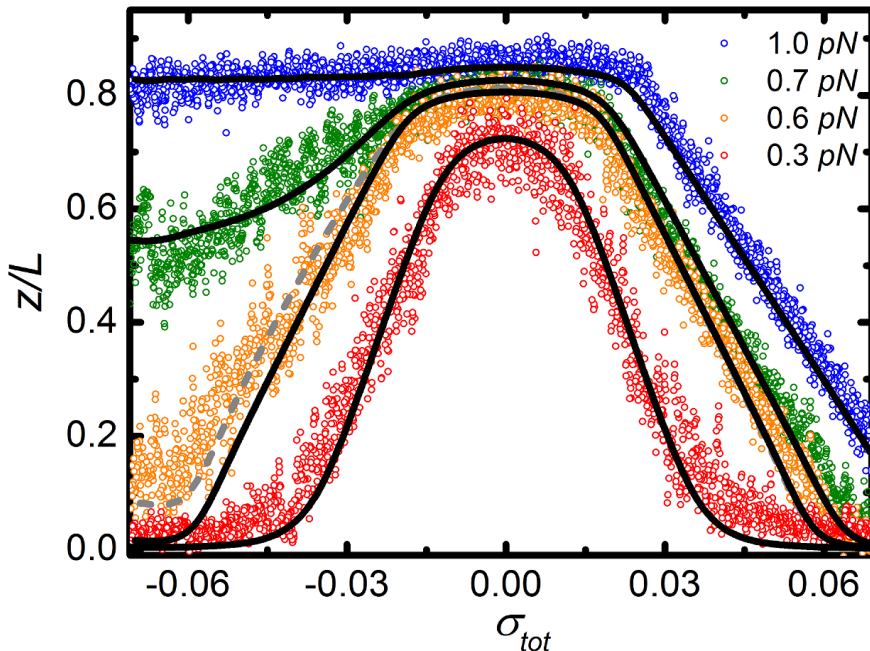
Figure 2.2: Experimental data of the relative extension of a $7.0\ kbps$ DNA molecule as a function of the total linking number density at various forces (circles). The relative extension as calculated by Equation 2.9 is shown by lines. Calculations are based on the parameters summarized in Table S1. Black solid lines represent a constant melting energy of $1.6\ k_B T/bp$. For the gray dashed line a force dependent melting energy was used, see Fig. S3 *B*, resulting in a better match with the experimental data at $0.6\ pN$.

bead. The height of the bead, corresponding to the extension of the DNA molecule, is measured in real time using video microscopy and image processing [21]. Unlike previous reports [14, 24, 25], we do not average the extension over a given time interval, so changes in extension are directly revealed. The bandwidth to detect these changes is limited by the viscous drag of the bead, the stiffness of the DNA tether, and the frame rate of the camera (see Supporting Material and Fig. S7). Typically, for the conditions of the measurements reported here, fluctuations in extension can be detected at 20-60 Hz. Because each state has a different extension (see Equation 2.8), the distribution of states can only be determined indirectly from the total extension of the molecule.

We carried out twisting experiments on $7.0\ kbps$ and $2.4\ kbps$ DNA molecules at

forces up to 1.0 pN and linking number densities up to $|\sigma_{tot}| < 0.07$ (Figs. 2.2 and S1 A for 7.0 and 2.4 $kbps$ respectively). Over- and under-twisting the DNA molecule at 0.3 pN resulted in a symmetric decrease in end-to-end distance (Fig. 2.2, red circles). At this force, DNA buckles at both negative and positive torque. The resulting supercoils reduce the end-to-end distance of the DNA molecule. Increasing the force to 1.0 pN results in an asymmetric extension-twist curve (Fig. 2.2, blue circles). The extension remains constant for under-twisting due to DNA melting [13, 16, 17, 26]. Over-twisting the DNA creates plectonemes at all forces. The extension at these two conditions can be fully captured by considering the equilibrium between two states: a twisted-melted state or a twisted-plectonemic state [17].

The twist-extension curves at 0.6 pN and 0.7 pN fall in between these two regimes (Fig. 2.2, orange and green circles). We therefore consider the coexistence of twisted, plectonemic, and melted DNA to describe these data. The black lines superimposed on the experimental data in Fig. 2.2 are the calculations using Equation 2.8. The used parameters for the mechanical properties of DNA are summarized in Table S1, using the same values as reported before [17] except for the twist modulus of melted DNA. We could only obtain a good agreement between experimental and simulated data using a twist modulus of melted DNA of 28 nm instead of 1 nm [27]. Thus it appears that small bubbles of melted DNA are more difficult to twist than previously reported.

Note that the model appears to underestimate extension of the DNA at very small extensions. This is caused by excluded volume forces that originate from the impossibility for the DNA and the bead to penetrate the glass surface [21]. We did not correct for this, leading to an underestimation of the effective force for short flexible tethers. Barring these deviations at very small extensions, we conclude that under conditions that resemble physiological salt concentrations, the 3-state model quantitatively captures experimental twist-extension curves of small topological domains at moderate forces and linking number densities.

2.3.2   Phase diagram

To summarize the distribution of base pairs in the 3-state model, we computed a phase diagram of the 7.0 $kbps$ DNA as a function of the linking number density and force (Fig. 2.3). The fractions of base pairs in each state are color coded, resulting in separate regions of twisted (blue) and plectonemic (green) DNA. Several regions show a mixed
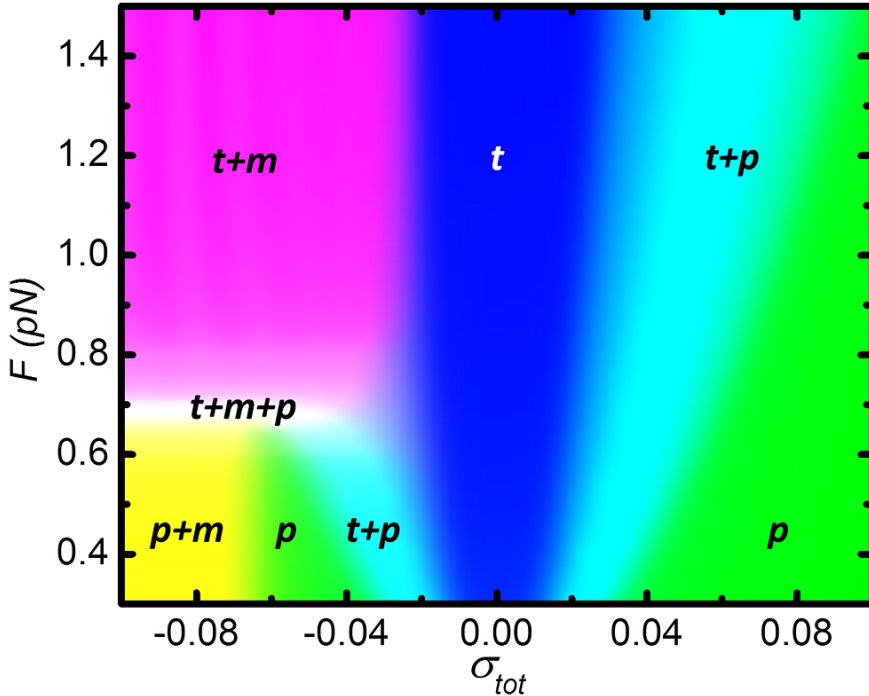
Figure 2.3: The force-linking number density phase diagram of a 7.0 $kbps$ DNA molecule. Gradual transitions occur between twisted (t), plectonememic (p), and melted (m) DNA. The fraction of base pairs in t, p, and m were used for the blue, green, and red hues. The fraction of melted bps was multiplied by 10 in all regions to optimize the contrast. The white region represents the 3-state coexistence phase.

distribution of two states: twisted and plectonemic DNA (cyan), twisted and melted DNA (pink), and plectonemic and melted DNA (yellow). These features, representing two-state conformations, follow previously reported phase diagrams [9, 15, 17].

The phase diagram also shows a phase, rather than a single triple point [28], where the three states coexist (white). This phase is a direct consequence of the small size of the topological domain, which invalidates the thermodynamic limit assumption and exposes states that are usually obscured in large systems. The phase diagram for 2.4 $kbps$ and 24.0 $kbps$ DNA (Fig. S2) reproduces the same trend, but the 3-state coexistence regime shrinks when the tether length increases. For 24.0 $kbps$ DNA we observe only a narrow line at $F = 0.69\ pN$. Because of the large difference in linking number be-

tween melted DNA and dsDNA, a small melting bubble is more efficient in relieving torsional stress than twisted or pelectonemic DNA. In larger tethers such a small bubble represents a smaller fraction of the total DNA size, reducing the size of the coexistence phase.

To better understand the 3-state coexistence, we looked into more details that can be calculated with the statistical mechanics model. Fig. 2.4 *A* shows the number of base pairs in the three states for 7.0 *kbps* DNA at $F = 0.7\ pN$. The majority of the DNA is in the twisted state for $|\sigma_{tot}| < 0.04$. For $|\sigma_{tot}| > 0.01$ plectonemic DNA starts to form, whereas at $\sigma_{tot} < -0.02$ melted DNA is formed. A small fraction of the DNA contributes to this melting bubble, though it grows to 250 *bps* for $\sigma_{tot} = -0.07$.

Though only a small fraction of the DNA molecule melts, these base pairs contribute to a large part of the total twist that is present in the DNA tether. Fig. 2.4 *B* shows the distribution of excess linking number among the three states. At small linking number densities all the twist is absorbed in twisted DNA. When σ_{tot} in the DNA molecule exceeds 0.02, the molecule buckles, and the additional twist is stored in plectonemes. For negative torque, however, at $\sigma_{tot} < -0.04$ most of the twist is stored in melted DNA. The large difference in helicity and free energy between dsDNA and melted DNA makes melted DNA a good buffer for torsional stress.

We extended our analysis to the quantification of torque within a 7.0 *kbps* DNA molecule for different forces and linking number densities (Supporting Material, Figs. 2.4 *C* and S4). Fig. 2.4 *C* shows that the torque increases linearly with twist when DNA exists in a single state. For example, the plectonemic state dominates at $F = 0.1 pN$ and $\sigma_{tot} > -0.05$ (with a small interruption at $\sigma_{tot} = 0$). Under these conditions the slope represents the twist stiffness of plectonemic DNA. At larger forces and small twist densities, DNA is predominantly twisted, yielding a larger slope because of the larger twist persistence length of twisted DNA. When multiple states coexist, an increase of torsional stress is accommodated by a redistribution of the states rather than increasing the twist in either of the states. Thus for mixed conformations the torque stays constant but the distribution of bps between states is shifted (Fig. 2.4 *A*). Remarkably, the negative torque reaches a minimum value of $-11\ pN\ nm$ for all forces probed. This torque corresponds to a free energy of 2.6 $k_B T$, which is just sufficient to melt and twist an additional basepair. Thus the maximum torque for negatively twisted DNA is limited. As a consequence, the linking number density in the plectonemic state, which comprises
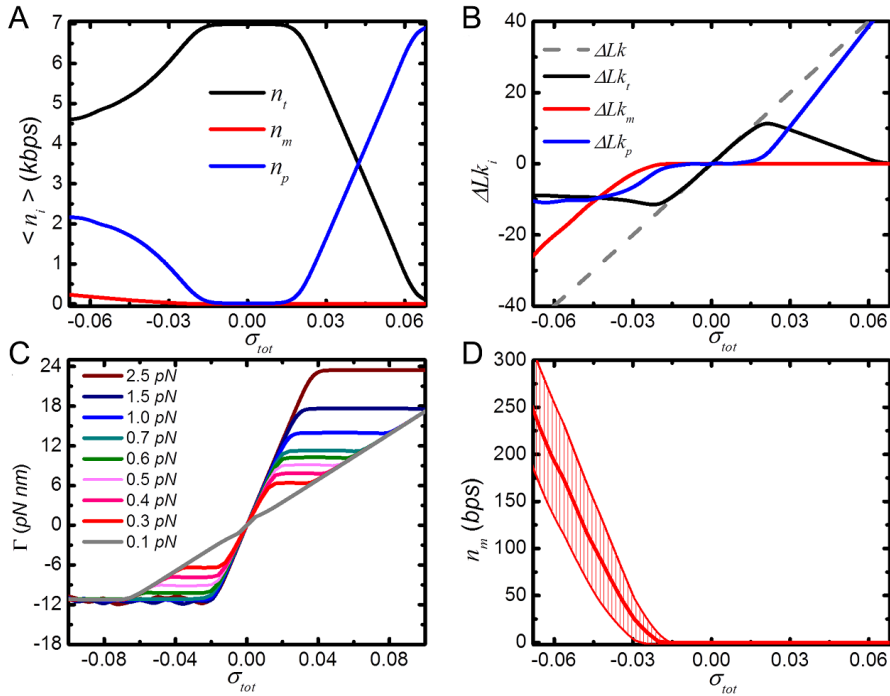
Figure 2.4: Calculations of the 3-state coexistence in a 7.0 *kbps* DNA molecule at 0.7 *pN* and different linking number densities. (*A*) The distribution of base pairs in each state. (*B*) The distribution of linking numbers in each state. The sum of linking numbers converges to the total linking number ΔLk, shown in gray. (*C*) The torque present in the DNA molecule calculated between 0.1 *pN* to 2.5 *pN*. (*D*) The distribution of melted base pairs. Error bars represent the standard deviation.

most of the DNA, is constrained, i.e. $< \sigma_p > = -0.065$, in excellent agreement with the natural linking number density observed in vivo [19, 29].

The model presented here differs from previous work in two aspects [17]. First, we consider all distributions of states, rather than only the lowest energy state. In small tethers there are a large number of states with a comparable free energy contributing to the average extension of the molecule. Fig. 2.4 *D* shows the expected value and standard deviation of n_m as a function of the applied linking number density calculated. It is clear from these calculations that the bubble size is not well defined, with variations ranging up to 50 *bps*, emphasizing the extent of the statistical fluctuations in a small DNA tether. Second, the torque is not fixed within the molecule, as shown in Fig. S4, the mean values of the torque in each phase follow the mean torque of the entire molecule, but significant variations in torque occur when phases coexist. Imposing a constant torque throughout the entire molecule still results in the coexistence of 3 states (Fig. S5). Fluctuations in torque between the different parts of the molecule therefore only contribute a small part of the states that define the average extension.

2.3.3 Fluctuations in extension

The relatively broad distribution of base pairs in each of the three states results in increased fluctuations in the extension of the molecule, due to the large differences in extension between the three states. Indeed, closer inspection of the extension-twist curves as shown in Fig. 2.2 reveals increased fluctuations in the extension in the 3-state coexistence region. In these experiments, the data were not time-averaged, revealing independent extension measurements while twisting the DNA molecule. The magnitude of these fluctuations can be calculated using Equations 2.6 and 2.8. Fig. 2.5 *A* shows twist-extension measurements of a 2.4 *kbps* and a 7.0 *kbps* DNA molecule along with the calculated median and variation in extension at $F = 0.7 \, pN$. The latter was calculated as the range that includes 68% of the extension distribution. Due to the variations among the three states, the extension is not Gaussian distributed for under-twisting as opposed to over-twisting (Figs. 2.5 *B* and S6 *B*), but displays an asymmetric distribution. The fluctuations caused by transitions between different states dominate over thermal fluctuations in extension that are always present in flexible polymers, as discussed in Supporting Material. Overall, we obtain a fair agreement between the calculated magnitude of the fluctuations in extension and experimental data. This shows that

the increased fluctuations in extension at under-twisting conditions can be attributed to transitions between different conformation of the molecule.

Fluctuations in extension at constant force and linking number measured in real time (Fig. 2.6) uniquely reveal the kinetics of the transitions between different states in the molecule. Such kinetics cannot be obtained from the statistical mechanics model presented here, which only describes the equilibrium situation. Remarkably, we observed distinct transitions between discrete levels (~110 *nm*) of extension of the molecule in the 3-coexistence state regime. Since the twisted and melted DNA have a comparable extension in this force regime, the discrete extension levels can only be explained by changes in the size of the plectoneme. Our model suggests the extension levels correspond to changes of about 400 *bps* of plectonemic DNA transferring back and forth into 380*bps* twisted and 20*bps* melted DNA. The transitions occur at intervals of several seconds. We attribute the discrete levels in extension to barriers originating from differences in the sequence of the DNA. Small stretches of GC base pairs, having one more hydrogen bond than AT base pairs, present a kinetic barrier for extension of the melting bubble. Such inhomogeneities will severely change the distribution and kinetics of the molecule's extension. For bubbles spanning several tens of bps, this results in a limited number of favored states, depending on the local DNA sequence.

We noted that the shape of the twist-extension curves is salt-dependent (Fig. S1). Increasing the ionic strength from 100 mM to 300 mM KAc shifts the twist-extension curves to smaller extensions for under-twisting. This is consistent with the well-known increase of the melting energy for DNA at higher salt concentrations [23], as also observed for force-induced melting without twist [30]. Increasing the melting energy from 1.6 $k_B T$ to 2.0 $k_B T$ per base pair recovered a good agreement between experimental and calculated data.

Though in principle it should be straightforward to extend the current 3-state model with a sequence dependent melting energy, such calculations will require large computational effects, even for small molecules. It is important to note that this sequence heterogeneity can have a significant effect on the phase diagram. We expect that small melting bubbles will preferably be formed in AT rich regions, but as the force increases such AT-rich regions will expand into GC-rich parts at their boundaries. We modeled this increased contribution of GC base pairs by increasing the melting energy in a linear fashion from 1.5 to 2.1 $k_B T$ for forces between 0.6 and 1.2 *pN*. For *F* = 0.6 *pN*, the
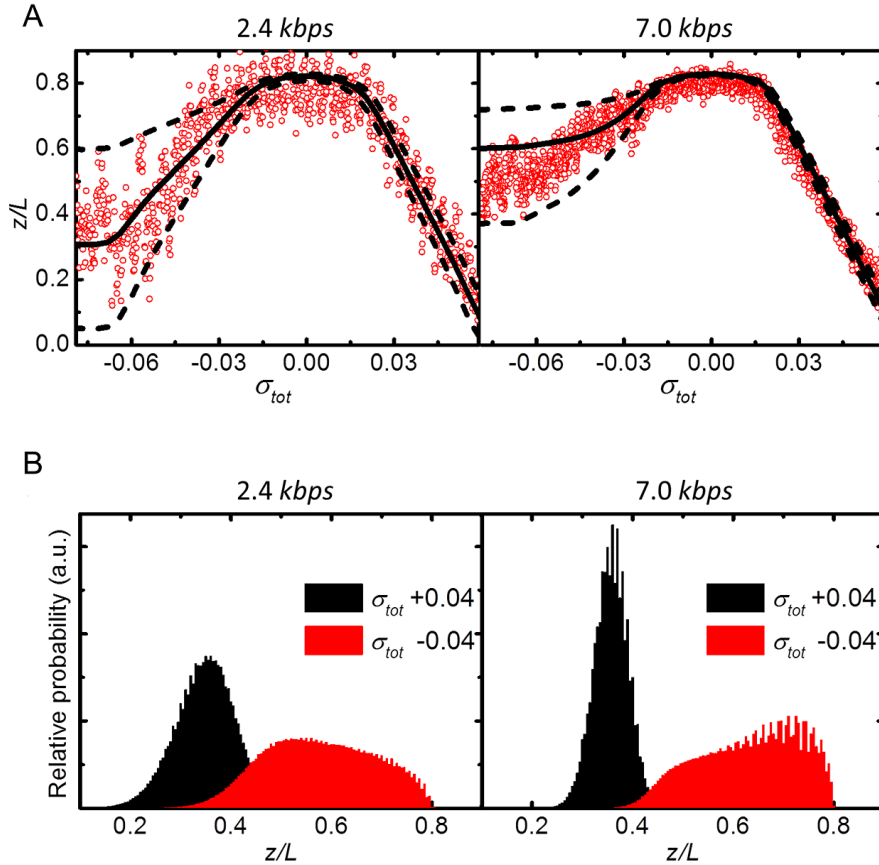
Figure 2.5: (*A*) Experimental data of the relative extension versus linking number density (red circles) at $0.7 \, pN$ for $2.4 \, kbps$ (left) and $7.0 \, kbps$ DNA (right). The calculated median extension value is shown as a solid black line. Dashed lines represent 68% range in extension. (*B*) Calculated extension distribution distribution for $2.4 \, kbps$ (left) and $7.0 \, kbps$ DNA (right) at $\sigma_{tot} = -0.04$ (red) and $\sigma_{tot} = +0.04$ (black). Note the broad and asymmetric extension distribution compared to the Gaussian profile for negative and positive twist respectively.
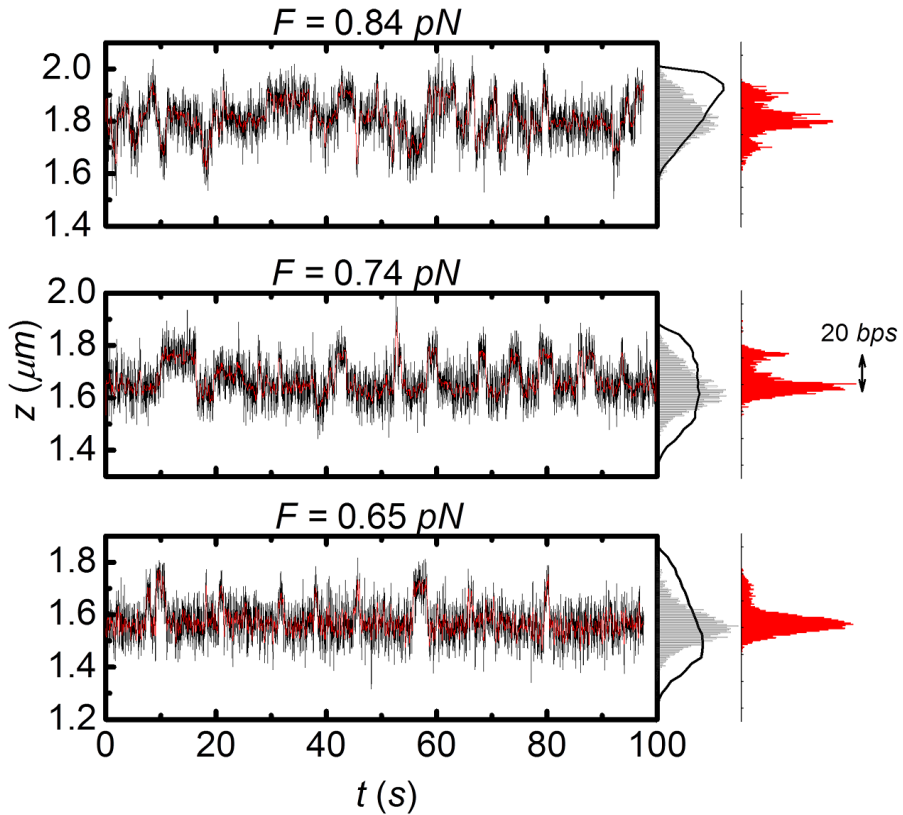
Figure 2.6: Constant force measurements at a linking number density σ_{tot} = −0.03. Three different forces are shown, from top to bottom: 0.84 *pN*, 0.74 *pN*, and 0.65 *pN*. The data in red shows the 20 points median filtered data, emphasizing the discrete transitions in extension. Histograms of the extension are shown on the right side of the time traces (black and red bars). The calculated extension distribution is superimposed on the histogram (solid black lines). The discrete levels are attributed to approximately 400*bps* of plectonemic DNA transferring back and forth into 380*bps* twisted and 20*bps* melted DNA.

adjusted twist extension curves show a small increase in extension at negative twist (Fig. 2.2, gray dashed line), yielding a better agreement with the experimental data (Fig. S1 A, dashed lines 2.4 $kbps$ DNA). The resulting phase diagram is globally similar to that presented in Fig. 2.3, but displays a larger area in which the three states coexist (Fig. S3). Thus, though the sequence dependence of melting bubbles is not included explicitly in our model, the data give clear indications that there is a significant effect of sequence heterogeneity, resulting in both discrete, 20 bp steps in the size of the melting bubble and in a larger area in which the three states coexist.

2.4   Discussion and conclusions

We described the coexistence of twisted, plectonemic, and melted DNA in small topological domains. Using a numerical 3-state model, we computed a force-twist phase diagram that reproduces earlier descriptions of supercoiled DNA. However, we observe gradual transitions and a region of three-state coexistence rather than a sharp first-order phase transition and a single triple point. DNA melting induced by large forces is well studied in recent works [31–34], including the effect of torque [9, 15]. Here we studied these effects at low forces and moderate linking number densities. This situation is particularly relevant in vivo, where topological domains are likely to be several kbps, forces are not likely to exceed several pNs, and linking number densities are generally close to -0.06. Moreover, we computed that melting bubbles of several tens of bps appear in such a domain. The continuous presence and the large dynamics of such bubbles may have important consequences for processes involving ssDNA.

Sheinin et al. [15] showed that long stretches of melted DNA are organized in a L-DNA structure with < σ_m >= −1.8, corresponding with a helical repeat of ~ 13 $bp/turn$, and a twist modulus of 20 nm. They also observed that the torque in under-twisted DNA is limited to −11 $pN\,nm$ under extreme twist densities of σ_{tot} down to -2.0 and $F > 5\,pN$. We show here that also under less extreme conditions this torque limit applies. Strick et al. reported that melted DNA remains in a disordered conformation resembling two strands of ssDNA with < σ_m >= −1 [13, 14]. The twist modulus of a DNA bubble was considered very small, about 1 nm. We obtained the best agreement between experimental and simulated data for < σ_m >= −1.05 and a twist modulus of 28nm. This may indicate that small melting bubbles are more difficult to twist than long ssDNA molecules and may point to alternative interactions between the melted bases

that are not present in larger stretches of melted DNA. Further studies are required to reveal possible structure in small melting bubbles.

It is clear that the finite size of the melting bubble and the large impact of sequence inhomogeneities have a significant effect on the twist-extension curves of DNA. From our studies we cannot resolve the position of the bubble. A melting bubble could for example be positioned at the tip of the plectoneme, rather than in the twisted section of the DNA. Such a melting bubble in the plectonemic region would not lead to an increase of the extension, relative to plectonemic DNA, but would reduce the torsional stress. DNA sequence may also result in highly curved DNA stretches that could localize the plectoneme at specific locations. The good agreement of the experimental data with a simple 3-state statistical physics model that does not include sequence effects suggests that such dependencies only play a minor role.

One of the most remarkable findings is that distinct steps in extension of the DNA molecule are clearly visible under small force and negative torque. Such steps can easily be confused with protein-induced changes in extension when studying protein-DNA interactions. Because long DNA substrates, such as lambda-DNA with a contour length of 48 *kbps*, are generally replaced by shorter DNA molecules in more recent studies, the presence of bubble-plectoneme transitions may be relevant for many force-spectroscopy studies.

The lifetime of the distinct levels of DNA extension (Fig. 2.6) that we attribute to DNA melting are much longer than the lifetime of melting bubbles obtained from Fluorescence Correlation Spectroscopy (FCS) measurements, i.e. ~ 50 μs [35]. This may be due to the force that is applied in the magnetic tweezers, which is absent in FCS. Moreover, the melting bubbles described here may be larger than those captured in the FCS experiments. We cannot exclude the presence of very short-lived states, because of the limited response time of the bead-tether mechanics.

The simulations are amendable for further refinements. In addition to introducing a sequence dependent melting energy, which may resolve the discrete levels of extension, one can include an entropic penalty for the formation of a melting bubble [26]. Similarly, a penalty may be included for the formation of a DNA buckle [36–38]. Without such penalties we do not discriminate between single or multiple domains within one DNA molecule. More advanced modeling of overtwisted DNA, which includes

electrostatic interactions between DNA segments, suggests that the formation of multiple plectonemes or melting bubbles in the same topological domain may have a significant effect on twist-extension curves [18]. However, experiments show that small molecules at moderate force and torque only feature single domains of bubbles and plectonemes [39, 40]. Though this indicates that the free energy for formation of a new domain exceeds that of the free energy increase per base pair, it may be relatively small compared to the total free energy of the entire domain. Therefore Equation 2.4 will be adequate for describing the different conformations of a small DNA tether.

In summary, our work resolved and quantitatively described the coexistence of three different states in DNA. This new insight may have implications for the interaction mechanism of proteins that interact with DNA in torsionally constraint domains, such as topoisomerases, transcription factors, histones and DNA based molecular motors such as DNA and RNA polymerases and chromatin remodellers.

2.5 Acknowledgements

2.6 Supporting material

2.6.1 Parameters used in the 3-state model

The free energy per base pair in each state follows a parabolic function in σ [15, 17]:

$$G_i(F, \sigma_i) = -g_i(F) + \frac{c_i(F)}{2}(\sigma_i - \sigma_{o,i})^2 + \varepsilon_i,$$

where i denotes the twisted (t), plectonemic (p), or melted (m) state. The values of the individual parameters are shown in Table S1:

	$g_i\,(F)$	$c_i\,(F)$	$\sigma_{0,i}$	$\varepsilon_i\,(k_BT/bp)$	$A_i\,(nm)$	$C_i\,(nm)$
t	$F - \sqrt{k_BTF/A_t}$	$\omega_0^2\,k_BTC_t[1 - \frac{C_t}{4A_t}(\frac{k_BT}{AF})]$	0	0	50	100
p	0	$\omega_0^2\,k_BTC_p$	0	0	0	24
m	$1.2(F - \sqrt{\frac{k_BTF}{A_m}})$	$\omega_0^2\,k_BTC_m$	-1	1.6	4	28

Table S1: The force and torque dependent descriptions for the free energy per base pair of the 3 state model

A_i and C_i are the persistence length and twist modulus. $\omega_o = 2\pi/3.6\,nm = 1.75\,nm^{-1}$, is the inverted pitch of the double helix. All parameters used are the same as [15, 17], except for the twist modulus of melted DNA.

2.6.2 Torque calculation

The torque was calculated separately for each state. The torque is defined as

$$\Gamma_i = \frac{1}{\omega_o}\frac{\partial G_i}{\partial \sigma_i} = k_B T \omega_o \cdot C_i(\sigma_i - \sigma_{o,i}). \tag{2.10}$$

The mean torque is calculated as:

$$< \Gamma > = \frac{\sum\limits_{i=t,\,p,\,m} n_i\Gamma_i}{N}. \tag{2.11}$$

2.6.3 Fluctuations in extension

In Fig. S6 A, we plot the calculated standard deviations (SD) in the extension of a $7.0 \ kbps$ DNA molecule from experimental and modeled data (colored and dashed lines, respectively) as a function of the force applied at different linking number densities. Transitions between states are not the only cause of fluctuations in the experimental twist-extension curves. Thermal fluctuations due to the low stiffness of the tether also contribute. Such thermal noise was not included in Fig. 2.5 A. The magnitude of these fluctuations can be calculated using the equipartition theorem:

$$SD_{thermal} = \sqrt{k_B T / k_z}, \tag{2.12}$$

where k_z equals $\frac{\partial F}{\partial z}$. In the case of a worm-like chain[41]:

$$k_z \quad = \quad \frac{k_B T}{AL} \left(1 + \frac{1}{2\left(1 - \frac{z}{L}\right)^3} \right). \tag{2.13}$$

In Fig. S6 A the SD in the extension caused by thermal fluctuations is shown as gray dashed lines. The SD by our 3-state model is obtained by

$$SD_{statistical} = \sqrt{< (\frac{z}{L})^2 > - < \frac{z}{L} >^2}. \tag{2.14}$$

The black dashed line in Fig. S6 A shows the SD at $\sigma_{tot} = -0.045$. For $F > 1.2 \ pN$, where only two states coexist, the experimental data largely follow the thermal fluctuations of the molecule. Between 0.6 and 1.0 pN, we observe increased fluctuations due to the coexistence of the three states. We observe the same trends in the experimental and calculated data, though the amplitude of the fluctuations in the experimental data sometimes exceeds the predicted amplitude.

Some reduction of the fluctuations in extension can be attributed to the slow response time of the bead or to the limited frame rate of the camera. The temporal resolution in the extension is calculated from the corner frequency f_c[42].

$$f_c = \frac{k_z}{12\pi^2 \eta R}. \tag{2.15}$$

The results calculated for a $7.0 \ kbps$ DNA molecule are shown in Fig. S7 (black line) using a viscosity $\eta = 1.0 \times 10^{-3} \ Pa \, s$, and a radius of the magnetic bead $R = 0.5 \mu m$. Imperfect alignment of the magnetic field with the optical axis of the microscope

results in small oscillations in extension when the external magnets of the tweezers are rotated[43]. This artifact can be omitted by following the extension of the tether at a fixed linking number.

2.6.4   Supporting figures
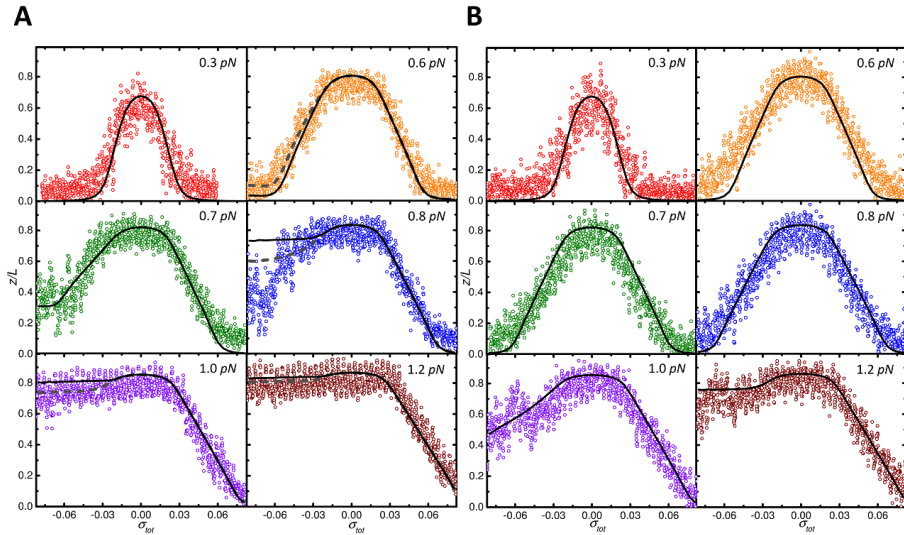
Figure S1

The relative extension as a function of the linking number density of a 2.4 $kbps$ DNA molecule in (A) 100 mM KAc at various forces (colored circles). The relative extension as calculated by the numerical model is shown as black solid lines. The dashed lines are the theoretical results for a melting energy that increases linearly with force between $\varepsilon_m = 1.5\,k_B T$ at 0.6 pN to $\varepsilon_m = 2.1\,k_B T$ at 1.2 pN. Such a force dependent melting energy results in a better overlap with the experimental data. (B) Same experiments at 300 mM KAc (colored circles). The relative extension as calculated by the numerical model is shown as black solid lines using a melting energy of 2.0 $k_B T/bp$.
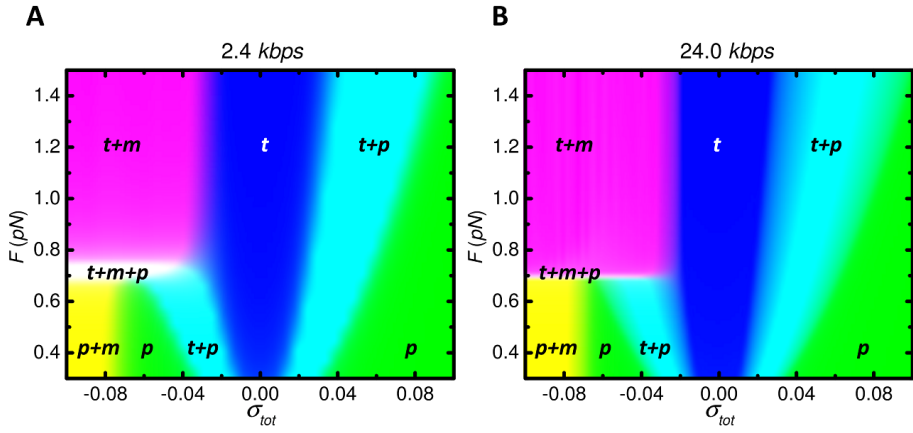
Figure S2

Force-linking number density phase diagrams. (A) A 2.4 $kbps$ DNA molecule shows transitions between extended twist-extended (t), plectonemic (p), and melted (m) DNA results, (B) A 24.0 $kbps$ DNA molecule shows the same trend as 2.4 $kbps$ DNA but a highly reduced 3-state coexistence region.
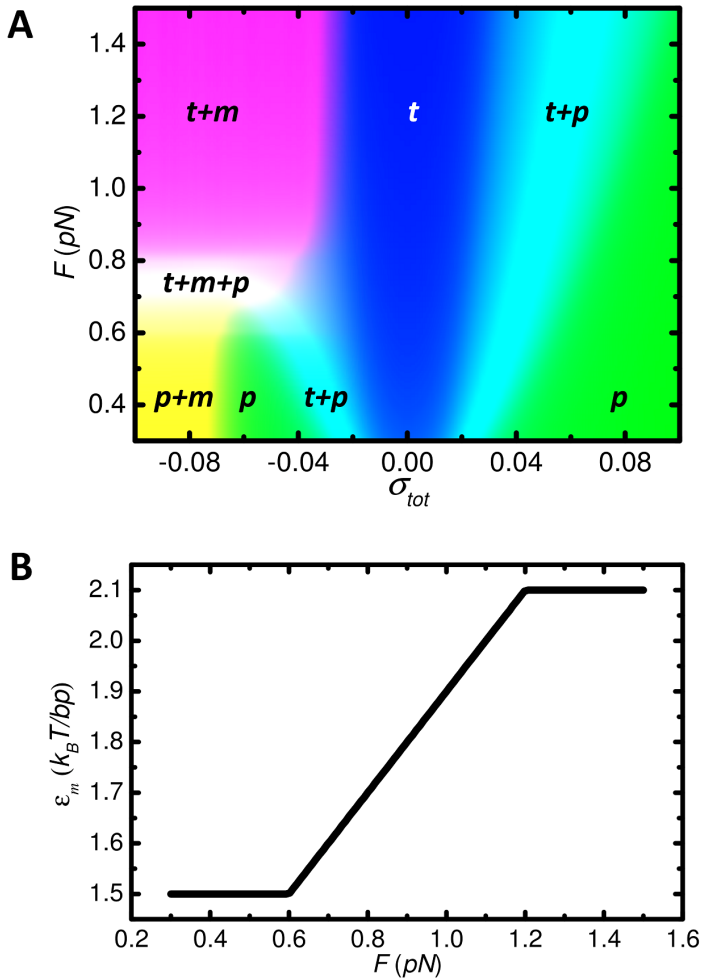
Figure S3

(A) The force linking number density phase diagram of a 7.0 $kbps$ DNA with a force dependent free melting energy. (B) The melting energy as a function of the applied stretching force as used for computing the density phase diagram in (A).
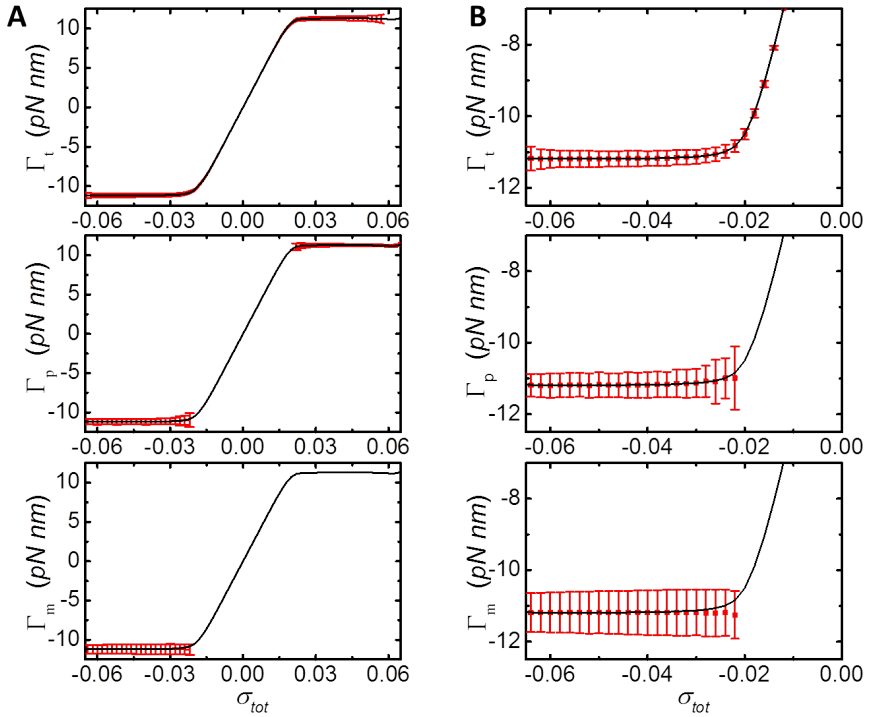
Figure S4

The torque distribution in each state of a 7.0 *kbps* DNA molecule at 0.7 *pN*. (A) The black line is the average torque in the molecule, whereas the red dots with their respective error bars represent the torque and its standard deviation in each of the occupied states. When the corresponding state is not occupied, the red dots are not shown. (B) Zoom in for a negative linking number density showing significant variations in the torque while the 3-state coexistence region is occupied.
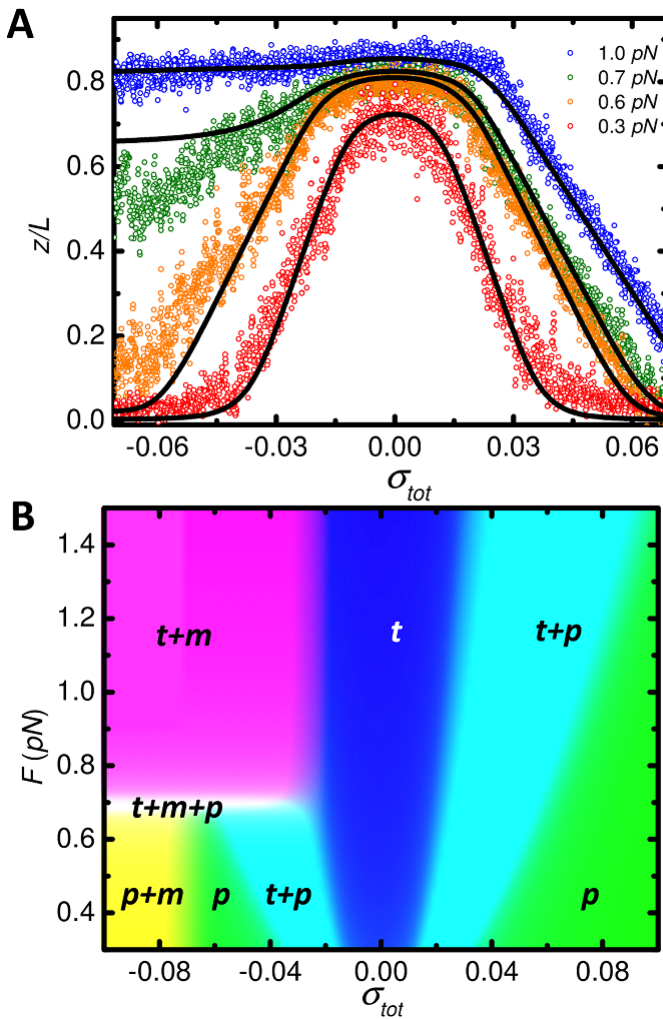
Figure S5

Torque-fixed calculation results of a $7.0\,kbps$ DNA molecule. (A) The relative extension as calculated by the numerical model with a constant torque throughout the molecule as black solid lines, compared with experimental data. (B) Force-linking number density phase diagram.

A

B
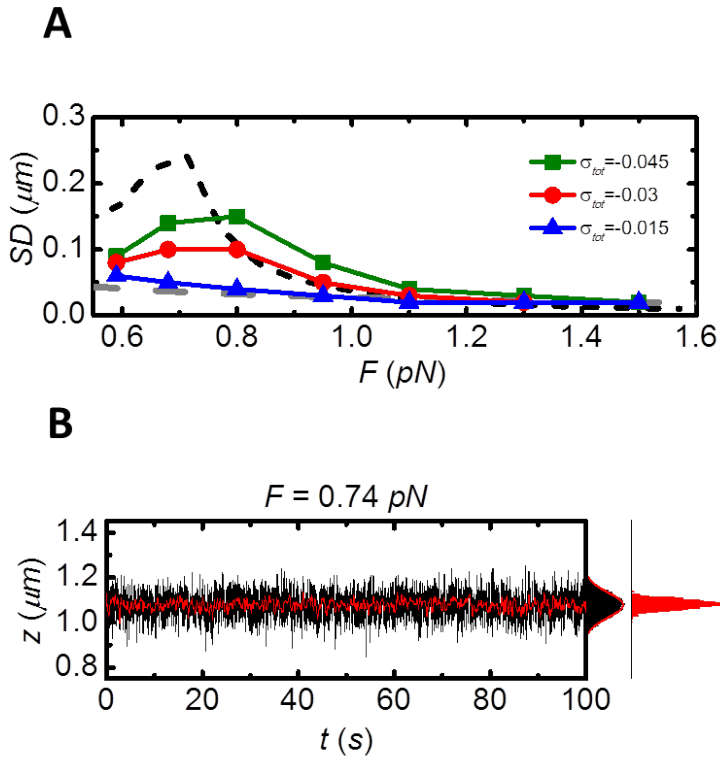
Figure S6

(A) Experimental data of the standard deviation of the extension of a $7.0\ kbps$ DNA molecule at different linking number densities with respect to the force applied. Data show increased fluctuations in extension at $0.7\ pN$. Fluctuations in the extension calculated based on thermal fluctuations only (gray dashed line) cannot capture this effect. SD calculated with the 3-state model (black dashed line) at $\sigma_{tot} = -0.045$ shows however a similar trend. (B) Constant force measurement of a $7.0\ kbps$ DNA molecule at $\sigma_{tot} = +0.03$. The red data is the 20 points median filtered data which do not reveal discrete steps as observed for negative linking number densities (Fig. 2.6). Histograms of the extension are shown on the right side of time traces (black and red bars). The raw data histogram is well fit by a Gaussian (red solid lines).
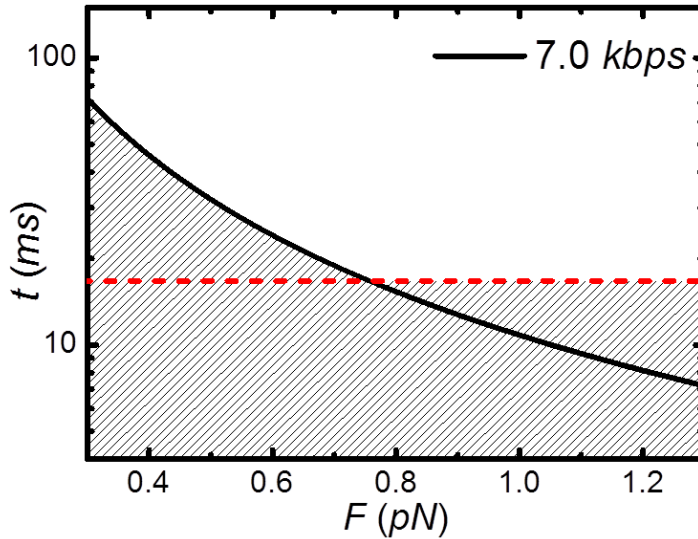
Figure S7

The temporal resolution of the experimental setup at different stretching forces. The black solid line represents the response time of a 7.0 *kbps* DNA molecule as calculated by Equation 2.15. The red solid line represents the frame rate of the CCD camera used. The shadowed region denotes the dynamics which cannot be resolved in this experiment.

References II

[1] Champoux, J. J. 2001. DNA topoisomerases: structure, function, and mechanism. *Annual review of biochemistry*. 70:369–413.

[2] Postow, L., C. D. Hardy, J. Arsuaga, and N. R. Cozzarelli. 2004. Topological domain structure of the Escherichia coli chromosome. *Genes & development*. 18:1766–79.

[3] Pruss, G. J., and K. Drlicat. 1989. DNA Supercoiling and Pmkatyotic Transcription. *Cell*. 56:521–523.

[4] Murakami, K. S., S. Masuda, E. A. Campbell, O. Muzzin, and S. A. Darst. 2002. Structural basis of transcription initiation: an RNA polymerase holoenzyme-DNA complex. *Science (New York, N.Y.)*. 296:1285–90.

[5] Postow, L., B. J. Peter, and N. R. Cozzarelli. 1999. Knot what we thought before: the twisted story of replication. *BioEssays : news and reviews in molecular, cellular and developmental biology*. 21:805–8.

[6] Revyakin, A., C. Liu, R. H. Ebright, and T. R. Strick. 2006. Abortive initiation and productive initiation by RNA polymerase involve DNA scrunching. *Science (New York, N.Y.)*. 314:1139–43.

[7] Kurth, I., R. E. Georgescu, and M. E. O'Donnell. 2013. A solution to release twisted DNA during chromosome replication by coupled DNA polymerases. *Nature*. 496:119–22.

[8] Ma, J., L. Bai, and M. D. Wang. 2013. Transcription under torsion. *Science (New York, N.Y.)*. 340:1580–3.

[9] Bryant, Z., M. D. Stone, J. Gore, S. B. Smith, N. R. Cozzarelli, and C. Bustamante. 2003. Structural transitions and elasticity from torque measurements on DNA. *Nature*. 424:338–41.

[10] Deufel, C., S. Forth, C. R. Simmons, S. Dejgosha, and M. D. Wang. 2007. Nanofabricated quartz cylinders for angular trapping : DNA supercoiling torque detection. *Nature methods*. 4:223–225.

[11] Lipfert, J., J. W. J. Kerssemakers, T. Jager, and N. H. Dekker. 2010. Magnetic torque tweezers: measuring torsional stiffness in DNA and RecA-DNA filaments. *Nature methods*. 7:977–80.

[12] Strick, T. R., J. F. Allemand, D. Bensimon, a. Bensimon, and V. Croquette. 1996. The elasticity of a single supercoiled DNA molecule. *Science (New York, N.Y.)*. 271:1835–7.

[13] Strick, T. R., V. Croquette, and D. Bensimon. 1998. Homologous pairing in stretched supercoiled DNA. *Proceedings of the National Academy of Sciences of the United States of America*. 95:10579–83.

[14] Strick, T. R., J. F. Allemand, D. Bensimon, and V. Croquette. 1998. Behavior of supercoiled DNA. *Biophysical journal*. 74:2016–28.

[15] Sheinin, M. Y., S. Forth, J. F. Marko, and M. D. Wang. 2011. Underwound DNA under Tension: Structure, Elasticity, and Sequence-Dependent Behaviors. *Physical Review Letters*. 107:108102.

[16] Allemand, J. F., D. Bensimon, R. Lavery, and V. Croquette. 1998. Stretched and overwound DNA forms a Pauling-like structure with exposed bases. *Proceedings of the National Academy of Sciences of the United States of America*. 95:14152–7.

[17] Marko, J. 2007. Torque and dynamics of linking number relaxation in stretched supercoiled DNA. *Physical Review E*. 76:021926.

[18] Emanuel, M., G. Lanzani, and H. Schiessel. 2013. Multiplectoneme phase of double-stranded DNA under torsion. *Physical Review E*. 88:022706.

[19] Lee, D. H., and R. F. Schleif. 1989. In vivo DNA loops in araCBAD: size limits and helical repeat. *Proceedings of the National Academy of Sciences of the United States of America*. 86:476–480.

[20] Salerno, D., a. Tempestini, I. Mai, D. Brogioli, R. Ziano, V. Cassina, and F. Mantegazza. 2012. Single-Molecule Study of the DNA Denaturation Phase Transition in the Force-Torsion Space. *Physical Review Letters*. 109:118303.

[21] Kruithof, M., F. Chien, M. de Jager, and J. van Noort. 2008. Subpiconewton dynamic force spectroscopy using magnetic tweezers. *Biophysical journal*. 94:2343–8.

[22] Wang, J. C. 1979. Helical repeat of DNA in solution Biochemistry : Wang. 76:200–203.

[23] Schildkraut, C., and S. Lifson. 1965. Dependence of the Melting Temperature of DNA. *Biopolymers*. 3:195–208.

[24] Lipfert, J., S. Klijnhout, and N. H. Dekker. 2010. Torsional sensing of small-molecule binding using magnetic tweezers. *Nucleic acids research*. 38:7122–32.

[25] Shao, Q., S. Goyal, L. Finzi, and D. Dunlap. 2012. Physiological levels of salt and polyamines favor writhe and limit twist in DNA. *Macromolecules*. 45:3188–3196.

[26] Jeon, J.-h., and W. Sung. 2008. How Topological Constraints Facilitate Growth and Stability of Bubbles in DNA. *Biophysical Journal*. 95:3600–3605.

[27] Kahn, J., E. Yun, and D. Crothers. 1994. Detection of Localized DNA flexibility. *Nature*. 368:163–166.

[28] Marko, J. F. 2009. Mathematics of DNA Structure, Function and Interactions. *In* Mathematics of DNA Structure, Function and Interactions. C. J. Benham, S. Harvey, W. K. Olson, D. W. Sumners, and D. Swigon, editors, *The IMA Volumes in Mathematics and its Applications*, volume 150. Springer New York, New York, NY. 225–249.

[29] Goldstein, E., and K. Drlica. 1984. Regulation of bacterial DNA supercoiling: plasmid linking numbers vary with growth temperature. *Proceedings of the National Academy of Sciences of the United States of America*. 81:4046–50.

[30] Huguet, J. M., C. V. Bizarro, N. Forns, S. B. Smith, C. Bustamante, and F. Ritort. 2010. Single-molecule derivation of salt dependent base-pair free energies in DNA. *Proceedings of the National Academy of Sciences of the United States of America*. 107:15431–6.

[31] Gross, P., N. Laurens, L. B. Oddershede, U. Bockelmann, E. J. G. Peterman, and G. J. L. Wuite. 2011. Quantifying how DNA stretches, melts and changes twist under tension. *Nature Physics*. 7:731–736.

[32] Zhang, X., H. Chen, H. Fu, P. S. Doyle, and J. Yan. 2012. Two distinct overstretched DNA structures revealed by single-molecule thermodynamics measurements. *Proceedings of the National Academy of Sciences of the United States of America*. 109:8103–8.

[33] Zhang, X., H. Chen, S. Le, I. Rouzina, P. S. Doyle, and J. Yan. 2013. Revealing the competition between peeled ssDNA, melting bubbles, and S-DNA during DNA overstretching by single-molecule calorimetry. *Proceedings of the National Academy of Sciences of the United States of America*. :1–6.

[34] King, G. a., P. Gross, U. Bockelmann, M. Modesti, G. J. L. Wuite, and E. J. G. Peterman. 2013. Revealing the competition between peeled ssDNA, melting bubbles, and S-DNA during DNA overstretching using fluorescence microscopy. *Proceedings of the National Academy of Sciences of the United States of America*. 110:3859–64.

[35] Altan-Bonnet, G., A. Libchaber, and O. Krichevsky. 2003. Bubble Dynamics in Double-Stranded DNA. *Physical Review Letters*. 90:138101.

[36] Forth, S., C. Deufel, M. Sheinin, B. Daniels, J. Sethna, and M. Wang. 2008. Abrupt Buckling Transition Observed during the Plectoneme Formation of Individual DNA Molecules. *Physical Review Letters*. 100:148301.

[37] Brutzer, H., N. Luzzietti, D. Klaue, and R. Seidel. 2010. Energetics at the DNA supercoiling transition. *Biophysical journal*. 98:1267–76.

[38] Marko, J. F., and S. Neukirch. 2012. Competition between curls and plectonemes near the buckling transition of stretched supercoiled DNA. *Physical Review E*. 85:011908.

[39] van Loenhout, M. T. J., M. V. de Grunt, and C. Dekker. 2012. Dynamics of DNA supercoils. *Science (New York, N.Y.)*. 338:94–7.

[40] Jeon, J.-H., J. Adamcik, G. Dietler, and R. Metzler. 2010. Supercoiling Induces Denaturation Bubbles in Circular DNA. *Physical Review Letters*. 105:208101.

[41] Marko, J. F., and E. D. Siggia. 1995. Stretching DNA. *Macromolecules*. 28:8759–8770.

[42] Neuman, K. C., and A. Nagy. 2008. Single-molecule force spectroscopy : optical tweezers , magnetic tweezers and atomic force microscopy. *Nature methods*. 5:491–505.

[43] De Vlaminck, I., T. Henighan, M. T. J. van Loenhout, D. R. Burnham, and C. Dekker. 2012. Magnetic forces and DNA mechanics in multiplexed magnetic tweezers. *PloS one*. 7:e41432.

Chapter 3

Chromatin Fiber Structure Revealed through Quantitative Analysis of Single-Molecule Force Spectroscopy[1]

Single-molecule techniques allow for picoNewton manipulation and nanometer accuracy measurements of single chromatin fibers. However, the complexity of the data, the heterogeneity of the composition of individual fibers, and the relatively large fluctuations in extension of the fibers complicate a structural interpretation of such force-extension curves. Here we introduce a statistical mechanics model that quantitatively describes the extension of individual fibers in response to force. Four conformations can be distinguished when pulling a chromatin fiber apart. A novel, transient conformation is introduced that coexists with single wrapped nucleosomes between 3 and 7 pN. Comparison of force-extension curves between single nucleosomes and chromatin fibers shows that embedding nucleosomes in a fiber stabilizes the nucleosome by 10 $k_B T$. Chromatin fibers with 20 and 50 bp linker DNA follow a different unfolding pathway. These results have implications for accessibility of DNA in fully-folded and partially unwrapped chromatin fibers and are vital for understanding force unfolding experiments on nucleosome arrays.

3.1 Introduction

The condensation of meters of DNA into the nucleus of a eukaryotic cell requires dense packing of the DNA into a structure called chromatin. This organization of eukaryotic DNA has attracted increasing interest because it is now evident that epigenetic changes to chromatin provide the cell with a means to fine-tune the regulation of its genes [1]. The physical mechanisms that are responsible for such epigenetic regulation clearly depend on the detailed structural arrangements of the molecules involved, but resolving the structure of chromatin at this scale has proven to be an enormous challenge.

The first level of DNA compaction, the nucleosome, is formed by wrapping 147 bp of DNA around a positively-charged histone protein core [2, 3]. It is now well-established that the nucleosome is a rather dynamic entity, allowing for spontaneous and force induced DNA unwrapping [4, 5], exchange of H2A-H2B histones [6] and thermal [7] and enzymatic repositioning [8, 9]. Several post-translational modifications have been shown to modulate the dynamics of these processes [10, 11]. Overall, single nucleosomes have been well-characterized yielding a dynamic structure in which DNA can transiently unwrap from the histone core.

The next level of organization is much more elusive. Despite great insights into the structure of nucleosome arrays from crystallography [12], electron microscopy (EM) [13, 14], and sedimentation analysis [15, 16], our understanding of the folding of an array of nucleosomes into a condensed fiber is limited. Part of the difficulty in studying the structure of chromatin fibers is the heterogeneity of the fiber's composition. The use of tandem arrays of the synthetic Widom 601 DNA nucleosome positioning sequence [17] for making well-defined nucleosomal arrays has greatly aided the study of chromatin folding [13], but still there is no consensus on the structure of chromatin. In fact, these regular arrays may not be representative for the situation in vivo [18], where nucleosomes are distributed along the DNA with irregular spacings. It also appears that higher order folding of chromatin fibers is critically dependent on buffer conditions as well as on the length of the linker DNA in between nucleosomes [19, 20]. Rather than looking for regular higher order structures, it may therefore be more illuminating to characterize the interactions between nucleosomes that define the folding of nucleosomal arrays into condensed chromatin fibers.

Single-molecule force spectroscopy is a powerful tool for probing molecular interactions. Pulling experiments on single nucleosomes reconstituted on a long DNA

fragment containing a single 601 element revealed a detailed picture of force induced DNA unwrapping [5]. Two transitions have been revealed, one at ~3 pN, corresponding to the unwrapping of about one turn of DNA, followed by a higher force (~8-9 pN) transition, representing the unwrapping of the remaining DNA. Such three-state behavior has since been confirmed by others [21–23]. The low force unfolding transition is reversible. Constant force measurements allowed for quantification of the free energy and rate constants of wrapping and unwrapping. The second transition is only reversible when the force is reduced to several pN. Theoretical modeling has indicated that the bending of linker DNA plays an important role in defining the structures of these meta-stable conformations [24]. The stability of a nucleosome under tension is therefore related to the DNA handles that are used to pull on it.

Nucleosome arrays have also been subject to manipulation with optical and magnetic tweezers. Early work on nucleosome arrays largely focused on the high-force unwrapping transition[4, 25]. The equivalent of approximately 72 bp is released in a step-wise irreversible fashion at 10-20 pN. At such forces the increased distance between the nucleosomes, due to stretching and unwrapping, is large enough to exclude interactions between nucleosomes. Only a few studies have focused on the low-force regime [26, 27], where a level of condensation is found that is comparable to the extension of folded chromatin fibers, as observed by EM [13]. Force-extension curves in this low force regime feature a transition to a large extension at ~3 pN as well. It is therefore non-trivial to distinguish DNA unwrapping, as observed in mono-nucleosomes, from the possible disruption of direct nucleosome-nucleosome interactions in folded chromatin fibers.

These single-molecule force spectroscopy data as well as other structural studies have led to a wealth of theoretical descriptions of the structure and mechanical properties of chromatin fibers, including full atom simulations [28], course-grained models [15, 29–31], and more analytical approaches [32–34]. While these works have set physical boundaries for the parameters that describe chromatin folding, most models are not detailed enough or use too many parameters to directly retrieve physical parameters from the experimental force spectroscopy data.

Here we aim to disentangle unfolding transitions in chromatin fibers, using new experimental data as well as a novel quantitative model for all aspects of a force-induced unwrapping of a chromatin fiber. With this statistical mechanics model, we quanti-

tatively compare pulling traces of mononucleosomes with those of fully-folded fibers. Despite using arrays of Widom 601 positioning elements and careful titration of the reconstitution dialysis [13], we find it necessary to include some heterogeneity of the chromatin fibers in terms of nucleosome composition. When these heterogeneities are accounted for, we are able to determine consistent values for DNA unwrapping free energies and extensions of each nucleosome conformation. A novel intermediate conformation is exposed, existing between 2.5 and 7 pN. Moreover, the qualitative difference in rupture behavior between chromatin fibers with 197 bp nucleosome repeat lengths (NRL) and 167 bp NRL indicates a different folding topology. Finally, by comparing the thermodynamical parameters of a mononucleosome with those of nucleosomes in a folded chromatin fiber, we unequivocally resolve the magnitude of stabilization of nucleosomes embedded in a folded fiber.

3.2   Results

3.2.1   Nucleosomes unfold differently in chromatin fibers as compared to mononucleosomes

To capture all aspects of chromatin folding, we measure and analyze here the force-extension relation of single chromatin fibers from small, sub-pN forces up to several tens of pN. Fig. 3.1A shows a force-extension curve of a chromatin fiber reconstituted with a tandem array of 15 repeats of a 197 bp Widom 601 nucleosome positioning sequence. A slow increase in extension is observed between 0.5 and 3 pN, followed by an extension of several hundred nanometers as force increases and, starting at about 9 pN, multiple stepwise unfolding events. These features have been described before as stretching of the chromatin fiber [27], rupture of roughly one turn of DNA from each of the nucleosomes [4], and at last the rupture of the second wrap of DNA from the histone core.

Whereas the stepwise unwrapping events at high force can unequivocally be attributed to the rupture of individual nucleosomes, the low force events are more difficult to interpret. In fact, it has been suggested that this characteristic force-extension relation at forces below 10 pN can be understood without nucleosome-nucleosome interactions and represents the gradual unwrapping of the outer turn of DNA from the nucleosomes [31]. Indeed, the force extension trace of a single nucleosome under identical conditions, shown in Fig. 3.1B, has remarkably similar characteristics, featuring
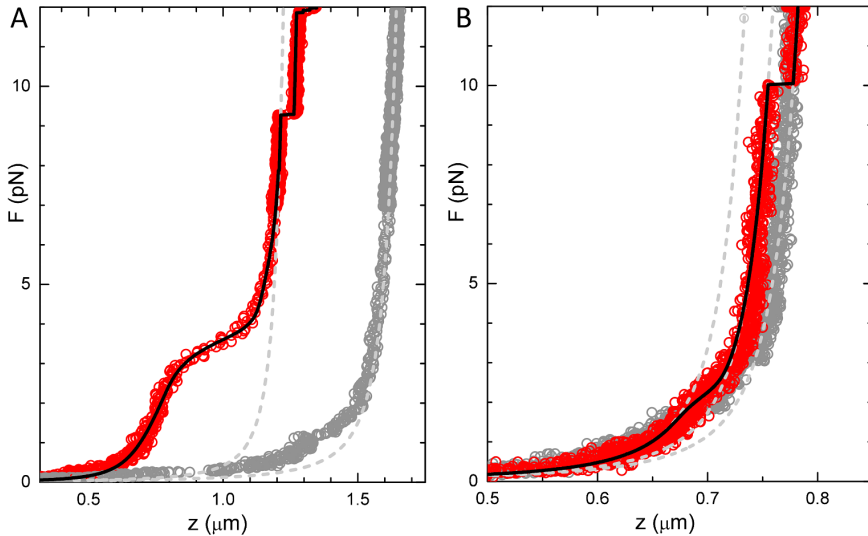
Figure 3.1: Comparison between force extension curves of (A) a chromatin fiber and (B) a mononucleosome. Red circles represent the pulling trace, grey circles represent the release trace. All force extension measurements are reversible, but a significant hysteresis is observed when the the force exceeds 6 pN. Light grey dashed lines represent WLC descriptions of the bare DNA and the state in which all nucleosomes are in the extended conformation (see Fig. 3.2). A third dashed line in B represents a WLC with a contour length 147 bp shorter than the bare DNA. Black lines are fits to Eq. 3.8 yielding for a) n_{fiber} = 13, $n_{unfolded}$ = 4, k = 0.28 pN/nm, z_{ext} = 4.6 nm, G_1 = 20.6 $k_B T$ and G_2 = 5.5 $k_B T$. For b): z_{ext} = 6.5 nm, G_1 = 8.8 $k_B T$ and G_2 = 3.5 $k_B T$.

three stages of unwrapping in the same force regimes, as reported before [5, 34, 35]. Because there are no neighboring nucleosomes in this case, all events should be attributed to the rupture of histone-DNA contacts. However, closer inspection shows that the first force plateau is slightly lower for the mono-nucleosome, 2.5 pN, than for the chromatin fiber, 3.5 pN, suggesting additional nucleosome-nucleosome interactions that stabilize the nucleosome in a folded fiber.

Another difference between mononucleosomes and chromatin fibers is that the latter show a rather large variation in the force-extension at low force. Despite careful titration of the histone-DNA stoichiometry and selection of the best batch using native gel electrophoresis [13], we generally observe significant variations in the low

force regime. Previously, we circumvented this problem by selecting only the most condensed chromatin fibers [27], assuming that those would be fully reconstituted with nucleosomes. However, chromatin fibers can be unstable under the highly diluted conditions that are typically used for single-molecule force spectroscopy. Claudet et al. pointed out that H2A-H2B dimers can readily dissociate, leaving $(H3-H4)_2$ tetramers on the DNA [36]. Despite the dissociation of dimers, the characteristic stepwise rupture events at 7-20 pN remain, showing that their occurrence can not be used as an indication for the presence of a full nucleosome, but rather reflect the number of tetramers in a particular nucleosomal array. The ability to resolve this heterogeneity between chromatin fibers is one of the unique features of single molecule techniques, though the occurrence of such variations in composition complicates a quantitative interpretation of force-extension relations of chromatin fibers in terms of structure and interaction energies.

In the next section we will set up a statistical mechanics framework that includes such heterogeneity. The thermodynamics is based on a free energy landscape for fiber unfolding that exhibits several metastable conformations, characterized by the roughness of the free energy landscape, as shown in Fig. 3.2. The structures of the individual nucleosome conformations are schematically depicted above the free energy diagram. Importantly, after the first transition each nucleosome follows the same unfolding pathway, independent of the number of nucleosomes in the fiber. This makes it possible to directly compare the unfolding of individual nucleosomes. By careful quantification of the free energy and extension of each of these conformations, we aim to separate possible nucleosome-nucleosome interactions from DNA unwrapping from the histone cores, as measured in single nucleosomes.

3.2.2 A multistate, statistical mechanics model

We describe a chromatin fiber as n_{tot} nucleosomes, which can be in any one of four conformations, see Fig. 3.2. Here we propose the nucleosome in a folded fiber has different mechanical properties compared with mono-nucleosome. Next to a nucleosome embedded in a fiber, a partially unfolded nucleosome comprising one turn of DNA and a fully unwrapped nucleosome in which all histones are still bound to the stretched DNA, we introduce a new metastable conformation in between the last two conformations, based on quantification of our experimental data (see next section).
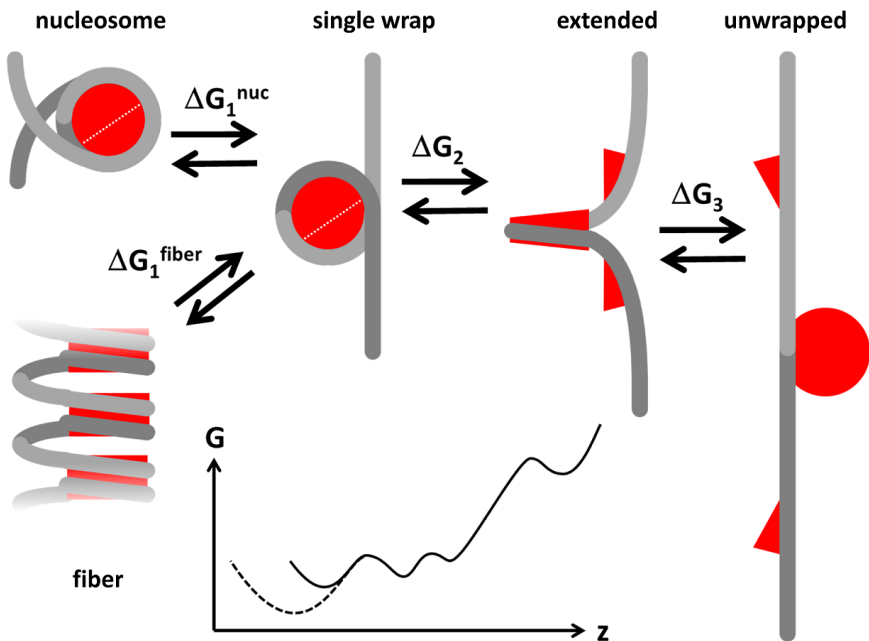
Figure 3.2: Schematic representation of the transitions between all metastable conformations of the nucleosomes. As force increases a single nucleosome unwraps part of its DNA. A single full turn of DNA remains wrapped around the histone core. The next, so far unresolved, conformation is slightly extended, which may be due to further unwrapping of the DNA, conformational changes within the nucleosome and/or deformation of the linker DNA. We propose the extended conformation may involve dissociation of H2A/H2B dimers from histone core (see Discussion). In the last conformation all histone proteins remain attached to the DNA, but the DNA can stretch fully. When a nucleosome is embedded in a chromatin fiber and interactions between nucleosomes fold the fiber into a dense structure, the extension per nuclesome is further reduced, as depicted in the bottom left. After the first transition, involving a change in free energy of ΔG_1, which may be different for a mono nucleosome and a nucleosome embedded in a fiber, all transitions will follow the same free energy landscape, as schematically plotted in the inset.

In our experiments, the DNA substrate includes about 1 kb of DNA handles that facilitate manipulation of the fiber. These DNA handles do not contain strong nucleosome positioning sequences and would, ideally, not contain any nucleosomes. The total extension of the tether, z_{tot}, increases with force, f, as both the chromatin fiber and

the DNA handles stretch elastically. On top of this elastic stretching, the nucleosomes will change conformation as force increases the fraction of nucleosomes in unwrapped, more extended conformations.

The extension of a DNA molecule follows an extensible Worm Like Chain (WLC) model. The free energy of the molecule depends on force [37]:

$$G_{DNA}(f, L) = -L \left[f - \sqrt{\frac{f \, k_B T}{A}} + \frac{f^2}{2S} \right] + f \, z_{DNA} \qquad (3.1)$$

with contour length L, persistence length A, stretching modulus S and thermal energy $k_B T$, yielding an extension:

$$z_{DNA}(f, L) = -\frac{d(G_{DNA} - f \, z_{DNA})}{df} = L \left[1 - \frac{1}{2} \sqrt{\frac{k_B T}{fA}} + \frac{f}{S} \right]. \qquad (3.2)$$

When nucleosomes are reconstituted on the DNA, the contour length of the free DNA is reduced by the amount of DNA that is wrapped around the histone cores. In the case of a single nucleosome the contour length is reduced by 147 bp. The extension of a one-turn wrapped nucleosome, including its linker DNA, follows Eq. 3.2, where L equals the NRL minus 89 bp, the amount of DNA in a single full wrap around the histone core. The free energy of this conformation is comprised of a part for stretching the free DNA, following Eq. 3.1, and a term for rupturing the wrapped DNA, ΔG_1^{nuc}. As shown below, the experimental data suggest an intermediate conformation between the one-turn wrapped and the fully unwrapped nucleosome. We assign an additional extension z_{ext} and free energy ΔG_2 to this conformation. The most extended conformation, the fully unwrapped nucleosome, can be described by a WLC with a contour length that equals the NRL and an additional free energy ΔG_3 that is required to rupture the remaining DNA from the histone core.

In absence of interactions between nucleosomes the above four conformations would suffice to quantitatively describe the entire force-extension behaviour of a chromatin fiber. When nucleosomes interact however, the linker DNA is also constrained, further reducing the extension per nucleosome. Within the force range in which the folded chromatin fiber is stable, we observe a linear increase in extension with force, pointing to a harmonic potential [27]:

$$G_{fiber}(f) = \frac{f^2}{2k} \tag{3.3}$$

and a Hookean extension

$$z_{fiber}(f) = -\frac{d(G_{fiber} - f\,z_{fiber})}{df} = f/k + z_0, \tag{3.4}$$

with a stiffness of k. An extra extension z_0 was added to include the finite size of the folded fiber. This additional extension corresponds to the nucleosome line density that can be obtained from EM micrographs [13, 38]. Note that this representation does not imply a structural model of the fiber, but it does suggest that the fiber is short and stiff enough that entropic contributions do not significantly reduce its extension, as opposed to a flexible polymer like DNA.

The thermodynamic properties of each of the conformations i, as schematically depicted in Fig. 3.2, are summarized in Table 3.1, in which all physical dependencies between the different conformations are explicitly captured in a minimal number of parameters.

The extension and free energy of the entire tether, containing n_{tot} nucleosomes, can now simply be calculated by summing the contributions of each of the nucleosomes and the DNA handles:

$$
\begin{aligned}
z_{tot}(f) &= \sum_i n_i z_i(f) + z_{DNA}(f) & (3.5) \\
G_{tot}(f) &= \sum_i n_i G_i(f) + G_{DNA}(f) & (3.6)
\end{aligned}
$$

When the DNA contains multiple nucleosomes, the chromatin fiber can be in a large, but finite number of states that are defined by the distribution of nucleosome conformations along the tether, $state = \{n_{fiber}, n_{single\,wrap}, n_{extended}, n_{unwrapped}\}$. This number can be reduced significantly by grouping states that have an equal number of nucleosomes in each of the conformations, but are arranged in a different order. These states cannot be distinguished based on extension only and are taken care of by including a degeneracy factor, which is calculated from a binomial distribution between the pairs of conformations i and j in each state:

$$D(state) = \prod_{i<j} \binom{n_i + n_j}{n_i} \tag{3.7}$$

The mean equilibrium extension of the fiber as a function of force can now be computed using standard statistical mechanics, summing over all states:

$$< z_{tot}(f) > = \frac{\sum_{states} z_{tot}(f)\, D(state)\, e^{-((G_{tot} - F z_{tot})/k_B T)}}{\sum_{states} D(state)\, e^{-((G_{tot} - F z_{tot})/k_B T)}} \tag{3.8}$$

3.2.3 DNA unwrapping at high forces involves less than one full wrap

The discrete steps in extension at forces above 6 pN represent the sequential unwrapping of the last DNA from each nucleosome and have been studied abundantly with optical tweezers [4, 22]. Here we describe these transitions as measured with Magnetic Tweezers (MT). MT act as a force clamp rather than a position clamp, resulting in a staircase-like force extension curve in stead of the typical sawtooth pattern obtained with optical tweezers. Fig. 3.3A shows a zoom in on these high force transitions. The corresponding step size distribution is shown in Fig. 3.3B. A step size of 22±3 nm was found, in range with previous optical tweezers studies on various DNA substrates and under different buffer conditions.

It should be noted though that the reported step sizes vary significantly: 22 nm [5], 24 nm [36], 25 nm [22], 27 nm [4] and 30 nm [39]. This high force transition is generally interpreted as a conformational change from a nucleosome with one turn of wrapped DNA to the fully unwrapped nucleosome. Such a transition would involve the release of about 89 bp of DNA, corresponding to approximately 30 nm. We attribute the difference to a so far unresolved metastable conformation prior to full unwrapping, as schematically depicted in Fig. 3.2. The extra extension of this conformation results in a large offset when multiple transitions occur in the same tether. For comparison, we plotted the extension of each of the intermediate states that contain a mixture of this extended conformation and fully unwrapped nucleosomes in grey dashed lines. We obtained the best match between multiple independent experimental datasets and this intermediate state for z_{ext} = 4.6 nm. Indeed, only when this extended conformation of the nucleosomes is included, do the force extension curves calculated with Eq. 3.8 overlap with the experimental data and can each data point unequivocally be assigned

to a specific state, as shown by the black line in Fig. 3.3A. This analysis shows that the last transition involves less than a full wrap of DNA.

Because the transitions are not in equilibrium, it is not possible to extract the free energy ΔG_3 that is associated with this transition. These high-force unfolding events are generally reversible however, when the force is decreased [22]. This indicates that the histones do not dissociate from the DNA, though extended exposure to higher forces slowly reduces the number of observed transitions. Interestingly, the variation in step sizes is larger than the accuracy of the measurement (7 nm vs 2 nm) showing that not all nucleosomes behave exactly the same. In Fig. 3.3A we observe for example a gradual extension beyond what can be explained by a WLC between 10 and 12 pN. This shift is made up for by a slightly smaller transition at 15 pN, after which the data accurately follow the theoretical curves again.

In the example trace shown in Fig. 3.3A there are 17 clearly distinguishable steps, even though the chromatin fiber was reconstituted on 15 repeats of the 601 nucleosome positioning sequence. We frequently observed a mismatch between the number of high force rupture events and the number of 601 repeats, demonstrating that the number of reconstituted nucleosomes is not strictly defined by the number of nucleosome positioning elements. The variation between individual fibers is small within a single reconstitution, and appears to depend on the precise histone/DNA ratio during reconstitution. Quantitative analysis of the high force transitions allows for counting of the number of nucleosomes that can wrap at least one turn of DNA in each fiber and indicates that these transitions involve a conformation that is more extended than a nucleosome containing a single wrap.
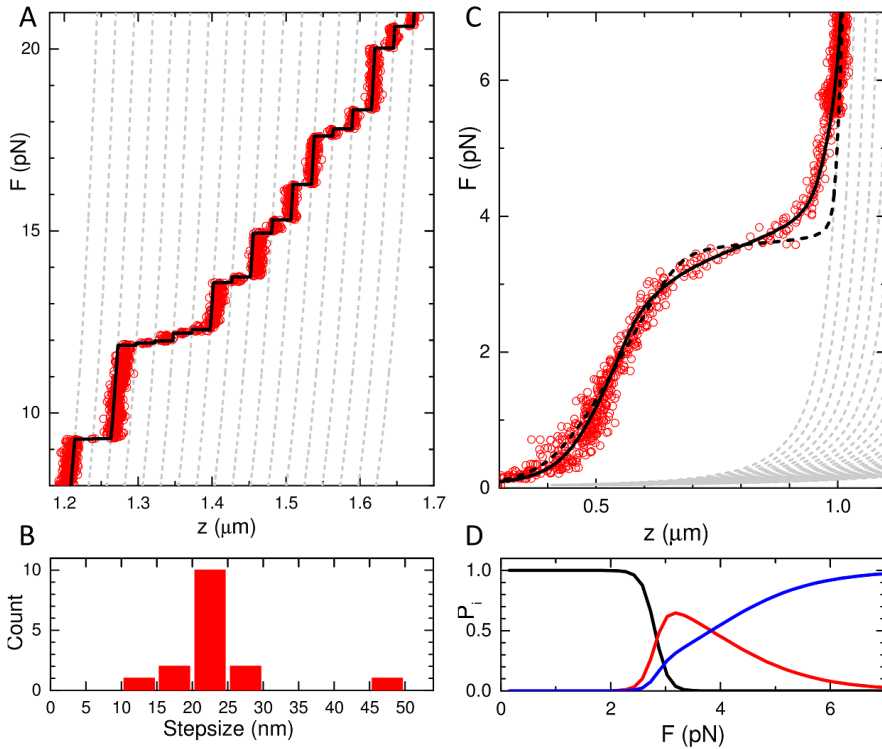
Figure 3.3: Detailed analysis of the unfolding of a single chromatin fiber. (A) A zoom in on the high force region shows discrete steps in extension. Dashed grey lines represent the extensions of all states that are composed of extended and fully unwrapped nucleosomes. The best match was obtained for z_{ext} = 4.6 nm. The black line shows the best match between individual data points and the various states of unwrapping after 10 bp median filtering. (B) Step size distribution of the data shown in (A) obtained from a 10 bp window t-test analysis. (C) Unfolding of a 15*197 NRL chromatin fiber at low force. Below 7 pN the extension starts to deviate from a string of extended nucleosomes (grey dashed lines). A single transition (black dashed line) does not capture the force extension data. The black line shows a fit to eq. 8, while constraining L_{wrap} = 89 bp and z_{ext} = 4.6 nm, yielding ΔG_1^{fiber} = 21.2±0.1 $k_B T$, ΔG_2 = 4.3±0.1 $k_B T$. (D) The corresponding probability for a nucleosome to be in a fiber (black), a single wrap (red) or in the extended conformation (blue).

3.2.4 Fiber unfolding at low forces shows a novel unfolding inter-mediate state

The force plateau at 3.5 pN represents the transitions from a folded fiber to a string of nucleosomes in the extended conformation, prior to the last unwrapping transition. A zoom in on this region for a fiber reconstituted on a 15*197 NRL DNA template is shown in Fig. 3.3C. The experimental data only converge to the force-extension curve corresponding to the state with all nucleosomes in the extended conformation at 7 pN. Thus the unfolding of the fiber occurs in a rather large force region. Following our previous work, we fitted the extension of the folded chromatin fiber with a Hookean spring. The broad transition between the folded fiber and a string of extended nucleosomes, cannot be captured in a single transition, as shown by the black dashed line. We obtained a good fit by including two transitions, with the constraints L_{wrap} = 89 bp and z_{ext}= 4.6 nm (as discussed above), yielding ΔG_1^{fiber}= 21.2±0.1 $k_B T$, ΔG_2= 4.3±0.1 $k_B T$. The necessity to include two transitions for an accurate description of the unfolding of a single chromatin fiber is a second indication that there is an additional metastable conformation of the nucleosome held under force.

Fitting the force extension curve of a mononucleosome in this force regime, Fig. 3.1B, results in an improved fit when the extended state is included, yielding z_{ext}=5.3±0.5 nm, ΔG_2= 5.0±0.5 $k_B T$ and ΔG_1^{nuc}= 8.3±0.2 $k_B T$. The free energy for the first transition is very similar to previous reports (9.0 $k_B T$ by Mihardja et al. [5]) and can unequivocally be attributed to the unwrapping of DNA from the histone core. It therefore provides a good reference for comparison with chromatin fibers in which nucleosome-nucleosome interactions may further stabilize DNA in the nucleosome. The fitted free energy of the first transition in unfolding the fiber is more than double of the value obtained for a single nucleosome, clearly demonstrating the extra stabilization of a nucleosome by neighboring nucleosomes.

Using the parameters obtained above, we plot in Fig.3.3D the probability of a nucleosome to be in each of the conformations that describe the fiber unfolding pathway. It is evident that multiple conformations coexist in a force region between 2 and 7 pN. This wide force range is due to the sequential order of events, that only allow the second transition to occur when the first unfolding event has taken place. The smaller change in extension in this second step makes this transition less sensitive to force than the first unfolding transition.
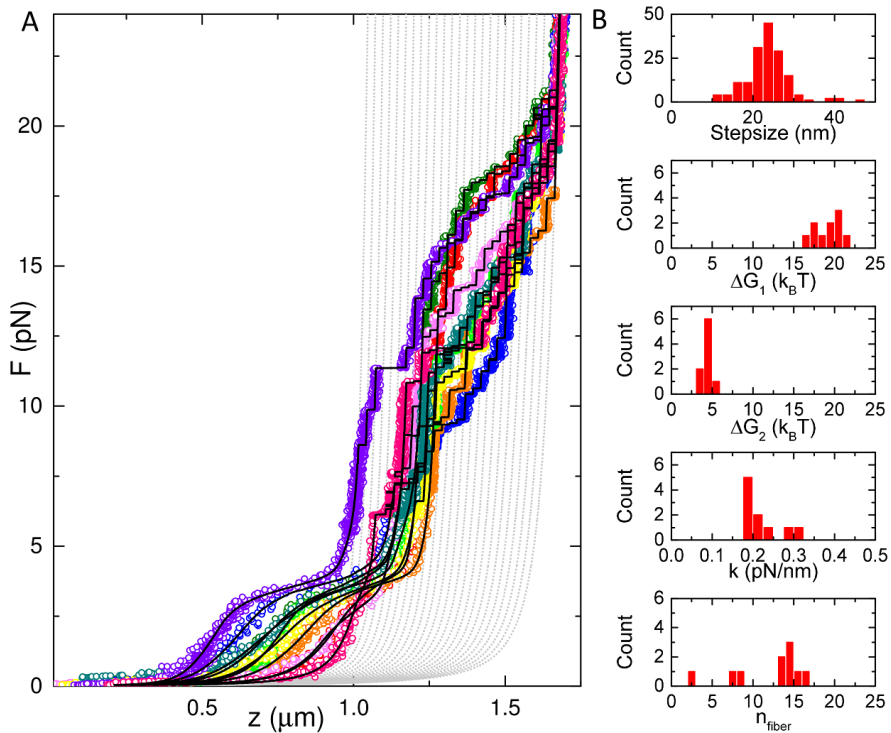
Figure 3.4: Different fibers show a large variation in condensation. (A) 10 chromatin fibers reconstituted on a 15*197 NRL DNA template. The high force transitions align well with states that describe the last unfolding transition, plotted in grey dashed lines. All curves have a force plateau at 3 pN, but the size of the force plateau and the extension at lower forces varies significantly. Black lines represent fits to Eq. 3.8. (B) Distribution of fit parameters obtained from (A). The stepsizes in the top histogram were determined independently using a t-test step finding algorithm. Except for the number of nucleosomes in the fiber, all parameters show a narrow distribution.

One of the most striking features of these fits is that the unfolding of the chromatin fiber can be fully captured in four conformations, including the novel extended conformation. We did not observe evidence for an intermediate conformation of a fully wrapped nucleosome without nucleosome-nucleosome interactions, often referred to as a beads-on-a-string structure. If such an intermediate would be present, we would expect a further broadening of the force plateau on the small extension side. The absence of such broadening may have important structural implications.

3.2.5 Variations between individual chromatin fibers result from different compositions

Whereas all chromatin fibers feature similar unfolding characteristics, we observed a rather large variation in the force extension behavior between fibers. Fig. 3.4 shows the force extension curves of 10 different fibers. Because the last unfolding transition is not in thermodynamic equilibrium, the rupture forces for this transition are distributed stochastically. Nevertheless, all curves align well with the set of unfolding states that contain extended and fully unwrapped nucleosome, indicated with the grey dashed lines. The first two transitions at forces below 7 pN on the other hand are fully reversible resulting in overlapping pull and release curves (data not shown). Nevertheless, we observe large variations in extension between fibers in this low force range. We attribute these differences to the variations in the composition of the fiber.

Over-saturation of the DNA substrate with nucleosomes, incomplete reconstitution, and/or partial dissociation of nucleosomes after reconstitution may result in inhomogeneity of the fiber composition within a batch. Repetitive pulling cycles exceeding 5 pN for example, show a gradual decrease of the condensation in the low force regime (data not shown), which would be consistent with dissociation of several H2A-H2B dimers. Such a loss of H2A-H2B dimers would not only prohibit the formation of a fully wrapped nucleosome, it would also prevent nucleosome-nucleosome interactions that are thought to be mediated by interactions between the H4 tail and the acidic patch on the H2A-H2B dimer of a neighbouring nucleosome [20]. As a consequence, the number of rupture events at low force would be smaller than the number of rupture events detected at high force.

To deal with this heterogeneity, we fitted the number of nucleosomes in the fiber, n_{fiber}, independently of the number of nucleosomes that undergo the last transition by introducing an additional parameter $n_{unfolded}$. The latter complexes do not fold into a fiber or in a single wrap conformation, and only undergo the last unwrapping event. Importantly, we could not resolve separate populations in the last transition, suggesting that such unfolded nucleosomes indeed share the same unwrapping pathway. With this addition all experimental curves gave good fits to the model and yielded a narrow distribution of fit parameters, as shown in Fig. 3.4B and Table 3.2. The fitted number of nucleosomes in the fiber gave a much better correlation with the number of nucleosome positioning elements in the DNA substrate, but we still do not observe a perfect match.

A quantitative interpretation of the force extension data therefore requires analysis of the composition of each fiber individually, as all parameters that define fiber folding scale with the number of nucleosomes in the fiber.

3.2.6   167 NRL fibers are folded in a different manner than 197 NRL fibers

The force extension data of 197 NRL fibers closely follow the model based on independent transitions for all rupture events, including the first transition, see Fig. 3.5A. This may be surprising in view of the large interaction energy and the high level of condensation up to 3 pN. Such independent rupturing can only be achieved when nucleosome-nucleosome interactions form exclusively between neighbors, as schematically drawn in the inset of Fig. 3.5A. If non-neighbouring nucleosomes would play a significant role in stabilizing chromatin folding, the nucleosomes at the ends would be more fragile than those embedded in the fiber. In fact, this scenario was already discussed by Cocco et al. [40], who argued that in that case, the degeneracy would be lifted for the transition. Indeed, removing the degeneracy in Eq. 3.7 for the first transition does not give a good fit to the experimental curve, indicating that the data can best be interpreted in terms of interactions between neighbouring nucleosomes only.

For chromatin arrays that have 20 bp of linker DNA the crystal structure of tetranucleosomes clearly shows stacking of non-neighbouring nucleosomes [12]. Cross-linking experiments further support a zig-zag folding in which odd and even nucleosomes interact into two parallel columns of nucleosomes [41]. Such a structure would not only yield a 2 times smaller extension per nucleosome and a significantly higher stiffness, as we reported before [27], it would also invalidate the independence of rupture events. Unlike the 197 NRL fibers, the force-extension curve of a 30*167 NRL chromatin fiber cannot be fitted with the degenerate unfolding model, see Fig. 3.5B. The experimental data show a narrower force plateau as compared to the 197 NRL fiber. When the degeneracy of the first transition is taken out of the model, a good fit is recovered. This notably changes the shape of the force-extension curve, it also shifts the onset of the force-plateau to a slightly higher value from 3.0 to 3.5 pN. As summarized in Table 3.2, all fit parameters, including the transition energy ΔG_1^{fiber} are similar to those obtained for the 197 NRL fibers, except for the stiffness of the fiber. These observations reinforce the idea that 167 NRL and 197 NRL chromatin are arranged in a different structure.
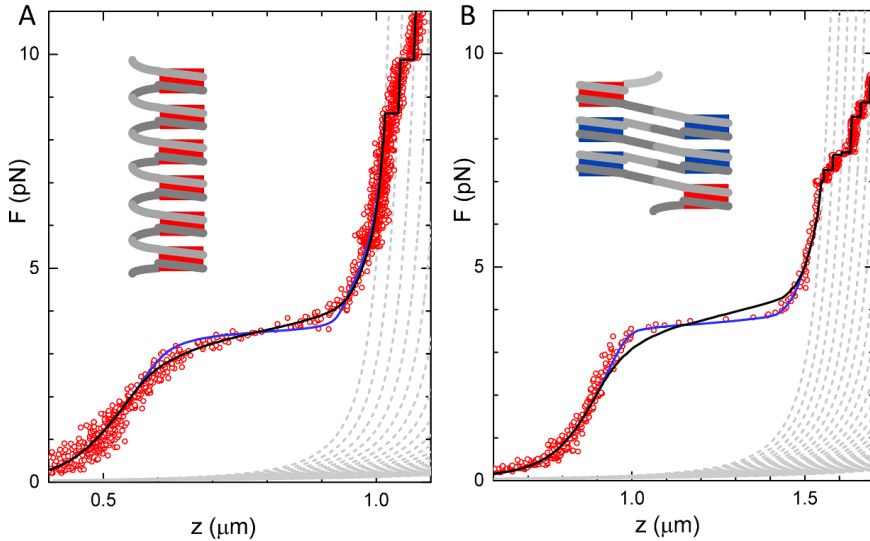
Figure 3.5: Chromatin fibers with 167 bp NRL follow a qualitatively different unfolding mechanism than 197 bp NRL fibers. (A) A 15*197 NRL chromatin fiber fits well with Eq. 3.8, black line. A model in which the degeneracy for the first transition is lifted, blue line, does not capture the unfolding transitions (blue line). (B) A 30*167 NRL chromatin fiber is better described by non-degenerate states for the first transition. This qualitative difference can be explained by a different structure of the fibers, as schematically shown in the insets. In particular, the nucleosomes that are embedded in the fiber, drawn in blue in the schematic drawing of a zig-zag folded fiber, are less susceptible for unfolding than the red nucleosomes at the ends of the fiber. In contrast, the nucleosomes arranged in a single stack are all equivalent, inset of (A), and rupturing of any of the nucleosomes will lead to the same amount of extension of the fiber.

3.3 Discussion

The folding of chromatin fibers and the mechanism of how they unfold under force have generated numerous debates. In this study we present and quantitatively interpret for the first time force spectroscopy on the unfolding of single chromatin fibers over a wide force range, spanning from less than 0.5 pN to more than 25 pN. These data include the well studied high-force regime and allow for a detailed analysis of the entire stretching curve. Based on the measured extensions, we resolved a novel metastable conformation of the nucleosome, we quantified the compositional hetero-

geneity of individual fibers in terms of number of nucleosomes and number of partially folded nucleosomes, and we showed that the unfolding mechanism of chromatin fibers depends on the linker length. These data reinforce our previous structural interpretation of the force-extension curves [27] and allow for detailed, quantitative comparison between fibers and with single nucleosomes without biasing the results by selection of well-behaved fibers.

For a quantitative interpretation of the data it was essential to allow for compositional heterogeneity. This should not be surprising given the strong dependence of the reconstitution on the precise DNA/histone stoichiometry [13] and the known fragility of the nucleosome under typical single-molecule conditions [36]. Moreover, we opted for a DNA construct with 1 kb of DNA on both sides of the chromatin fiber. Though such DNA extensions may allow for additional nucleosomes in the fiber, the long DNA handles proved useful to prevent or identify interactions between the reconstituted chromatin fiber and the surface of the flow cell or the bead. Though careful titration and handling of the sample can reduce this heterogeneity, we could not reliably produce perfectly defined fibers. Generally we found that the number of nucleosomes that fold in a fiber reflects the number of Widom 601 positioning elements, but additional tetramers may be reconstituted and nucleosomes do partially dissociate into tetramers when exposed to excessive force over a longer time. This may be illustrative of the dynamics of chromatin in vivo, where H2A-H2B dimers are highly mobile [42, 43], it also shows that assuming such perfect stoichiometry for single molecule force spectroscopy may not be correct and that any analysis that does not take possible heterogeneity into account can be significantly flawed.

The novel extended conformation of the nucleosome between 3 and 7 pN that we report here explains the discrepancy between the reported stepsizes for the last unwrapping event, which vary between 20 and 30 nm, and the structural insight from the crystal structure, showing that a single wrap of DNA would constrain 89 bp, which would amount to 30 nm. Here we measured a stepsize of 24 ± 7 nm. The rather large variation exceeds our experimental accuracy and can only be explained by occasional deviations from the unfolding pathway, as sketched in Fig. 3.2. Nevertheless, in individual force extension traces it is possible to unequivocally assign a state of chromatin unfolding at any time in the experiment.

We could not differentiate different classes of rupture events in the last transition,

though it is clear that all previous transitions only occur in nucleosomes that start off as fully folded. It is therefore likely that the novel metastable state structurally resembles that of a tetramer. This interpretation implies that the transition from a single wrap nucleosome to the extended conformation involves dissociation of the H2A-H2B dimers from histone core, rather than dissociation of DNA from the histone octamer (See Fig. 3.2). The transition is usually reversible, which is only possible when the H2A-H2B dimers remain bound to the DNA. Such a mechanism of nucleosome unfolding was recently resolved with single molecule FRET in absence of force [6]. Note that DNA does not extend from a tetrasome in exactly opposite directions, as it does in a single wrap nucleosome, which makes the force-extension relation non-trivial [32]. Pending more detailed structural information of this conformation we therefore opt to model this conformation as having a constant extension in addition to a single wrap nucleosome. The forces at which these conformational changes take place is well within the range that may be expected in vivo, so this metastable conformation may have functional properties. Independent of its structure or function it is clear that this conformation should be included in a quantitative analysis of fiber unfolding under force.

We compared force-extension data of single nucleosomes with data of folded chromatin fibers with the same buffer conditions, histone composition and pulling protocol. As should be expected, single nucleosomes and nucleosomes embedded in chromatin fibers share the same stepwise unfolding pathway, except for the first transition into a single wrap nucleosome. This first transition involves a 10 $k_B T$ higher free energy per nucleosome in embedded nucleosomes than in a single nucleosome, which leads to a higher rupture force for DNA unwrapping from a chromatin fiber. Remarkably, the measured free energy of the folded conformation was the same for fibers with 197 and 167 bp NRL, despite possible different higher order structure of the fibers. The results that we obtained here with highly regular reconstituted chromatin fibers may therefore be more generic, and may be applicable for more disordered chromatin fibers, as found in vivo.

It is tempting to directly attribute the difference in free energy between the mononucleosome and a fiber embedded nucleosome to the nucleosome-nucleosome interaction energy. However, the situation may be more intricate. We could not resolve any indication of a fully wrapped nucleosome conformation in our fiber pulling data, i.e. a transition between the left two conformations drawn in Fig. 3.2 . This may simply be because the force for rupturing nucleosome-nucleosome interactions exceeds that

of histone-DNA interactions, and when the nucleosomes are torn apart DNA unwrapping directly follows within the time resolution of the experiment. Similar arguments however would apply to the transition into an extended nucleosome, which is clearly resolved as a broadening of the force plateau. Alternatively, it may be that the nucleosomes in the folded fiber are not fully wrapped and that part of the nucleosomal DNA is released from the histone core when the fiber folds into its higher order structure. FRET experiments on free nucleosomes have shown that unwrapping the first tens of bps of nucleosomal DNA is energetically not expensive [44]. Such unwrapping would allow for less bending of the linker DNA, and may therefore be required for fiber folding. FRET experiments on nucleosomes in folded fibers may be able to test this hypothesis. Indirect evidence from restriction enzyme accessibility indicated that indeed nucleosomal DNA can be more accessible in chromatin fibers than in single nucleosomes [45], which do not have that constraint.

Though the free energy difference is the same, the first rupture event is qualitatively different in fibers with different NRLs. It appears that nucleosomes in 197 NRL fibers rupture independently, whereas in 167 NRL fibers nucleosome rupture events appear to follow a cooperative mechanism. This observation is hard to reconcile with a gradual unwrapping of the first part of the wrapped DNA, as has been proposed before to explain the shape of the force-extension data [31], but quantitatively agrees with a different unfolding mechanism where nucleosomes are less stable at the ends of the fiber due to missing nucleosome-nucleosome interactions, as sketched in Fig. 3.5. In this scenario the nucleosomes would rupture sequentially from the ends, which is consistent with a solenoidial folding of 197 NRL fibers and a zig-zag folding of 167 NRL fibers. The maximum extension at the rupture force (13 vs 7 nm per nucleosome for 197 and 167 bp NRL fibers) and the almost 4 times higher stiffnes for 167 NRL fibers also support this interpretation.

Despite the complexity of the fiber we were able to resolve a clear mechanism of fiber unfolding that is consistent for various architectures of chromatin. With the model and the parameters that described force induced structural changes in chromatin it should now be possible to resolve the effects of post-translational modifications on the structure and dynamics of chromatin at the molecular scale. It should also be possible to extend the experiments and model to torsionally constraint topological domains of chromatin. In addition, because we can describe the mechanics of chromatin fibers at the level of individual nucleosomes, it will be interesting to move towards fibers that are

heterogeneous in terms of linker length, mimicking the situation in vivo more closely. These steps will lead to a fundamental structural understanding of chromatin fiber folding, without oversimplification or imposing regularity that is often required to interpret structural data.

3.4 Materials and methods

3.4.1 Chromatin reconstitution

A DNA substrate based on pUC18 (Novagen) with inserts containing 15 times 197 bp and 30 times 167 bp repeats of the Widom 601 nucleosome positioning sequence was used for reconstitution of chromatin fibers. After digestion with BsaI and BseYI enzyme, single stranded ends were filled with a dUTP-digoxigenin at the BsaI and a dUTP-biotin at the BseYI end by Klenow reaction. The linear DNA fragment was mixed with 147 bp competitor DNA and histone octamers purified from chicken erythrocytes, and reconstituted into chromatin fibers using salt dialysis following [13].

3.4.2 Sample preparation

A clean cover slip was coated with 1% polystyrene-tuolene solution and mounted on a poly-di-methysiloxane (PDMS, Dow Corning) flow cell containing a $10 \times 40 \times 0.4$ mm^3 flow channel. The flow cell was incubated with 1 μg/ml anti-digoxigenin for 2 hours and 2% BSA (w/v) solution over night. 20 ng/ml fibers in 10 mM Hepes pH 7.6, 100 mM KAc, 2 mM MgAc$_2$ and 10 mM NaN$_3$ was flushed into the flow cell and incubated for 10 minutes, followed by flushing in 2.8 μm streptavidin-coated superparamagnetic microspheres (M270, Invitrogen) in the same buffer. Loose beads were flushed out after another 10 minutes of incubation.

3.4.3 Magnetic tweezers

The home-built magnetic tweezers have been described by Kruithof et al. [46]. During an experiment, a single chromatin fiber was tethered between the end of a superparamagnetic bead and the surface of a microscope coverslip. The force was varied by moving the pair of magnets at 0.1 mm/s. The extension of the DNA was measured in real time at a frame rate of 60 Hz with a CCD camera (Pulnix TM-6710CL).

3.4.4 Data analysis

Data analysis and curve fitting was done using a custom software written in LabView. The offset of each force-extension curve was adjusted by aligning the extension at high force, after the last rupture event, with a WLC using the known contour length, a persistence length of 50 nm and a stretch modulus of 1200 pN. This procedure circumvents errors due to off-center attachment [47, 48] and the roughness of the bead and surface. In some cases a linear drift was subtracted to enforce overlap from successive pulling experiments. This drift correction was validated by the (partial) overlap of pull and release curves. All data are presented and analyzed without further filtering or averaging.

Rupture events at high force were automatically detected with a t-test step finding algorithm, using a 10 points window [49]. At forces larger than the first rupture event the fitted extension was assigned to the extension of the state that matched the experimental data point best. To eliminate erroneous assignments due to the relatively large amplitude of thermal fluctuations in the extension this part of the fitted curve was filtered using a 10 point median filter. At forces below the first rupture event the data were fitted to Eq. 3.8 using a Levenberg-Marquardt algorithm. Instabilities due to the discrete nature of of the number of nucleosomes were circumvented by linear interpolation of these parameters. Generally the fit results yielded numbers of nucleosomes that were within 0.1 of an integer number. Data points acquired a forces below 0.5 pN were not included in the fit to exclude artifacts due to bead-surface interactions.

3.5 Tables

Table 3.1: Structural and thermodynamic parameters per nucleosome for different conformations sketched in Fig. 3.2.

i	L_i (bp)	z_i (nm)	G_i (k_BT)
nucleosome	$NRL - 147$	$z_{DNA}(f, L_i)$	$G_{DNA}(f, L_i)$
fiber	-	$f/k + z_o$	$\frac{1}{2}f^2/k$
single wrap	$NRL - L_{wrap}$	$z_{DNA}(f, L_i)$	$G_{DNA}(f, L_i) + \triangle G_1$
extended	$NRL - L_{wrap}$	$z_{DNA}(f, L_i) + z_{ext}$	$G_{DNA}(f, L_i) + \triangle G_1 + \triangle G_2$
unwrapped	NRL	$z_{DNA}(f, L_i)$	$G_{DNA}(f, L_i) + \triangle G_1 + \triangle G_2 + \triangle G_3$

Table 3.2: The mean parameters obtained from fitting multiple force extension traces

	mono nucleosome	15*197 NRL	30*167 NRL
n_{fiber}	1	12 ± 4	27 ± 2
k (pN/nm)	-	0.22 ± 0.04	0.6 ± 0.2
$G_1(k_B T)$	8.8 ± 0.5	19 ± 2	18 ± 3
$G_2(k_B T)$	3.5 ± 1.0	4.4 ± 0.7	5.0 ± 0.4
Step size (nm)	24 ± 2	24 ± 7	24 ± 8
$n_{unfolded}$	-	8 ± 6	10 ± 5

References III

[1] Li, B., M. Carey, and J. L. Workman. 2007. The role of chromatin during transcription. *Cell*. 128:707–19.

[2] Luger, K., A. W. Ma, R. K. Richmond, D. F. Sargent, and T. J. Richmond. 1997. Crystal structure of the nucleosome core particle at 2 . 8 A resolution. *Nature*. 389:251–260.

[3] Makde, R. D., J. R. England, H. P. Yennawar, and S. Tan. 2010. Structure of RCC1 chromatin factor bound to the nucleosome core particle. *Nature*. 467:562–6.

[4] Brower-Toland, B. D., C. L. Smith, R. C. Yeh, J. T. Lis, C. L. Peterson, and M. D. Wang. 2002. Mechanical disruption of individual nucleosomes reveals a reversible

multistage release of DNA. *Proceedings of the National Academy of Sciences of the United States of America*. 99:1960–5.

[5] Mihardja, S., A. J. Spakowitz, Y. Zhang, and C. Bustamante. 2006. Effect of force on mononucleosomal dynamics. *Proceedings of the National Academy of Sciences of the United States of America*. 103:15871–6.

[6] Böhm, V., A. R. Hieb, A. J. Andrews, A. Gansen, A. Rocker, K. Tóth, K. Luger, and J. Langowski. 2011. Nucleosome accessibility governed by the dimer/tetramer interface. *Nucleic acids research*. 39:3093–102.

[7] Flaus, A., and T. Owen-Hughes. 2011. Mechanisms for ATP-dependent chromatin remodelling: the means to the end. *The FEBS journal*. 278:3579–95.

[8] Rippe, K., A. Schrader, P. Riede, R. Strohner, E. Lehmann, and G. Längst. 2007. DNA sequence- and conformation-directed positioning of nucleosomes by chromatin-remodeling complexes. *Proceedings of the National Academy of Sciences of the United States of America*. 104:15635–40.

[9] van Vugt, J. J. F. a., M. de Jager, M. Murawska, A. Brehm, J. van Noort, and C. Logie. 2009. Multiple aspects of ATP-dependent nucleosome translocation by RSC and Mi-2 are directed by the underlying DNA sequence. *PloS one*. 4:e6345.

[10] Neumann, H., S. M. Hancock, R. Buning, A. Routh, L. Chapman, J. Somers, T. Owen-Hughes, J. van Noort, D. Rhodes, and J. W. Chin. 2009. A method for genetically installing site-specific acetylation in recombinant histones defines the effects of H3 K56 acetylation. *Molecular cell*. 36:153–63.

[11] North, J. a., M. X0160 Imon, M. B. Ferdinand, M. a. Shoffner, J. W. Picking, C. J. Howard, A. M. Mooney, J. van Noort, M. G. Poirier, and J. J. Ottesen. 2014. Histone H3 phosphorylation near the nucleosome dyad alters chromatin structure. *Nucleic acids research*. :1–12.

[12] Schalch, T., S. Duda, D. F. Sargent, and T. J. Richmond. 2005. X-ray structure of a tetranucleosome and its implications for the chromatin fibre. *Nature*. 436:138–41.

[13] Robinson, P. J. J., L. Fairall, V. a. T. Huynh, and D. Rhodes. 2006. EM measurements define the dimensions of the "30-nm" chromatin fiber: evidence for a compact, interdigitated structure. *Proceedings of the National Academy of Sciences of the United States of America*. 103:6506–11.

[14] Routh, A., S. Sandin, and D. Rhodes. 2008. Nucleosome repeat length and linker histone stoichiometry determine chromatin fiber structure. *Proceedings of the National Academy of Sciences of the United States of America*. 105:8872–7.

[15] Grigoryev, S. a., G. Arya, S. Correll, C. L. Woodcock, and T. Schlick. 2009. Evidence for heteromorphic chromatin fibers from analysis of nucleosome interactions. *Proceedings of the National Academy of Sciences of the United States of America*. 106:13317–22.

[16] Allahverdi, A., R. Yang, N. Korolev, Y. Fan, C. a. Davey, C.-F. Liu, and L. Nordenskiöld. 2011. The effects of histone H4 tail acetylations on cation-induced chromatin folding and self-association. *Nucleic acids research*. 39:1680–91.

[17] Lowary, P. T., and J. Widom. 1998. New DNA sequence rules for high affinity binding to histone octamer and sequence-directed nucleosome positioning. *Journal of molecular biology*. 276:19–42.

[18] Nishino, Y., M. Eltsov, Y. Joti, K. Ito, H. Takata, Y. Takahashi, S. Hihara, A. S. Frangakis, N. Imamoto, T. Ishikawa, and K. Maeshima. 2012. Human mitotic chromosomes consist predominantly of irregularly folded nucleosome fibres without a 30-nm chromatin structure. *The EMBO journal*. 31:1644–53.

[19] Li, G., and D. Reinberg. 2011. Chromatin higher-order structures and gene regulation. *Current opinion in genetics & development*. 21:175–86.

[20] Luger, K., M. L. Dechassa, and D. J. Tremethick. 2012. New insights into nucleosome and chromatin structure: an ordered state or a disordered affair? *Nature reviews. Molecular cell biology*. 13:436–47.

[21] Kruithof, M., and J. van Noort. 2009. Hidden Markov analysis of nucleosome unwrapping under force. *Biophysical journal*. 96:3708–15.

[22] Mack, A. H., D. J. Schlingman, R. P. Ilagan, L. Regan, and S. G. J. Mochrie. 2012. Kinetics and thermodynamics of phenotype: unwinding and rewinding the nucleosome. *Journal of molecular biology*. 423:687–701.

[23] Sheinin, M. Y., M. Li, M. Soltani, K. Luger, and M. D. Wang. 2013. Torque modulates nucleosome stability and facilitates H2A/H2B dimer loss. *Nature communications*. 4:2579.

[24] Kulić, I., H. Mohrbach, V. Lobaskin, R. Thaokar, and H. Schiessel. 2005. Apparent persistence length renormalization of bent DNA. *Physical Review E*. 72:041905.

[25] Simon, M., J. a. North, J. C. Shimko, R. a. Forties, M. B. Ferdinand, M. Manohar, M. Zhang, R. Fishel, J. J. Ottesen, and M. G. Poirier. 2011. Histone fold modifications control nucleosome unwrapping and disassembly. *Proceedings of the National Academy of Sciences of the United States of America*. 108:12711–6.

[26] Cui, Y., and C. Bustamante. 2000. Pulling a single chromatin fiber reveals the forces that maintain its higher-order structure. *Proceedings of the National Academy of Sciences of the United States of America*. 97:127–32.

[27] Kruithof, M., F.-T. Chien, A. Routh, C. Logie, D. Rhodes, and J. van Noort. 2009. Single-molecule force spectroscopy reveals a highly compliant helical folding for the 30-nm chromatin fiber. *Nature structural & molecular biology*. 16:534–40.

[28] Ettig, R., N. Kepper, R. Stehr, G. Wedemann, and K. Rippe. 2011. Dissecting DNA-histone interactions in the nucleosome by molecular dynamics simulations of DNA unwrapping. *Biophysical journal*. 101:1999–2008.

[29] Korolev, N., A. Allahverdi, Y. Yang, Y. Fan, A. P. Lyubartsev, and L. Nordenskiöld. 2010. Electrostatic origin of salt-induced nucleosome array compaction. *Biophysical journal*. 99:1896–905.

[30] Dobrovolskaia, I. V., and G. Arya. 2012. Dynamics of forced nucleosome unraveling and role of nonuniform histone-DNA interactions. *Biophysical journal*. 103:989–98.

[31] Victor, J. M., J. Zlatanova, M. Barbi, and J. Mozziconacci. 2012. Pulling chromatin apart: Unstacking or Unwrapping? *BMC biophysics*. 5:21.

[32] Kulić, I., and H. Schiessel. 2004. DNA Spools under Tension. *Physical Review Letters*. 92:228101.

[33] Schiessel, H. 2006. The nucleosome: a transparent, slippery, sticky and yet stable DNA-protein complex. *The European physical journal. E, Soft matter*. 19:251–62.

[34] Sudhanshu, B., S. Mihardja, E. F. Koslover, S. Mehraeen, C. Bustamante, and a. J. Spakowitz. 2011. Tension-dependent structural deformation alters single-molecule transition kinetics. *Proceedings of the National Academy of Sciences of the United States of America*. 108:1885–90.

[35] Bintu, L., T. Ishibashi, M. Dangkulwanich, Y.-Y. Wu, L. Lubkowska, M. Kashlev, and C. Bustamante. 2012. Nucleosomal elements that control the topography of the barrier to transcription. *Cell*. 151:738–49.

[36] Claudet, C., D. Angelov, P. Bouvet, S. Dimitrov, and J. Bednar. 2005. Histone octamer instability under single molecule experiment conditions. *The Journal of biological chemistry*. 280:19958–65.

[37] Bustamante, C., S. B. Smith, J. Liphardt, and D. Smith. 2000. Single-molecule studies of DNA mechanics. *Current opinion in structural biology*. 10:279–85.

[38] Bassett, A., S. Cooper, C. Wu, and A. Travers. 2009. The folding and unfolding of eukaryotic chromatin. *Current opinion in genetics & development*. 19:159–65.

[39] Pope, L. H., M. L. Bennink, K. a. van Leijenhorst-Groener, D. Nikova, J. Greve, and J. F. Marko. 2005. Single chromatin fiber stretching reveals physically distinct populations of disassembly events. *Biophysical journal*. 88:3572–83.

[40] Cocco, S., J. F. Marko, R. Monasson, a. Sarkar, and J. Yan. 2003. Force-extension behavior of folding polymers. *The European physical journal. E, Soft matter*. 10:249–63.

[41] Dorigo, B., T. Schalch, A. Kulangara, S. Duda, R. R. Schroeder, and T. J. Richmond. 2004. Nucleosome arrays reveal the two-start organization of the chromatin fiber. *Science (New York, N.Y.)*. 306:1571–3.

[42] Kimura, H., and P. R. Cook. 2001. Kinetics of core histones in living human cells: little exchange of H3 and H4 and some rapid exchange of H2B. *The Journal of cell biology*. 153:1341–53.

[43] Jamai, A., R. M. Imoberdorf, and M. Strubin. 2007. Continuous histone H2B and transcription-dependent histone H3 exchange in yeast cells outside of replication. *Molecular cell*. 25:345–55.

[44] Koopmans, W. J. a., R. Buning, T. Schmidt, and J. van Noort. 2009. spFRET using alternating excitation and FCS reveals progressive DNA unwrapping in nucleosomes. *Biophysical journal*. 97:195–204.

[45] Poirier, M. G., E. Oh, H. S. Tims, and J. Widom. 2009. Dynamics and function of compact nucleosome arrays. *Nature structural & molecular biology*. 16:938–44.

[46] Kruithof, M., F. Chien, M. de Jager, and J. van Noort. 2008. Subpiconewton dynamic force spectroscopy using magnetic tweezers. *Biophysical journal*. 94:2343–8.

[47] Klaue, D., and R. Seidel. 2009. Torsional Stiffness of Single Superparamagnetic Microspheres in an External Magnetic Field. *Physical Review Letters*. 102:028302.

[48] De Vlaminck, I., T. Henighan, M. T. J. van Loenhout, D. R. Burnham, and C. Dekker. 2012. Magnetic forces and DNA mechanics in multiplexed magnetic tweezers. *PloS one*. 7:e41432.

[49] Carter, B. C., M. Vershinin, and S. P. Gross. 2008. A comparison of step-detection methods: how well can you do? *Biophysical journal*. 94:306–19.

Chapter 4

Torsional stress controls the folding and unfolding of the chromatin fiber[1]

In eukaryotic cells, DNA exists as chromatin fibers with different degrees of compaction. Folding and unfolding of chromatin plays a key role in gene regulation. However, the structural changes of a compacted chromatin fiber induced by torsional stress are poorly understood. Here we studied the stability of single supercoiled chromatin fibers, reconstituted on tandem repeats of 601 nucleosome positioning sequence. By applying tension and torsion with magnetic tweezers, we find that the fiber has a strong asymmetric response to supercoiling. Negative supercoiling stabilizes the fiber against unfolding. Positive supercoiling can be absorbed by the fiber. This anisotropy of the fiber reflects the chirality of a left-handed helix. When the force exceeds ~2.5 pN, the fiber unfolds, unwrapping one turn of DNA. The level of unfolding is regulated by supercoiling. An equilibrium statistical mechanics model based on chromatin topology and elasticity is presented, which captures the full complexity of chromatin folding and unfolding at different degrees of supercoiling. These results reveal for the first time the effects of supercoiling on a folded chromatin fiber and present a new quantitative model of chromatin supercoiling.

---

[1]The contents of this chapter are based on : H. Meng and J. van Noort. "Torsional stress controls the folding and unfolding of the chromatin fiber", manuscript in preparation.

4.1 Introduction

In eukaryotic cells, genomic DNA is organized in chromatin, a DNA-protein complex which results in a formidable compaction of DNA in the nucleus. The basic unit of chromatin is the nucleosome. Both the structure of DNA and the structure of nucleosome are known from X-ray crystallography. DNA forms a right-handed helix with 10.4 basepairs (bp) per helical turn [1]. The nucleosome consists of 147 bp of DNA wrapped 1.7 times around a wedge-shaped octamer of histone proteins in a left-handed superhelix [2]. Nucleosomes are connected by short DNA segments (linker DNA), typically 10 to 90 bp long, forming an array of nucleosomes with a diameter of about 10 nm. These arrays are thought to fold into chromatin fibers by short-range interactions between neighboring nucleosomes. In vitro, under physiological salt conditions, these fibers thicker fibers have a diameter of 30 nm, and are commonly known as the 30-nm fiber [3]. However, the higher order structure of the 30-nm fiber is controversial.

It is becoming clear that native chromatin structures are not nearly as uniform as those formed by reconstitution in vitro [4]. The structure of the chromatin fiber is sensitive to the length of linker DNA, the salt conditions, histone modifications and linker histones [5, 6]. Understanding chromatin structure is therefore complicated and it is unlikely that a "one-model-fits-all" solution to the problem exists. Furthermore, recent studies suggest that there may not be an higher order structure such as the 30-nm fiber but that chromatin in vivo rather folds into 10-nm fibers [7–9]. Chromatin compaction modeling work based on Hi-C data unfortunately doesn't have the resolution to reveal such details [10, 11]. These studies demonstrated, by modeling, that chromatin compaction as measured by Hi-C techniques is insensitive for changes of the model from a 10-nm fiber to a 30-nm fiber.

The function of chromatin is not only to compact DNA, but also to control gene regulation. Transcription regulation involves next to a plethora of post transcriptional modifications and chromatin remodellers [12] also the effects of supercoiling [13]. During transcription, RNA polymerase (RNAP) generates large torsional stress on DNA, which is estimated to be seven DNA supercoils per second [14]. A common model to describe the RNAP elongation is the "twin supercoiled domain" model, in which the RNAP moves along the DNA helix and generates positive supercoiling (overwound DNA) ahead and negative supercoiling (underwound DNA) behind [15]. Following this model, one hypothesis [16, 17] is that positive supercoiling ahead of the RNAP will

destabilize nucleosomes, and negative supercoiling behind it will promote reassembly of nucleosomes. Recently, a psoralen based cross-linking technique was introduced to measure the local DNA supercoiling density genome wide [18, 19]. These results clearly show that the genome has separate domains with various degrees of supercoiling, supporting the idea that supercoiling is dependent on transcription, with active genes being more negatively supercoiled than inactive genes. High-resolution genome-wide nucleosome mapping also [17] suggest indirectly that positive torsional stress contributes to such destabilization of nucleosomes. However, there is no direct data on how a chromatin fiber responds to supercoiling.

Single-molecule techniques such as magnetic and optical tweezers provide powerful tools to study the effects of supercoiling. The effect of supercoiling on naked DNA is widely studied, and so is the mechanism of transcription on bare DNA [20]. However, in vivo, RNAP encounters DNA folded into chromatin fibers consisting of arrays of nucleosomes rather than naked DNA. Hence, the effects of supercoiling have to be considered in the context of chromatin, but this is poorly understood so far [21]. A recent study demonstrated the mechanical stability of single nucleosomes under torsion [22]. Interestingly, torque was shown to have only a moderate effect on nucleosome unwrapping. The chromatin fiber's response to torque may be quite different. Though supercoiling effects on chromatin fibers were first investigated at forces below 0.5 pN [23, 24], which is significantly lower than the DNA unwrapping force about of 3~5 pN, these experiments could therefore not reveal the effect of torque on nucleosome unwrapping. Moreover, these experiments were done at salt conditions much lower than physiological buffer conditions. The data was interpreted as a chiral transition from a left-handed nucleosome to a right-handed reversome. Because of the buffer conditions, these results could not show how folded chromatin fibers unfold by supercoiling and therefore neglected all nucleosome-nucleosome interactions.

Previously, we showed that the chromatin fibers reconstituted on the 601 sequence repeats with 50 bp linker DNA fold in accordance with the one start solenoid model [25]. Although the model has been questioned [26], one needs additional, more detailed data to resolve this discussion. The chirality of such a solenoidally folded fiber has direct implications on the mechanical properties of the fiber. Here we focus on the effects of supercoiling on the stability of the higher order structure of the fiber. We performed a comprehensive investigation of force spectroscopy on torsionally constrained chromatin fibers, under physiological buffer conditions and at different degrees of su-

percoiling. The torsionally constrained fiber has an anisotropic response to torsion. We show that the fiber does not unfold until forces exceed 2.5 pN, and has an end-to-end distance which corresponds to the fiber being stretched to a single file of stacked, interacting nucleosomes. Above this force, the unfolding of the fiber depends on the degree of supercoiling. Positive supercoiling facilitates the unfolding, but superfluous positive supercoiling refolds the fiber. We developed a torsional spring model for the chromatin fiber that captures the anisotropy of the fiber to supercoiling. We demonstrate that the chromatin fiber folds in a left-handed helix. Interestingly, this interpretation is consistent with very early diffraction studies of the fiber's chirality [27]. Our model captures all unfolding and refolding events in a quantitative manner. These findings give a detailed structural insight in how a chromatin fiber responds to supercoiling and directly test the "twin supercoiled model", yielding a better understanding of the role of chromatin during transcription.

4.2 Results

4.2.1 Torsionally unconstrained chromatin fibers

Before describing the structural changes in a chromatin fiber under torsional stress, we first review the elasticity of torsionally unconstrained chromatin fibers. A force-extension (F-E) curve of a torsionally unconstrained chromatin fiber reconstituted with 25 nucleosomes is shown in Fig. 4.1A. The fiber has about 1 kb of DNA handles on each side of the chromatin fiber. At low forces (F < 0.5 pN), the largest part of the increase in extension is due to the entropic elasticity of these DNA handles [28, 29]. A linear increase in extension is observed at intermediate forces (0.5 pN < F < 2.5 pN). In this part of the F-E curve, the elasticity of the fiber can be described by a Hookean spring [25]. Near 3 pN, a force plateau occurs, as nucleosomes in the fiber unfold into an array of singly wrapped nucleosomes (Fig. 4.1B).

The entire F-E curve can be described by a statistical mechanics model that takes into account the elasticity of the DNA and chromatin fiber, as well as the conformational changes of the nucleosomes, as shown before. In Chapter 3, we show that an intermediate state of the nucleosome between the unfolded fiber and the fully unwrapped nucleosome exists. To simplify the analysis, we combine these two conformations in a single transition. Fitting this model to the data yields a stretch modulus of the fiber,

$s_f \approx 0.5 \, pN$, an unfolding energy $G_u \approx 18.5 \, k_B T$ and an elongation per unfolded nucleosome of 20 nm, corresponding to DNA unwrapping of about 58 bp. All the parameters are scaled per nucleosome and are summarized in Table 4.1.

4.2.2 Torsionally constrained chromatin fibers

Figs. 4.1C and 1E show the F-E curves for a chromatin fiber containing 25 nucleosomes, similar to the fiber in Fig. 4.1A, but torsionally constrained by multiple bonds between the DNA and the bead and the glass surface. Interestingly, compared to the torsionally unconstrained chromatin fiber, at ΔLk = 0, no force plateau occurs around 3 pN, but the extension increases linearly up to 4 pN. When decreasing the excess linking number from ΔLk = 0 to ΔLk = −20, the extension of the fiber decreased at forces below 1.8 pN. Between 1.8 pN and 4 pN, the extension increased linearly with force, independent of ΔLk.

To understand the response of folded chromatin fibers to supercoiling, it is important to separate the changes in extension of the DNA handles from the compliance of the fiber itself. F-E curves of bare DNA without nucleosomes are shown in Fig. S1 as comparison. Negative supercoiling results in plectonemes in the DNA, which reduce the extension of the tether [30, 31]. Like in the case of a bare DNA molecule, we observe a reduction of the extension of the fiber. This should be attributed mostly to the response of the DNA handles supercoiled into plectonemes. This plectonemic DNA transfers into melted and twisted DNA when increasing the force up to 1.8 pN. The net result is an extension that is equivalent to that of torsionally unconstrained DNA. Apparently, the DNA handles, rather than the fiber, absorb negative supercoiling.

Interestingly, when positive twist is applied, we observed hardly any change in extension compared to the torsionally unconstrained chromatin fiber at forces below 2.5 pN. This is remarkable because the presence of a 25 nucleosomes chromatin fiber, appears to prevent the 2 kb of DNA handles to form plectonemic DNA, as it does for negative twist. Above 2.5 pN, the force plateau, which is indicative of fiber unfolding, appears as more positive twist is applied, like in the case of torsionally unconstrained fibers. A maximum extension occurs at ΔLk = 20. When more twist is applied, the extension of the plateau reduces again, which is, as we will show below, due to fewer nucleosomes unfolding.
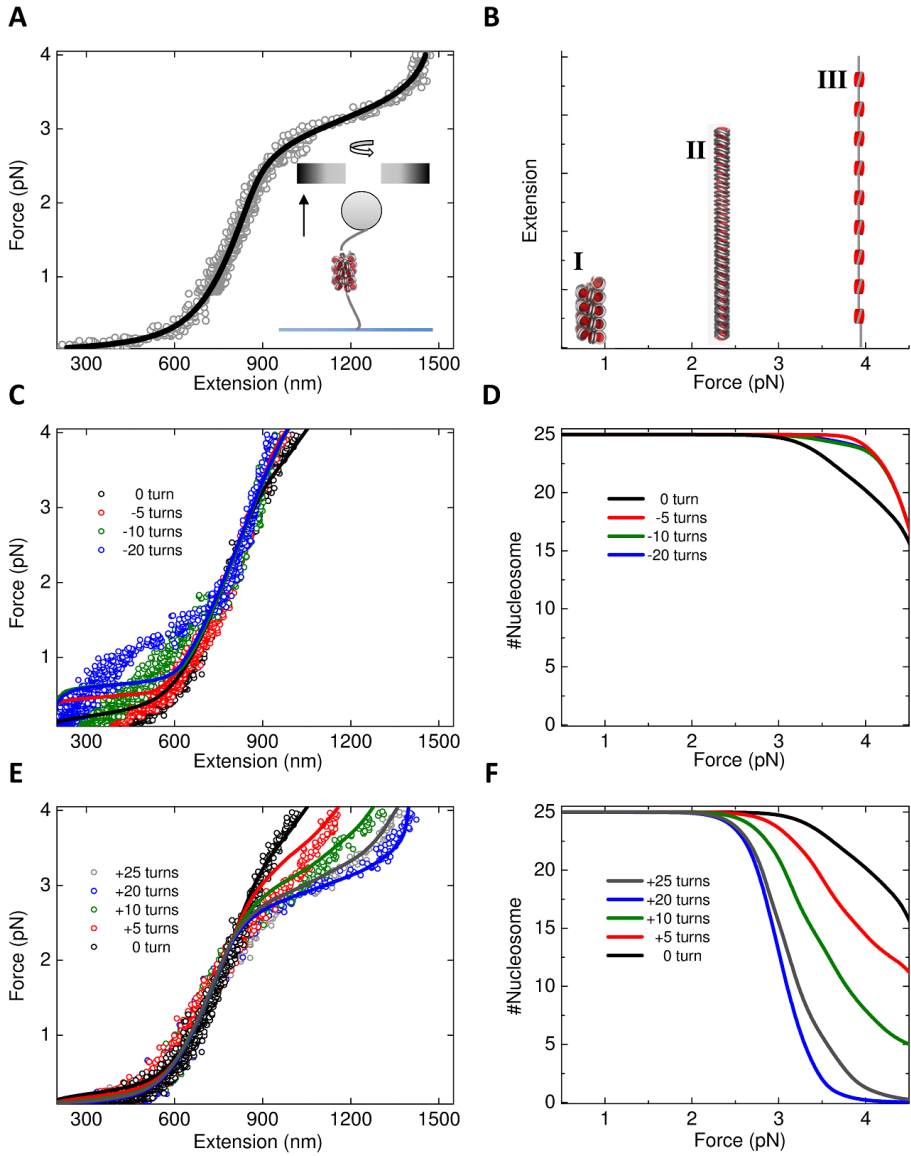
Figure 4.1: Pulling single torsionally (un)constrained chromatin fibers. (A) Force-extension curve for a torsionally unconstrained chromatin fiber reconstituted with 25 nucleosomes. The solid line is a statistical mechanics model that describes the fiber as a Hookean spring and the DNA handles as a Worm-like-chain (see Supplemental Information). Inset: Experimental setup: a single compacted chromatin fiber with DNA handles (~ 1 kb each), is tethered between a 1 μm bead and a cover-glass. Tension and torsion on the fiber is controlled by moving or rotating the magnets above the bead. (B) Schematic illustration of a chromatin fiber's conformational changes with increasing tension. I: low force regime, nucleosomes are folded into a 30-nm fiber; II: intermediate force regime, the fiber is stretched to a single stack of nucleosomes; III: high force regime, the fiber unfolds to form an array of nucleosomes that have only a single turn of wrapped DNA. (C) Force-extension curves for a single torsionally constrained chromatin fiber with 25 nucleosomes at various degrees of negative supercoiling (dots). The solid lines are global fits to Equation 4.6. (D) The number of folded nucleosomes calculated by the model as a function of force under negative supercoiling. (E) Force-extension curves for the same fiber at various degrees of positive supercoiling. Global fits are drawn with solid lines. (F) The calculated number of folded nucleosomes under positive supercoiling.

Thus, excess positive supercoiling appears to be absorbed by the fiber, whereas negative supercoiling stabilizes the fiber's structure. Positive supercoiling can be stored in the fiber at low forces, and restores chromatin fiber unfolding at high forces in torsionally constrained fibers. These are clear indications that the fiber is not folded in an isotropic structure, but rather displays features that point to a left-handed superhelix that can handle some undertwisting, but cannot be over-twisted.

4.2.3 A quantitative statistical mechanics model for unfolding a supercoiled chromatin fiber

To quantify the interpretation above, we extended our statistical mechanics model for a torsionally unconstrained chromatin fiber. We consider a Hookean torsional spring, yielding an elastic energy G_{fiber} [28, 32, 33]:

$$G_{fiber} = \frac{1}{2} \frac{s_f}{Nz_f^o} \left(\Delta z_{fiber} \right)^2 + \frac{1}{2} \frac{c_f}{Nz_f^o} \left(2\pi Lk_{fiber} \right)^2 + \frac{g_f}{Nz_f^o} \left(\Delta z_{fiber} \right) \left(2\pi Lk_{fiber} \right) \quad (4.1)$$

where s_f is the stretch modulus of the fiber; c_f is the twist modulus, and g_f is the twist-stretch coupling factor. N is the total number of fully folded nucleosomes and

z_f^o is the length of fiber in the absence of force, which is about 1.7 nm per nucleosome [5, 34]. Δz_{fiber} is the extension change of the fiber by pulling and twisting. The total extension of the folded fiber is $z_{fiber} = Nz_f^o + \Delta z_{fiber}$. Lk_{fiber} is the linking number of fiber. The force and torque on the fiber are calculated from the derivative of the free energy to the extension and to the linking number [35]:

$$F = \frac{s_f}{Nz_f^o}\Delta z_{fiber} + \frac{g_f}{Nz_f^o}\left(2\pi Lk_{fiber}\right)$$
$$\Gamma_{fiber} = \frac{c_f}{Nz_f^o}\left(2\pi Lk_{fiber}\right) + \frac{g_f}{Nz_f^o}\Delta z_{fiber} \tag{4.2}$$

The entire tether in our experiment consists of a part of chromatin fiber and a part of DNA handles. The mechanical properties of the DNA handles (free energy G_{DNA}, extension of DNA z_{DNA}, and the torque Γ_{DNA}) are described by twisted, plectonemic and melted conformations [36] (see Supplemental Information). The excess linking number of the tether is distributed between the two parts, with the torque considered equal in both parts of the tether. To capture the anisotropy of the fiber in response to twist, we include a linking number Lk_{fiber}^o per nucleosome, yielding a total twist in the fiber,

$$Lk_{fiber} \quad = \quad N \times Lk_{fiber}^o + \Delta Lk_{fiber} \tag{4.3}$$

Combining Equation 4.2 , 4.3 and the elasticity of DNA (details in Supplemental Information) yields the elastic response of a DNA-fiber tether:

$$z(F, \Delta Lk, N) = z_{DNA}(F, \Delta Lk_{DNA}) + z_{fiber}(F, \Delta Lk_{fiber}, N), \tag{4.4}$$

for forces small enough not to rupture the fiber.

The force-induced rupturing of the nucleosomes in the fiber yields nucleosomes with one turn wrapped of DNA. The linking number that is constrained by the nucleosome in the fiber will redistribute along the tether when such a rupture event takes place. The elasticity of the resulting unfolded nucleosome is defined by the linker DNA plus the length of DNA that is released from the nucleosome. In addition, an amount of free energy G_u for each nucleosome is released when nucleosome-nucleosome and nucleosome-DNA interactions break. Note that we describe the unfolding of the fiber as a single transition, as opposed to our previous modeling, in order to keep the model as simple as possible. We can numerically calculate the partition function for a finite number of nucleosomes:

$$Z = \sum_{i=0}^{N} \left(\begin{array}{c} N \\ i \end{array} \right) exp\left(-\frac{G_{DNA} + G_{fiber} + iG_u - Fz(F, \Delta Lk + iLk_{fiber}^{o}, i)}{k_B T}\right), \quad (4.5)$$

i is the number of nucleosomes that is unfolded, and $\left(\begin{array}{c} N \\ i \end{array} \right)$ is a binomial coefficient that takes the degeneracy of nucleosome unfolding into account. The expected value of total extension at a certain force and an excess linking number is then given by:

$$\langle z(F, \Delta Lk, N) \rangle = Z^{-1} \sum_{i=0}^{N} z(F, \Delta Lk + iLk_{fiber}^{o}, i) \left(\begin{array}{c} N \\ i \end{array} \right) exp\left(-\frac{G_{DNA} + G_{fiber} + iG_u - Fz}{k_B T}\right)$$

$$(4.6)$$

4.2.4   Comparison between data and model

We performed a global fit to our data for forces between 1.0 pN to 4.0 pN, and excess linking numbers ΔLk ranging from -5 to 25. The elastic parameters of the chromatin fiber were fit and those of DNA were fixed to known values.(solid lines in Figs. 4.1C and E). We obtain s_f = 0.48 ± 0.02 pN, c_f = 3.4 ± 0.2 pN nm², g_f = 0.03 ± 0.01 pN nm. An unfolding energy G_u = 17.80 ± 0.04 $k_B T$ was found, very similar to that of a torsionally unconstrained fiber, shown in Fig. 4.1A. The linking number per nucleosome yields Lk_{fiber}^{o} = −0.81 ± 0.01. Our model also recovers the number of folded nucleosomes at different forces and excess linking numbers. It can be seen in Figs. 4.1D and F that all the nucleosomes stay in the folded conformation at F< 2.5 pN. The change in extension of the tether at forces larger than 2.5 pN can be attributed to an increase in the number of unfolded nucleosomes. Interestingly, adding more positive supercoiling (ΔLk > 21 for 25 repeats) reduces the extension of the tether, suggesting that fewer nucleosomes unfold when excessive positive supercoiling is applied.

At low forces (F< 1.0 pN) and negative supercoiling, the model deviates from the data. This is remarkable as we obtain very good agreement between data and model for bare DNA (see Fig. S1). The reduced extension that we observe for low forces and negative supercoiling may indicate a more complex interplay among fiber structure, plectonemes and melting bubbles in the DNA handles. Apart from this small region in force and excess linking number, we obtain an excellent agreement between the model

	Linking number per basepair/ nucleosome Lk^0	Stretch modulus s (pN)	Twist-stretch coupling g (pN nm)	Twist modulus c (pN nm²)	Unfolding energy G_u (k$_B$T)
B-DNA	0.1	1000	-90	440	----
25x 197 torsionally unconstrained	----	0.46±0.05	----	----	18.31±0.04
(25x197) global	-0.81±0.01	0.48±0.02	0.03±0.01	3.4±0.2	17.80±0.04
(15x197) global	-0.86±0.01	0.51±0.04	-0.02±0.01	3.0±0.3	18.40±0.03

Table 4.1: Comparison of the elastic parameters of DNA (F<30 pN) from [32, 37, 38], with those of torsionally unconstrained chromatin fibers (25 repeats), and torsionally constrained chromatin fibers (25 nucleosomes and 15 nucleosomes).

and the data.

4.2.5 Extension-twist curves

Besides pulling the chromatin fiber at constant excess linking numbers, we also twisted the fiber at constant forces similar to experiments by Bancaud et al. [23, 24], but now under conditions that favour higher order folding of chromatin. A comparable response of the fiber to force and twist is evident in the Extension-Twist (E-T) curves, shown in Fig. 4.2A. At high force (F=3.4 pN), the fiber's extension hardly changes under negative twist, whereas under positive twist, the extension first increases and reaches a maximum value at ΔLk = 21 , and subsequently decreases symmetrically. At an intermediate force (F=1.8 pN), the extension hardly changes under both negative and positive twist in the range of $-20 < \Delta Lk < 40$. At low force (F=0.4 pN), fiber shortenes with negative twist, whereas under positive twist, the extension remains constant up to 30 turns. After 30 turns, a decease in extension occurs with a slope similar to that at negative twist.

When we plot the E-T curves calculated with our model, we obtain excellent agreement at F > 1.8 pN. Again, the data can be interpreted as the unfolding of the fiber at sufficient positive twist. Like in the pulling experiment, in the twisting experiment the calculated number of unfolded nucleosomes (Fig. 4.2C) indicates that the nucleosomes
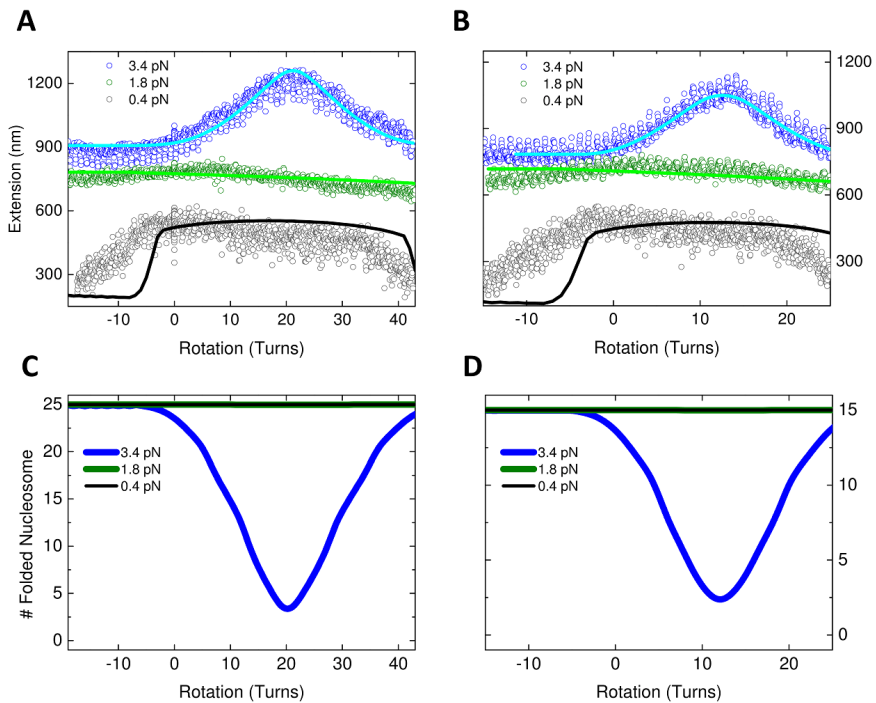
Figure 4.2: Extension versus twist data (dots) at constant force, together with the calculated extension using the parameters from the global fit to the F-E curves shown in Fig. 4.1 and Fig. S3 (solid lines). (A) Fiber reconstituted with 25 nucleosomes. (B) Fiber reconstituted with 15 nucleosomes. (C) and (D) are the calculated number of folded nucleosomes corresponding to (A) and (B).

first unfold from the fiber by increasing positive twist, and subsequently refold when additional positive twist is applied. At 0.4 pN, however, we observe the same discrepancy at negative twist that we found in the F-E data.

Experimental data of the chromatin fiber reconstituted on 15 repeats shows a similar response to force and twist (shown in Fig. 4.2B, Fig. S2,3). The global fit parameters of 15 repeats obtained from the F-E curves are very close to those found for 25 repeats (shown in Table 4.1), which indicates that the model properly takes the number of nucleosome into account. Overall, we get a good agreement between our model and the data, showing that the folded chromatin fiber can be described by a torsional spring with a left-handed chirality. Moreover, the effect of supercoiling on the stability of the fiber is accurately described by taking the mechanical and thermodynamical properties of such a torsional spring and of DNA into account.

4.2.6   Salt effects

In vitro studies have shown that the compaction of chromatin requires divalent ions [3]. We tested the influence of Mg^{2+} on the elasticity of torsionally constrained fibers. All the experiments done in 100 mM K^+, 2 mM Mg^{2+} , the E-T curves at F=0.5 pN show that forward twisting (adding excess linking numbers) and backward twisting (reducing excess linking numbers) curves overlap, indicating that all deformations of the fiber are reversible (Fig. 4.3A). When depleting Mg^{2+} the E-T curves at 0.5 pN hardly change (Fig. 4.3B). This indicates that the structure of the folded fiber is stable, and that Mg^{2+} depletion barely influences the mechanical properties of the folded fiber at low force.

The F-E curves for pulling and releasing at constant linking numbers also overlap in pulling experiments in buffers containing Mg^{2+}, (shown in Fig. 4.3C). This absence of hysteresis indicates that the fiber is in equilibrium during the folding and unfolding events. When the Mg^{2+} is depleted (Fig. 4.3B), F-E curves at ΔLk = 0 are hardly affected. F-E curves start to differ however, when positive twist is applied. The unfolding transitions above 2.5 pN in Mg^{2+} depleted buffer, show large hysteresis, indicating that an unfolded fiber refolds more slowly than it unfolds without Mg^{2+}. Thus, the effects of torsion are more persistent in the absence of Mg^{2+} .
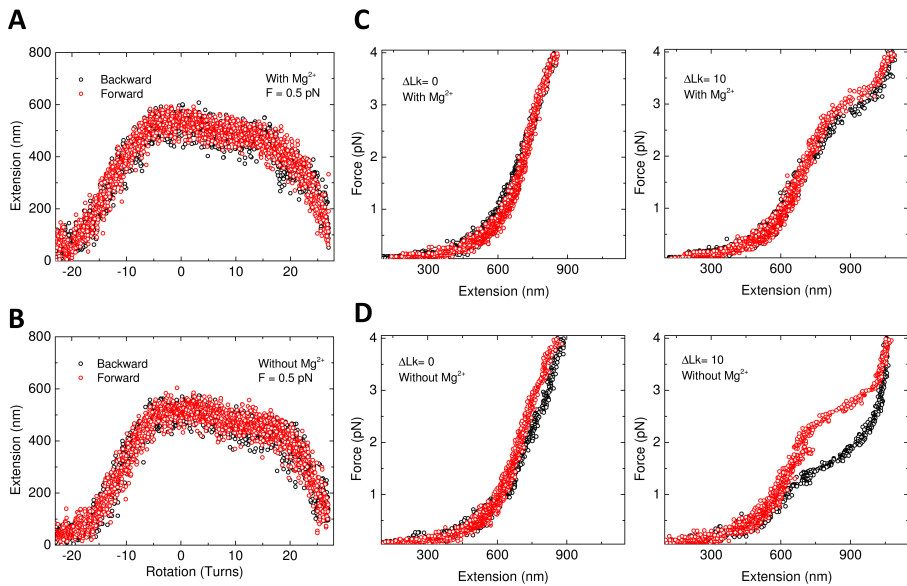
Figure 4.3: Salt dependence of chromatin fiber folding (15 nucleosomes) at different degree of supercoiling. Twist-Extension curves of the fiber at 0.5 pN, with (A) and without Mg^{2+}(B). Both curves show no hysteresis between forward twisting (adding excess linking numbers) and backward twisting (reducing excess linking numbers), indicating that depletion of Mg^{2+} doesn't induce structural changes at this force regime. (C) Pulling and releasing the fiber in 100 mM K^+ and 2 mM Mg^{2+}. The pulling and release traces overlap, indicating the folding and refolding is in equilibrium. (D) Replacing the buffer with 100 mM K^+ without Mg^{2+}. The pulling and release curves show large hysteresis, and irregular refolding and unfolding of the fiber.

4.3   Discussion and conclusions

In this work, we describe the anisotropic elastic response of torsionally constrained chromatin fibers, and quantify this response using a torsional spring model. In combination with the statistical mechanics describing the unfolding of the chromatin fiber, we found that the Hookean torsional spring model accurately describes the fiber's force-dependent extension, regardless of the total number of folded nucleosomes. The obtained fit parameters give a more detailed insight to the structure of chromatin fiber. A linking number per nucleosome $Lk_{fiber}^{o} \simeq -0.8$ indicates that chromatin fiber has a left-handed chirality.

To evaluate the role of higher order folding of the chromatin fiber, this number can be compared to the amount of supercoiling that is constraint in a single nucleosome. Though one nucleosome contains 1.7 turns of DNA, the linking number of a single nucleosome is only -1 [39, 40]. This difference is known as the linking number paradox [41]. Thus, the contribution of unwrapping the first turn to the change in the linking number is about -0.4. The rest of Lk_{fiber}^{o} must therefore be attributed to the higher-order structure of fiber that is stabilized by nucleosome-nucleosome and nucleosome-DNA interactions. Our model does not yield a satisfactory global fit to the data if we reduce the excess linking number Lk_{fiber}^{o} in the free energy term in Equation 4.1 and 4.5 to -0.4. Having two turns per five nucleosomes in the folded chromatin fiber, however, seems excessive. Modeling and EM reconstructions rather suggest about seven nucleosomes per helical twist in a solenodial fiber, yielding $Lk_{fiber}^{o} \simeq 0.14$. The remaining part could easily be maintained by undertwisting the linker DNA, which would lead to a twist density of -0.05 $(-(0.4 - 0.14)/(50/10.4))$. This is close to the twist densities that are found in vivo. The quantification of the excess linking number that we describe here is therefore fully compatible with a solenoid folding of the chromatin fiber with 50 bp linker DNA.

It is informative to compare our measured elastic parameters of torsionally constrained chromatin fibers with bare DNA and torsionally unconstrained chromatin fibers (Table 4.1). Both the stretch and twist modulus of the folded chromatin fiber are dramatically smaller than those of bare DNA. The small twist modulus, which is about hundred times smaller than that of DNA, implies that a chromatin fiber is very soft and it can absorb large twists without building up much torque. The twist-coupling factor g_f obtained here is a very small number, comparable to the uncertainty in the fit.

This suggests that in this force regime (F<4.0 pN), there is no significant twist-stretch coupling. The low stretch and twist modulus of the fiber that we report here, suggests that large changes in extension and linking number can readily be absorbed by neighboring chromatin within single topological domain. Thus excessive stresses may be effectively prevented by the soft chromatin fiber.

The unfolding energy G_u captures the unfolding transitions of a torsionally constrained fiber in a wide range of twist densities. Moreover, this energy is close to the value that is obtained in independent experiments with torsionally unconstrained chromatin fibers. This indicates that the energy barrier of a nucleosome between the folded and unfolded state of a nucleosome is independent of torsional stress. The change in rupture force that we report here can therefore be fully attributed to the energy associated with twisting the DNA. Recent measurements on the effect of torque on the stability of a mononucleosome [22] qualitatively show that the rupture force for the first turn unwrapping event is increased by positive torque. We tested if our model can quantitatively explain these experimental results. By replacing the fiber with a single nucleosome, leaving out the chirality, the stretch and the twist modulus of the fiber, and simply considering a constant unfolding energy G_u, we are able to reproduce the rupture force-torque relation similar to the experimental results (shown in Fig. S4). This reinforces our model in which we have a strict mechanical coupling between the nucleosomes, and the linker and handle DNA.

In this study we used highly regular, homogeneous chromatin fibers that are known to fold in regular 30-nm structures. In vivo, chromatin is likely to be far less structured, and the existence of such fibers is still heavily debated. We note that all the interactions that we describe here are between neighboring nucleosomes and the unfolding mechanism seems to be conserved over a wide range of linker DNA (20, 55 bp, data not shown). This lack of cooperativity, as demonstrated by the independence of the thermodynamical parameters on the number of nucleosomes in the fiber, indicates that these results can be applied to any pair of nucleosomes. Having a regular chromatin fiber greatly facilitates the interpretation of these nano-mechanical measurements, but we expect that the described mechanical coupling and interaction energies can also be applied to pairs of nucleosomes in irregular chromatin fibers.

Our experiments are conducted under moderate tension and torsion with force smaller than 4 pN, and excess linking number $|\Delta Lk| < 2$/nucleosome. Under more ex-

treme stresses conditions, the nucleosome may respond with various chiral transitions [24]. Furthermore, DNA with positive twist and forces larger than 3 pN may transfer into a new conformation, P-DNA [42]. The force and twist regime that we describe here is highly relevant for the situation in vivo. The activity of molecular motors, such as RNAP leads to the build up of torsional stress on the DNA. It has been speculated that this stress involves the disassembly and reassambly of chromatin [16, 17], and therefore may be a critical factor to regulate gene transcription. Previous studies reported that RNAP can overcome the obstacle of a nucleosome at F~4 pN under torsionally unconstrained conditions [43, 44]. According to the "twin supercoiled domain model" [15], RNAP generates positive twist ahead of transcription direction and negative twist behind. In our experiments, we show that positive supercoiling is readily absorbed by the fiber, which subsequently facilitates fiber unfolding. On the other hand, we show that negative twist can refold and stabilize the fiber. Interestingly, excessive positive twist will drive the nucleosome to refold. This might play a role in the transcription termination in eukaryotes, which is currently poorly understood [45].

In summary, we accurately quantified the elastic properties of a well-defined, folded, torsionally constrained chromatin fiber. The data and modelling suggests that the chromatin fiber folds into a left-handed helix. Both observations support the anticipated role of the "twin supercoiled domain model" in chromatin maintenance. It even suggests that higher-order folding of the fiber may contribute to reinforce this effect. Its anisotropic response to supercoiling may have important implications for all processes involving DNA during the cell cycle.

4.4   Materials and methods

4.4.1   Magnetic tweezers

The home-built magnetic tweezers was described before by Kruithof et al.[46]. During an experiment a DNA or chromatin molecule was constrained between the end of a superparamagnetic bead with diameter of 1 μm and the surface of a microscope coverslip. Tension and torsion on the fiber are manipulated by the pair of magnets. Moving the magnets up and down changes the force on the bead. Rotating the magnets changes the degree of supercoiling, i.e., the excess linking number (ΔLk). Each turn changes ΔLk by ±1. Supercoiling was induced by rotating the magnets at 1 turn/s. The extension of DNA was measured in real time at a frame rate of 60 Hz with a CCD camera (Pulnix TM-6710CL). No averaging or filtering was used. During experiments, we first twisted

a fiber at low force (0.05 pN) to a desired ΔLk, and then pulled on the fiber. Alternatively, we moved the magnets to a certain position [46] and measured extension versus ΔLk at constant force.

4.4.2   Chromatin constructs

Two DNA constructs with 25 or 15 tandem repeats of the 601 sequence were used based on Puc18 (A gift from D. Rhodes, Singapore). Both plasmids were digested with BsaI and BseYI yielding linear fragments of 2410 and 6960 bp with corresponding sticky ends. Digoxigenin and biotin-labeled handles were produced with PCR using 10% biotin-dUTP and digoxigen-dUTP on the pGem-3Z template using the following primers: 5' GAT AAA TCT GGA GCC GGT GA 3' and 5' CTC CAA GCT GGG CTG TGT 3'. After PCR amplification, the fragments were digested with BsaI and BseYI and ligated to the previously digested DNA 601 array. The ligation product was mixed with competitor DNA (-147 bp) and histone octamers purified from chicken erythrocytes, and reconstituted into chromatin fibers using salt dialysis [47].

4.4.3   Sample preparation

A clean cover slip was coated with 1% polystyrene-toluene solution. The cover slip was then mounted on a poly-di-methysiloxane (PDMS, Dow Corning) flow cell containing a $10 \times 40 \times 0.4$ mm flow channel. The flow cell was incubated with 1 μg/ml anti-digoxigenin for 2 hours and 2% BSA (w/v) solution over night. 20 ng/ml DNA folded into chromatin in 10 $mM\ Hepes$, pH 7.6, 100 $mM\ KAc$ and 10 $mM\ NaN_3$ was flushed into the flow cell and incubated for 10 minutes, followed by flushing in 1 μm streptavidin-coated superparamagnetic microspheres (MyOne, Invitrogen) diluted one thousand times in the same buffer. After 10 minutes excess beads were flushed away using the same buffer.

4.5 Supplemental Information

4.5.1 Variables and derived expressions

Below, we use the following parameters to describe the mechanical properties of DNA:

F = Force;

A_t = Bending persistence length (50 nm for twisted DNA);

$k_B T$ = Thermal energy;

$C_t = C \left(1 - \frac{C}{4A_t} \sqrt{\frac{k_B T}{A_t F}} \right)$ = Twist persistent length as a function of force (twisted DNA), with constant C = 100 nm;

C_p = Twist persistent length of plectonemic DNA (24 nm for plectonemic DNA);

L_o = Contour length;

$g = \left(F - \sqrt{\frac{F k_B T}{A_t}} \right)$ = Free energy per nm of torsionally unconstrained DNA.

4.5.2 Elasticity of supercoiled DNA

A supercoiled DNA molecule can be described by 3 different conformations, i.e, twisted, plectonemic, and melted states. The free energy of twisted DNA is given by a parabola function ($G'_{DNA} = G_{DNA} - F z_{DNA}$) [35, 48] :

$$G'_{DNA} = L_o \left(-g + \frac{k_B T C_t}{2} \left(\frac{2\pi \Delta Lk_{DNA}}{L_o} \right)^2 \right). \tag{4.7}$$

The extension of twisted DNA is calculated by taking the derivative of free energy to force:

$$z_{DNA} = -\frac{dG'_{DNA}}{dF} = L_o \left(1 - \frac{1}{2}\sqrt{\frac{k_B T}{A_t F}} - \frac{C^2}{16} \left(\frac{2\pi \Delta Lk_{DNA}}{L_o} \right)^2 \left(\frac{k_B T}{A_t F} \right)^{\frac{3}{2}} \right). \tag{4.8}$$

As twist is applied to the DNA, the restoring torque will increase linearly with the excess linking number it absorbed, before any conformational changes:

$$\Gamma_{DNA} = C_t \frac{2\pi \Delta Lk_{DNA}}{L_o} k_B T. \tag{4.9}$$

4.5.3 Positive supercoiling: plectonemic and twisted DNA

DNA under positive twist can be overwound, staying in a twisted conformation or transform into plectonemic conformation. An analytical solution yielded a constant torque when the DNA buckles into plectonemic states [35]:

$$\Gamma_c^+ = \sqrt{\frac{2k_B T C_p g}{1 - C_p/C_t}}.$$ (4.10)

The maximum linking number that can be absorbed by DNA before conformation change is then:

$$\Delta Lk_{\max}^+ = \Gamma_c^+ L_o / \left(2\pi k_B T C_t \right)$$ (4.11)

The total extension of DNA after buckling decreases linearly by increasing linking numbers, the slope in nm/turn is given by [35, 37]:

$$\Delta z_{DNA} = \frac{2\pi \left[1 - \frac{1}{2}\sqrt{\frac{k_B T}{A_t F}} - \frac{C^2}{16 C_t^2} \left(\frac{k_B T}{A_t F} \right)^{3/2} \left(\frac{\Gamma_c^+}{k_B T} \right)^2 \right]}{\frac{\Gamma_c^+}{k_B T} \left(\frac{1}{C_p} - \frac{1}{C_t} \right)}$$ (4.12)

The free energy of DNA will increase linearly; the gain in free energy per turn is:

$$\Delta G_{DNA}^+ = 2\pi \Gamma_c^+$$ (4.13)

4.5.4 Negative supercoiling: plectonemic, melted and twisted DNA

DNA under negative twist can stay in the twisted state, or can have conformational change to become melted or pelctonemic DNA. Without the existence of melted DNA, the mechanical properties of negative supercoiled DNA are identical to those for positive supercoiling. When we consider the coexistence of twisted and melted states, the constant torque is limited due to melting [36]:

$$\Gamma_c^- = -11 \ pN \ nm$$ (4.14)

To solve the problem of the different possible conformations of the DNA, we consider two scenarios. If the calculated buckling torque in Equation 4.10 is smaller than the constant torque in Equation 4.14 , then the DNA coexists in twisted and plectonemic states; if the calculated buckling torque in Equation 4.10 exceeds -11 pN nm, DNA

exists in twisted and melted states. The maximum linking number DNA can absorb before conformation change is then:

$$\Delta Lk^-_{\max} = \Gamma^-_c L_{\mathrm{o}} / \left(2\pi k_B T C_t\right) \tag{4.15}$$

The extension of DNA in the melted state is considered as the same as that of twisted DNA under small degrees of supercoiling, due to the small fraction of melted DNA. The free energy of DNA increases per turn:

$$\Delta G^-_{DNA} = 2\pi\Gamma^-_c \tag{4.16}$$

4.5.5   The analytical solution of a DNA-fiber tether

Having discussed the mechanical properties of the torsional spring in the main text, the extension and torque of the fiber are expressed as:

$$\Delta z_{fiber} = \frac{F - g'_f 2\pi Lk_{fiber}}{s'_f}$$
$$\Gamma_{fiber} = c'_f 2\pi Lk_{fiber} + g'_f \Delta z_{fiber} \tag{4.17}$$

Here, $s'_f = s_f / N z^{\mathrm{o}}_f$, $g'_f = g_f / N z^{\mathrm{o}}_f$ and $c'_f = c_f / N z^{\mathrm{o}}_f$. Equaling the torque in the fiber and in the DNA, and considering the total excess linking number is distributed between the DNA and the fiber, we find:

$$\Delta Lk = \Delta Lk_{DNA} + \Delta Lk_{fiber}$$
$$Lk_{fiber} = N \times Lk^{\mathrm{o}}_{fiber} + \Delta Lk_{fiber}$$
$$c'_f 2\pi Lk_{fiber} + g'_f \times \frac{F - g'_f 2\pi Lk_{fiber}}{s'_f} = C_t \frac{2\pi \Delta Lk_{DNA}}{L_{\mathrm{o}}} k_B T \tag{4.18}$$

Solving Equation 4.18 yields

$$\Delta Lk_{DNA} = -\frac{2\pi N s'_f c'_f Lk^{\mathrm{o}}_{fiber} + g'_f \left(F - 2\pi N g'_f Lk^{\mathrm{o}}_{fiber}\right) - 2\pi\left(\left(g'_f\right)^2 - s'_f c'_f\right)\Delta Lk}{2\pi\left(\left(g'_f\right)^2 - s'_f c'_f - \frac{s'_f k_B T}{L_{\mathrm{o}}} C_t\right)}$$
$$\Delta Lk_{fiber} = \Delta Lk - \Delta Lk_{DNA} \tag{4.19}$$

After plectonemic or melted states form in the DNA, we compare Equation 4.19 with Equation 4.11 and 4.15. For large excess linking numbers the torque will stay constant at $\Gamma^{\pm}_c$ and the linking number distribution is then given by:

$$\Delta Lk_{fiber} = \frac{Fg_f' - s_f'\Gamma_c^{\pm}}{2\pi\left(\left(g_f'\right)^2 - s_f'c_f'\right)} - N \times Lk_{fiber}^{o}$$
$$\Delta Lk_{DNA} = \Delta Lk - \Delta Lk_{fiber}$$
(4.20)

The extension of the tether at a certain force and excess linking number can now be calculated as:

$$z(F, \Delta Lk, N) = z_{DNA}(F, \Delta Lk_{DNA}) + z_{fiber}(F, \Delta Lk_{fiber}, N)$$
(4.21)

The extension of DNA is considered for all the three states, twisted, plectonemic and melted states by using Equation 4.8 and 4.12. When the unfolding of the chromatin fiber is considered, as discussed in the main text, the partition function is written in the terms of free energy:

$$Z = \sum_{i=0}^{N} \binom{N}{i} exp\left(-\frac{G_{DNA} + G_{fiber} + iG_u - Fz(F, \Delta Lk + iLk_{fiber}^{o}, i)}{k_B T}\right)$$
(4.22)

One should notice the free energy of the DNA is $G_{DNA} = G_{DNA}' + Fz_{DNA}$ as shown in Equation 4.7. Using the partition function, we calculate the expected values of the parameters that we are interested in.

4.5.6   Supporting figures

A

B
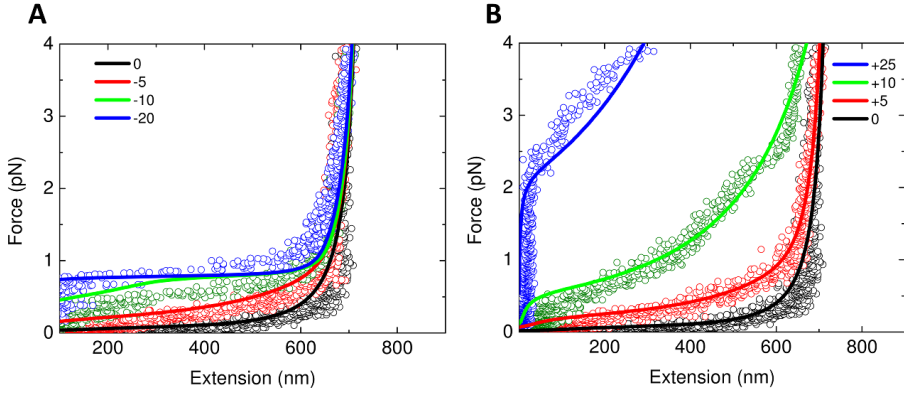
Figure S1

Force-Extension curves of torsionally constrained 2.4 kb DNA under negative super-coiling (A) and positive supercoiling (B). The solid lines are the calculation results by using Equations 4.8-4.15, which is similar to the numerical solution presented in [36]. Under negative twist, the extension of the molecule decreased when increasing the degree of supercoiling at forces below 1.0 pN. Above 1.0 pN, the extension of supercoiled DNA converged to the extension of DNA without twist. Under positive twist, the extension of the molecule decreased when increasing the degree of supercoiling up to F=4.0 pN.
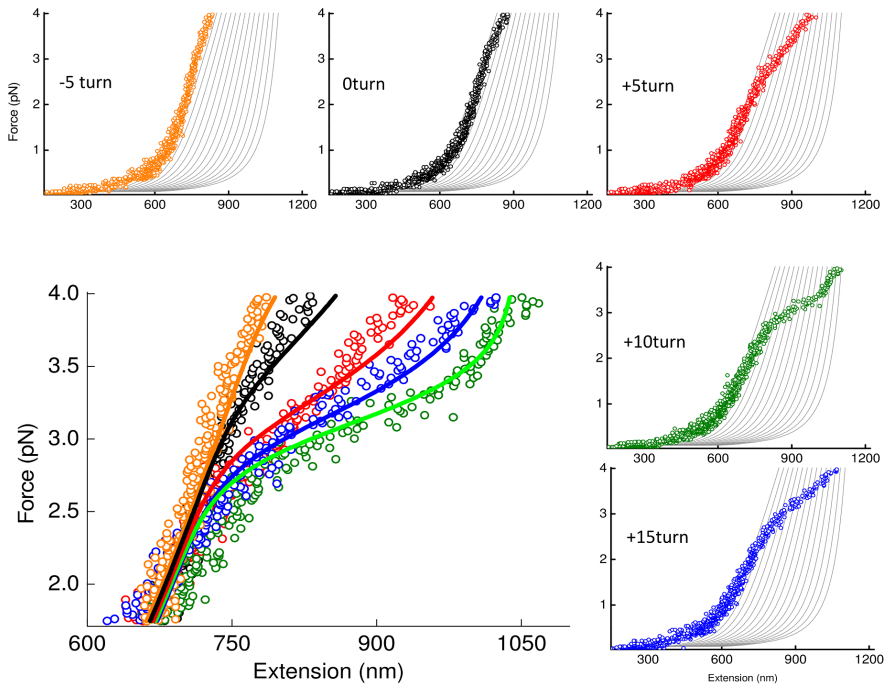
Figure S2

The force-extension curves of 197x15 repeats torsional constrained chromatin fiber. The global fit results for the five curves from 1.0 pN to 4.0 pN are shown as solid lines. The gray lines as background in each curve are the calculation results of torsionally unconstrained model by varying the number of folded nucleosome as references to the experimental data.
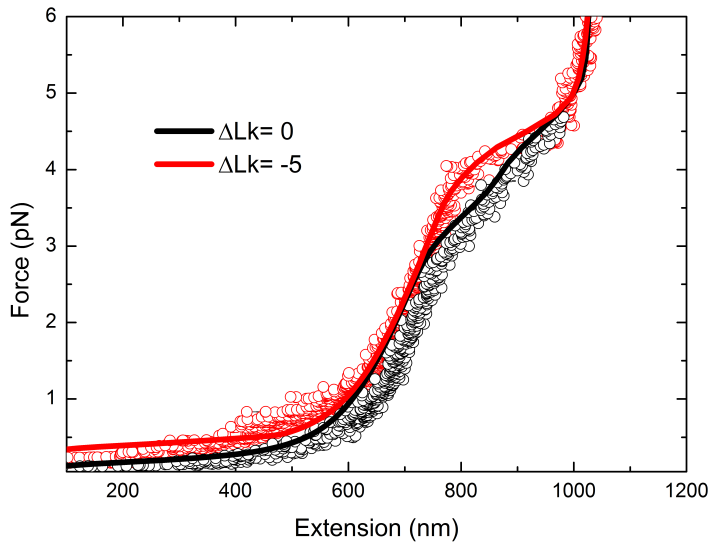
Figure S3

Force-extension curves of 197x15 repeats torsional constrained chromatin fiber with force up to 6 pN by using the magnetic bead with diameter 2.8 μm instead of 1.0 μm. It shows that under negative twist, around 4 pN the force-extension curve has a force plateau similar to the torsional unconstrained fiber at lower force. Solid lines are the calculations by using the parameters from global fit in main text Table 4.1. It shows a good agreement to the experimental data.
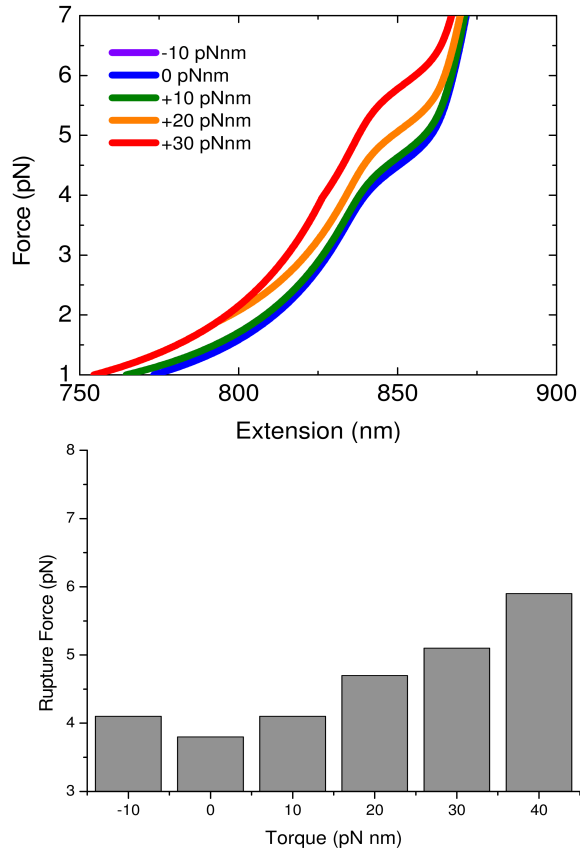
Figure S4

Simulated Force-extension curves for a mononucleosome under constant torque. By using our statistical mechanics model discussed in the main text, we decrease the number of nucleosomes to one, and we only use one parameter, the unfolding energy $G_u = 10\ k_B T$ to describe the mononucleosome. We converted the excess linking number to torque using Equation 4.9. The calculated curves and rupture forces give the same trend as reported in [22].

References IV

[1] Watson, J., and F. Crick. 1953. Molecular Structure of Nucleic Acids. *Nature*. 171:737–738.

[2] Luger, K., A. W. Ma, R. K. Richmond, D. F. Sargent, and T. J. Richmond. 1997. Crystal structure of the nucleosome core particle at 2 . 8 A resolution. *Nature*. 389:251–260.

[3] Li, G., and D. Reinberg. 2011. Chromatin higher-order structures and gene regulation. *Current opinion in genetics & development*. 21:175–86.

[4] Luger, K., M. L. Dechassa, and D. J. Tremethick. 2012. New insights into nucleosome and chromatin structure: an ordered state or a disordered affair? *Nature reviews. Molecular cell biology*. 13:436–47.

[5] Bassett, A., S. Cooper, C. Wu, and A. Travers. 2009. The folding and unfolding of eukaryotic chromatin. *Current opinion in genetics & development*. 19:159–65.

[6] Grigoryev, S. a., and C. L. Woodcock. 2012. Chromatin organization - the 30 nm fiber. *Experimental cell research*. 318:1448–55.

[7] Eltsov, M., K. M. Maclellan, K. Maeshima, A. S. Frangakis, and J. Dubochet. 2008. Analysis of cryo-electron microscopy images does not support the existence of 30-nm chromatin fibers in mitotic chromosomes in situ. *Proceedings of the National Academy of Sciences of the United States of America*. 105:19732–7.

[8] Maeshima, K., S. Hihara, and M. Eltsov. 2010. Chromatin structure: does the 30-nm fibre exist in vivo? *Current opinion in cell biology*. 22:291–7.

[9] Nishino, Y., M. Eltsov, Y. Joti, K. Ito, H. Takata, Y. Takahashi, S. Hihara, A. S. Frangakis, N. Imamoto, T. Ishikawa, and K. Maeshima. 2012. Human mitotic chromosomes consist predominantly of irregularly folded nucleosome fibres without a 30-nm chromatin structure. *The EMBO journal*. 31:1644–53.

[10] Fudenberg, G., and L. a. Mirny. 2012. Higher-order chromatin structure: bridging physics and biology. *Current opinion in genetics & development*. 22:115–24.

[11] Naumova, N., M. Imakaev, G. Fudenberg, Y. Zhan, B. R. Lajoie, L. a. Mirny, and J. Dekker. 2013. Organization of the mitotic chromosome. *Science*. 342:948–53.

[12] Li, B., M. Carey, and J. L. Workman. 2007. The role of chromatin during transcription. *Cell*. 128:707–19.

[13] Brooks, T. a., and L. H. Hurley. 2009. The role of supercoiling in transcriptional control of MYC and its importance in molecular therapeutics. *Nature reviews. Cancer*. 9:849–61.

[14] Darzacq, X., Y. Shav-Tal, V. de Turris, Y. Brody, S. M. Shenoy, R. D. Phair, and R. H. Singer. 2007. In vivo dynamics of RNA polymerase II transcription. *Nature structural & molecular biology*. 14:796–806.

[15] Wang, J. C., and A. S. Lynch. 1993. Transcription and DNA supercoiling. *Current opinion in genetics & development*. 3:764–8.

[16] Clark, D. J., and G. Felsenfeld. 1992. A nucleosome Core Is Transferred out of the Path of a Transcribing polymerase. *Cell*. 71:11–22.

[17] Teves, S. S., and S. Henikoff. 2014. Transcription-generated torsional stress destabilizes nucleosomes. *Nature structural & molecular biology*. 21:88–94.

[18] Naughton, C., N. Avlonitis, S. Corless, J. G. Prendergast, I. K. Mati, P. P. Eijk, S. L. Cockroft, M. Bradley, B. Ylstra, and N. Gilbert. 2013. Transcription forms and remodels supercoiling domains unfolding large-scale chromatin structures. *Nature structural & molecular biology*. 20:387–95.

[19] Kouzine, F., A. Gupta, L. Baranello, D. Wojtowicz, K. Ben-Aissa, J. Liu, T. M. Przytycka, and D. Levens. 2013. Transcription-dependent dynamic supercoiling is a short-range genomic force. *Nature structural & molecular biology*. 20:396–403.

[20] Ma, J., L. Bai, and M. D. Wang. 2013. Transcription under torsion. *Science*. 340:1580–3.

[21] Gilbert, N., and J. Allan. 2014. Supercoiling in DNA and chromatin. *Current Opinion in Genetics & Development*. 25:15–21.

[22] Sheinin, M. Y., M. Li, M. Soltani, K. Luger, and M. D. Wang. 2013. Torque modulates nucleosome stability and facilitates H2A/H2B dimer loss. *Nature communications*. 4:2579.

[23] Bancaud, A., N. Conde e Silva, M. Barbi, G. Wagner, J.-F. Allemand, J. Mozzi-conacci, C. Lavelle, V. Croquette, J.-M. Victor, A. Prunell, and J.-L. Viovy. 2006. Structural plasticity of single chromatin fibers revealed by torsional manipulation. *Nature structural & molecular biology*. 13:444–50.

[24] Bancaud, A., G. Wagner, N. Conde E Silva, C. Lavelle, H. Wong, J. Mozziconacci, M. Barbi, A. Sivolob, E. Le Cam, L. Mouawad, J.-L. Viovy, J.-M. Victor, and A. Prunell. 2007. Nucleosome chiral transition under positive torsional stress in single chromatin fibers. *Molecular cell*. 27:135–47.

[25] Kruithof, M., F.-T. Chien, A. Routh, C. Logie, D. Rhodes, and J. van Noort. 2009. Single-molecule force spectroscopy reveals a highly compliant helical folding for the 30-nm chromatin fiber. *Nature structural & molecular biology*. 16:534–40.

[26] Victor, J. M., J. Zlatanova, M. Barbi, and J. Mozziconacci. 2012. Pulling chromatin apart: Unstacking or Unwrapping? *BMC biophysics*. 5:21.

[27] Williams, S. P., B. D. Athey, L. J. Muglia, R. S. Schappe, H. Albert, and J. P. Langmore. 1986. Chromatin fibers are left-handed double helices with diameter and mass per unit length that depend on linker length. *Biophysical journal*. 49:233–245.

[28] Marko, J. 1997. Stretching must twist DNA. *Europhysics Letters*. 38:183–188.

[29] Bustamante, C., S. B. Smith, J. Liphardt, and D. Smith. 2000. Single-molecule studies of DNA mechanics. *Current opinion in structural biology*. 10:279–85.

[30] Strick, T. R., J. F. Allemand, D. Bensimon, A. Bensimon, and V. Croquette. 1996. The elasticity of a single supercoiled DNA molecule. *Science*. 271:1835–7.

[31] Strick, T. R., J. F. Allemand, D. Bensimon, and V. Croquette. 1998. Behavior of supercoiled DNA. *Biophysical journal*. 74:2016–28.

[32] Gore, J., Z. Bryant, M. Nöllmann, M. U. Le, N. R. Cozzarelli, and C. Bustamante. 2006. DNA overwinds when stretched. *Nature*. 442:836–9.

[33] Durickovic, B., A. Goriely, and J. H. Maddocks. 2013. Twist and Stretch of Helices Explained via the Kirchhoff-Love Rod Model of Elastic Filaments. *Physical Review Letters*. 111:108103.

[34] Robinson, P. J. J., W. An, A. Routh, F. Martino, L. Chapman, R. G. Roeder, and D. Rhodes. 2008. 30 nm chromatin fibre decompaction requires both H4-K16 acetylation and linker histone eviction. *Journal of molecular biology*. 381:816–25.

[35] Marko, J. 2007. Torque and dynamics of linking number relaxation in stretched supercoiled DNA. *Physical Review E*. 76:021926.

[36] Meng, H., J. Bosman, T. van der Heijden, and J. van Noort. 2014. Coexistence of Twisted, Plectonemic, and Melted DNA in Small Topological Domains. *Biophysical Journal*. 106:1174–1181.

[37] Forth, S., C. Deufel, M. Sheinin, B. Daniels, J. Sethna, and M. Wang. 2008. Abrupt Buckling Transition Observed during the Plectoneme Formation of Individual DNA Molecules. *Physical Review Letters*. 100:148301.

[38] Gross, P., N. Laurens, L. B. Oddershede, U. Bockelmann, E. J. G. Peterman, and G. J. L. Wuite. 2011. Quantifying how DNA stretches, melts and changes twist under tension. *Nature Physics*. 7:731–736.

[39] Simpson, R. T., F. Thoma, and J. M. Brubaker. 1985. Chromatin reconstituted from tandemly repeated cloned DNA fragments and core histones: a model system for study of higher order structure. *Cell*. 42:799–808.

[40] Hayes, J. J., T. D. Tullius, and a. P. Wolffe. 1990. The structure of DNA in a nucleosome. *Proceedings of the National Academy of Sciences of the United States of America*. 87:7405–9.

[41] Prunell, A. 1998. A topological approach to nucleosome structure and dynamics: the linking number paradox and other issues. *Biophysical journal*. 74:2531–44.

[42] Allemand, J. F., D. Bensimon, R. Lavery, and V. Croquette. 1998. Stretched and overwound DNA forms a Pauling-like structure with exposed bases. *Proceedings of the National Academy of Sciences of the United States of America*. 95:14152–7.

[43] Hodges, C., L. Bintu, L. Lubkowska, M. Kashlev, and C. Bustamante. 2009. Nucleosomal fluctuations govern the transcription dynamics of RNA polymerase II. *Science*. 325:626–8.

[44] Bintu, L., T. Ishibashi, M. Dangkulwanich, Y.-Y. Wu, L. Lubkowska, M. Kashlev, and C. Bustamante. 2012. Nucleosomal elements that control the topography of the barrier to transcription. *Cell*. 151:738–49.

[45] Kuehner, J. N., E. L. Pearson, and C. Moore. 2011. Unravelling the means to an end: RNA polymerase II transcription termination. *Nature reviews. Molecular cell biology*. 12:283–94.

[46] Kruithof, M., F. Chien, M. de Jager, and J. van Noort. 2008. Subpiconewton dynamic force spectroscopy using magnetic tweezers. *Biophysical journal*. 94:2343–8.

[47] Routh, A., S. Sandin, and D. Rhodes. 2008. Nucleosome repeat length and linker histone stoichiometry determine chromatin fiber structure. *Proceedings of the National Academy of Sciences of the United States of America*. 105:8872–7.

[48] Tinoco, I., and C. Bustamante. 2002. The effect of force on thermodynamics and kinetics of single molecule reactions. *Biophysical chemistry*. 101-102:513–33.

Summary

Since the discovery of the right-handed helical structure of DNA, 61 years have passed. The DNA molecule, which encodes genetic information, is also found twisted into coils. This extra twist of the helical structure, called supercoiling, plays important roles in both DNA compaction and gene regulation.

The DNA in eukaryotic cells is packaged into chromatin, with the basic unit called nucleosome. The nucleosome core is a protein-DNA complex, with 147 base pairs (bp) of DNA wrapped 1.7 turns in a left-handed helix around the histone octamer proteins. The strong electrostatic interactions between histones and DNA make the nucleosome one of the most stable protein-DNA complexes under physiological conditions. Because of this, it is well suited for its packaging function. It is generally accepted that arrays of nucleosomes can coil into a 30-nm-diameter helix to form the higher order structure of chromatin.

Chromatin is not a static structure, but it is highly dynamic to allow for vital processes such as replication and transcription. The two chains of DNA in the chromatin must get untwisted and separated during their activity. Many enzymes, acting on DNA, such as topoisomerases and RNA polymerases are constantly stretching and twisting the DNA helix. The effects of tension and torsion on bare DNA have been well studied by single-molecule techniques in the last 20 years. However, those effects on chromatin are still poorly understood. Understanding of this interplay has potential clinical implications, since some widely used anti-cancer drugs are known to interfere with the regulation of supercoiling. In this thesis, I give insights into chromatin fiber response to tension and torsion. With the results presented in this thesis, I aim to connect to the knowledge obtained from molecular biology and genomics on understanding the role of chromatin structure in maintaining our genes.

In order to quantify the effects of tension and torsion on a chromatin fiber, I first

studied the mechanical properties of supercoiled DNA (**Chapter 2**). I report the coexistence of twisted, plectonemic and melted states of DNA in a small topological domain. An extended experimental data set obtained with magnetic tweezers indicates the coexistence of these three states at sub-picoNewton force and linking number densities of about -0.06. A broadening of the transitions between the three states is found when the size of a topological domain reduces to several kilobasepairs. I presented a statistical mechanics model for such DNA domains by calculating the full partition function. Real-time analysis of short DNA tethers at constant force and torque shows discrete levels of extension, representing discontinuous changes in the size of the melted DNA. This new insight may have implications for the working mechanism of proteins that interact with DNA in topological domains, such as topoisomerases, transcription factors, histones and DNA based molecular motors, like DNA and RNA polymerases and chromatin remodellers.

Next, I quantitatively described the force spectroscopy of torsionally unconstrained regular chromatin fibers reconstituted with DNA containing Widom 601 sequence repeats (**Chapter 3**). Aiming to disentangle unfolding transitions in chromatin fibers, I presented new experimental data as well as a novel quantitative model for all aspects of force-induced unwrapping of the chromatin fiber. With this statistical mechanics model, I compared pulling traces of a mononucleosome with those of fully folded fibers. Despite using arrays of Widom 601 sequences and careful titration of the reconstitution dialysis, I found it necessary to include some heterogeneity of the chromatin fibers in terms of nucleosome composition into the model. When these heterogeneities were accounted for, I was able to determine consistent values for the DNA unwrapping free energy and the extension of each nucleosome conformation. A novel intermediate conformation was found, existing between 2.5 and 7 pN. Moreover, the qualitative difference in rupture behavior between chromatin fibers with 197 bp and 167 bp nucleosome repeat length indicated a different folding topology of the two repeat lengths. My results have implications for accessibility of DNA in fully-folded and partially unwrapped chromatin fibers and are essential for understanding force-unfolding experiments on nucleosome arrays.

Finally, based on the knowledge summarized above, I studied the stability of single supercoiled chromatin fibers (**Chapter 4**). By applying tension and torsion with magnetic tweezers, I found that the fiber has a strong asymmetric response to supercoiling. Negative supercoiling stabilizes the fiber against unfolding. Positive supercoiling is ab-

sorbed by the fiber. This anisotropy of the fiber reflects the chirality of a left-handed helix. When the force exceeds 2.5 pN, the fiber unfolds, and unwraps one turn of DNA. The level of unfolding depends on the degree of supercoiling. Interestingly, positive supercoiling facilitates the unfolding, but superfluous positive supercoiling refolds the fiber. An equilibrium statistical mechanics model based on chromatin topology and elasticity was presented, which captures the full complexity of chromatin folding and unfolding at different degrees of supercoiling. These results revealed for the first time the effects of torque on a folded chromatin fiber and present a new quantitative model of chromatin supercoiling.

In conclusion, using single-molecule force spectroscopy, I resolved force/torque-induced structural changes of DNA and chromatin fibers. I showed that the structural changes of chromatin fibers can be described by four conformations. I showed for the first time the folding and unfolding of a chromatin fiber under torsion. The anisotropic response of chromatin fibers to supercoiling reflects its left-handed chirality. These findings give a detailed structural insight of a supercoiled chromatin fiber, yielding a better understanding of the response of chromatin during transcription.

Samenvatting

Om de 2 meter DNA die elke menselijke cel bevat te passen in de kern van de cel zit het DNA opgevouwen in chromatine. Nucleosomen zijn de kleinste eenheid waarin het DNA in chromatine zit opgerold. Een nucleosoom bestaat uit 147 baseparen DNA die 1,7 keer gewikkeld zijn om een histon-octameer. De interacties tussen de histonen en DNA maken een nucleosoom een van de meest stabiele eiwit-DNA complexen onder fysiologische condities. Als gevolg van deze eigenschap is het zeer geschikt voor zijn verpakkingsfunctie.

Sinds in de jaren 70 van de vorige eeuw werd ontdekt dat in eukaryote cellen DNA gevouwen zit in chromatine, wordt gedacht dat de functie van deze structuur verder gaat dan alleen DNA compactie. Chromatine is niet statisch in de celkern, maar speelt een belangrijke regulerende rol in diverse levensprocessen, zoals replicatie en transcriptie. Voor deze processen moeten de twee ketens van DNA in chromatine, die om elkaar gedraaid zijn in een rechtsdraaiende dubbele helix, worden ontwonden en van elkaar gescheiden worden. Enzymen zoals topoisomerases en RNA polymerases zijn hiervoor voortdurend bezig de helix uit te rekken en te draaien.

Het effect van krachten als spanning en torsie op DNA zonder nucleosomen is een onderwerp dat door middel van enkel-molecuul technieken goed bestudeerd is in de afgelopen 20 jaar. De effecten die deze krachten uitoefenen op chromatine zijn echter nog nauwelijks onderzocht. In dit proefschrift laat ik zien hoe een enkele chromatine vezel reageert op span- en torsiekrachten die uitgeoefend worden met behulp van een magnetisch pincet. Deze resultaten geven een fysische beschrijving van de veranderingen in chromatine zoals deze plaatsvinden als genen worden uitgelezen, of tijdens de delingscyclus van de cel.

Om de effecten van span- en torsiekrachten op de chromatine vezel te onderzoeken, heb ik eerst de mechanische eigenschappen van supercoiled DNA bestudeerd

(**Hoofdstuk 2**). Experimentele data gemeten met een magnetisch pincet wijzen erop dat opgewikkelde, gedraaide, en gedenatureerde vormen van DNA in een gesloten topologisch gebied naast elkaar bestaan bij krachten kleiner dan 1 piconewton en 6% ontwinding van het DNA. Een verbreding van de overgang tussen deze drie toestanden ontstaat wanneer de grootte van het topologisch gebied wordt beperkt tot een paar duizend baseparen. Zulke korte DNA ketens laten bij een constante kracht en torsie discrete niveaus van extensie zien, die stapsgewijze veranderingen in de grootte van het gedenatureerde DNA voorstellen. Naast metingen presenteer ik in dit hoofdstuk een statistisch mechanisch model voor korte DNA gebieden door de complete partitiefunctie te berekenen. De resultaten van dit model beschrijven kwantitatief de stabiliteit van de drie verschillende toestanden in supercoiled DNA. Dit nieuwe inzicht heeft wellicht implicaties voor het mechanisme van eiwitten die interactie hebben met DNA en de topologie van het DNA beïnvloeden, zoals topoisomerases, transcriptie factoren, histonen en moleculaire motoren actief op DNA, zoals DNA- en RNApolymerases.

Vervolgens beschrijf ik krachtspectroscopie van torsievrije chromatine vezels, gereconstitueerd op DNA dat een aantal eenheden van de zogenaamde Widom 601 sequentie bevat (**Hoofdstuk 3**). Om de ontvouwing van chromatine vezels te begrijpen presenteer ik nieuwe experimentele data en een nieuw kwantitatief model voor alle aspecten van ontvouwing van een chromatine vezel door kracht. Aan de hand van dit statistisch mechanisch model vergelijk ik de ontvouwing van individuele nucleosomen met die van volledig gevouwen chromatine vezels, bestaande uit meerdere nucleosomen. Ondanks het gebruik van de Widom 601 sequentie en het behoedzaam titreren van histonen tijdens de reconstitutie dialyse, blijkt het nodig te zijn heterogeniteit van chromatine fibers wat betreft nucleosoomcompositie mee te nemen. Dit levert consistente waarden op voor de vrije energie van DNA ontvouwing en de extensies van elk van de vier nucleosoom conformaties. Ik heb een nieuwe intermediaire conformatie gevonden tussen 2,5 en 7 piconewton. Bovendien wordt een kwalitatief verschil getoond in het ontvouwingsgedrag van chromatine vezels met 50 baseparen en 20 baseparen DNA tussen de nucleosomen, wat duidt op een andere vouwingsstructuur. Deze resultaten geven een fysisch inzicht in hoe de toegankelijkheid van DNA in volledig gevouwen en gedeeltelijk ontvouwen chromatine vezels wordt gereguleerd.

Tenslotte heb ik de stabiliteit van supercoiled chromatine vezels bestudeerd (**Hoofdstuk 4**). Door span- en torsiekrachten uit te oefenen met het magnetische pincet kon ik een sterk asymmetrische reactie op het op- en ontwinden van de chromatine

vezel meten. Negatieve supercoiling stabiliseert de vezel tegen ontvouwing. Positieve supercoiling kan worden geabsorbeerd door de chromatine vezel. Deze anisotropie laat de chiraliteit van een linksdraaiende helix zien. Wanneer de kracht groter is dan ~2,5 piconewton ontvouwt de chromatine vezel, waarbij één winding van het DNA los komt van elk nucleosoom. De mate van ontvouwing is afhankelijk van de graad van supercoiling. Opmerkelijk is dat positieve supercoiling ontvouwing faciliteert, maar overtollige positieve supercoiling de vezel weer terugvouwt. Een statistisch mechanisch model wordt gepresenteerd waarin topologie, elasticiteit, chromatine vouwing en ontvouwing op verschillende niveaus van supercoiling zijn opgenomen. Deze inzichten beschrijven de effecten van torsie op een gevouwen chromatine vezel met behulp van een nieuw kwantitatief model voor chromatine supercoiling.

Samenvattend heb ik door individuele chromatine vezels zorgvuldig te manipuleren met behulp van een magnetisch pincet de effecten van kracht en torsie op de structuur van chromatine kunnen meten. Ik heb aangetoond dat deze veranderingen in chromatine vezels met 3 tussenstappen plaatsvinden. Daarnaast heb ik de anisotrope respons van chromatine fibers op supercoiling laten zien, wat de linkshandige chiraliteit van chromatine aantoont. De mechanische eigenschappen van de chromatine vezel geven belangrijke aanwijzingen over de veranderingen van chromatine tijdens bijvoorbeeld transcriptie, of bij de werking van enkele anti-kanker geneesmiddelen die direct ingrijpen in de controle van supercoiling in de cel. De nieuwe kennis van de mechanische eigenschappen van DNA en chromatine is belangrijk voor een fundamenteel begrip van deze en velerlei andere processen waarin DNA een rol speelt.

List of Publications

- Rosalie Driessen, **He Meng**, Gorle Suresh, Rajesh Shahapure, Giovanni Lanzani, U Deva Priyakumar, Malcolm F White, Helmut Schiessel, John van Noort, Remus Th Dame,
  "Crenarchaeal chromatin proteins Cren7 and Sul7 compact DNA by inducing rigid bends",
  Nucleic Acids Research , 2013, **41** (1): 196-205

- **He Meng**, Johan Bosman, Thijn van der Heijden, John van Noort,
  "Coexistence of Twisted, Plectonemic, and Melted DNA in Small Topological Domains",
  Biophysical Journal, 2014, **106** (5): 1174-1181

- **He Meng**, Kurt Andresen, John van Noort,
  "Chromatin Fiber Structure Revealed through Quantitative Analysis of Single-Molecule Force Spectroscopy",
  submitted

- **He Meng**, John van Noort,
  "Torsional stress controls the folding and unfolding of the chromatin fiber",
  in preparation

Curriculum Vitae

He Meng was born on August 25, 1985 in Jilin, China. In 2003, he finished his secondary education at the Jilin City No.1 High School. In the same year, he passed the National College Entrance Examination with a score of the top 0.1%, and he was admitted to the School of Physics, Peking University in Beijing. After finishing his undergraduate studies in 2007, he started his graduate study in the Institute of Physics, Chinese Academy of Science under the mentorship of Prof. Ming Li. Here he got interested in single-molecule biophysics. He graduated with a project on DNA (de)compaction induced by protamine and nucleophosmin. In 2010, he joined the group of Dr. John van Noort, Leiden University, as a PhD candidate, working on an experimental project of probing the chromatin structure by magnetic tweezers.

The results of this work are presented in this thesis. During the PhD period, he presented his work at several conferences in Europe and the USA. He assisted teaching four courses: "Absorption Spectroscopy Practical for Biologists"; "Practical of Optical Tweezers"; "Experimental Biophysics"; "Noise and Signal Processing". He was also responsible for organizing the biweekly seminar of the biophysics and molecular physics. During his PhD research, he supervised one bachelor project and two master projects.